BINDING CONFIGURATIONS OF SINGLE-STRANDED DNA BINDING PROTEIN AND THEIR INFLUENCE ON DNA RECOMBINASE

BY

SUKRIT SUKSOMBAT

DISSERTATION

Submitted in partial fulfillment of the requirements
for the degree of Doctor of Philosophy in Physics
in the Graduate College of the
University of Illinois at Urbana-Champaign, 2015

Urbana, Illinois

Doctoral Committee:

Professor Taekjip Ha, Chair
Associate Professor Yann R. Chemla, Director of Research
Associate Professor Aleksei Aksimentiev
Assistant Professor Sua Myong

Abstract

DNA inside a cell is continuously damaged through multiple mechanisms including environmental exposure to radiation, chemical agents, or UV light. Certain products of the cell's own metabolism, such as reactive oxygen species, can also damage the DNA. In the worst-case scenario, this damage results in double-stranded DNA (dsDNA) breaks. Double-stranded DNA breaks are lethal, and difficult to repair, with potential complications from genome rearrangement. To prevent this genetic instability, a cell can utilize a homologous chromosome as a template to accurately repair DSBs. This process is called homologous recombination.

Homologous recombination begins when an enzyme complex binds to a blunt end of a dsDNA break. The complex unzips the dsDNA through its helicase activity, and simultaneously cleaves the newly-generated 5' end of the ssDNA. This process leaves the remaining ssDNA strand exposed to the surrounding environment and prone to nucleolytic and chemical attacks. Cells have evolved single-stranded DNA binding (SSB) proteins to wrap and protect this ssDNA. In *E. coli*, SSB is known to wrap ssDNA in a variety of binding configurations, or modes. Three different binding modes, $(SSB)_{65}$, $(SSB)_{56}$, and $(SSB)_{35}$, which wraps 65, 56, and 35 nucleotides (nt) respectively, have been observed *in vitro* [1]. Previous studies have suggested that SSB binding in different modes may exhibit different levels of binding cooperativity. SSBs in the $(SSB)_{65}$ binding mode form isolated clusters (limited cooperativity), while SSBs in the $(SSB)_{35}$ binding mode form long filaments (unlimited cooperativity) [2, 3]. These different levels of binding cooperativity have been proposed to be used selectively in different DNA metabolic processes, including DNA replication, recombination, and repair.

In homologous recombination, recombinase RecA must bind and form nucleoprotein filaments on the ssDNA, in direct competition with SSB. Prior studies have shown that RecA is capable of forming filaments on ssDNA wrapped by SSBs in the $(SSB)_{65}$ binding mode, but

filament formation on ssDNA wrapped by SSBs in the $(SSB)_{35}$ binding mode is inhibited [3]. Recent single-molecule studies have been conducted to investigate this competitive process, but the detailed mechanisms remain unclear [4–6].

Here, we use high-resolution optical tweezers with simultaneous fluorescence microscopy to observe directly the activity of ssDNA-SSB, ssDNA-RecA, and ssDNA-SSB-RecA complexes under tension, and characterize their mechanical properties. The instrument allows us to simultaneously probe and visualize the interactions of RecA and SSB with ssDNA in real time and with nanometer resolution.

We confirm that individuals SSBs bind and compact ssDNA in discrete modes. Under low tension (1-3 pN), a single SSB wraps ssDNA in the $(SSB)_{65}$ or $(SSB)_{56}$ binding mode. At higher tension (4-8 pN), SSB exhibits transient wrapping-unwrapping, switching between the $(SSB)_{56}$, $(SSB)_{35}$, and $(SSB)_{17}$ wrapping modes. When multiple SSBs are present on the ssDNA, the SSBs form isolated clusters in those solution conditions that favor the $(SSB)_{65}$ binding mode. The configuration of the SSBs changes to a long and stable filament when solution conditions that favor the $(SSB)_{35}$ binding mode are used.

In the absence of SSB, RecAs nucleate filament rapidly on ssDNA. The nucleation rate of RecA is slowed down by several times when RecA is added to ssDNA coated with isolated clusters of SSBs in the $(SSB)_{56}$ mode. The nucleation rate of RecA decreases further when long and stable filaments of SSBs in the $(SSB)_{35}$ binding mode are present on the ssDNA. The same experiments also demonstrate that RecA is capable of removing these SSBs from the ssDNA in a step-wise manner.

Our results reveal the importance of SSB binding modes and their oligomerization to DNA recombination, and further confirm that $(SSB)_{65}/(SSB)_{56}$ binding modes are more likely to facilitate the activity of recombinase RecA during the DNA repair. The $(SSB)_{35}$ binding mode, on the contrary, inhibits RecA filament formation, and is believed to not play an important role in this recombination process.

To my parents

Acknowledgments

This project would not been possible without the support of many people. First of all, I would like to thank my advisor, Yann Chemla, for enlightening me to the field of Biophysics. He took me as a rotation student, and gave me an opportunity to work in the lab since day one. Yann taught me everything necessary to do research. I learned how to select, design, and perform experiment in a very thoughtful approach. His programming, data analysis, and theoretical modeling skills also guided me to think critically and systematically. Yann inspired me with his data presentation. He taught me to present my data in a concise but informative way. His care for an audience always reminded me of how good a teacher he is. I was very fortunate to receive a hands-on help from Yann, something that is impossible in most research groups.

I would like to thank many wonderful professors and teachers who encouraged me to pursue my dream in science including my thesis committee members Professor Taekjip Ha, Professor Aleksei Aksimentiev, and Professor Sua Myong. Their guidance, support, and suggestion have shaped me into who I am today.

I would like to give special thanks to my mentor and best friend, Dr. Isaac Li. Isaac taught me how to be creative and efficient in experimental work. His observational and critical thinking skill also impressed me beyond my expectation. I learned so much from him, and my progress as a graduate student would be nowhere near it is now without Isaac's influence.

I would like to thank our collaborators, Professor Timothy Lohman and Dr. Alexander Kozlov from Washington University School of Medicine, for their help with providing *E. coli* SSB and stimulating many useful and interesting discussions. I would also like to thank Dr. Rustem Khafizov and Professor Matthew Comstock for helping me get this project started.

In addition to those mentioned above, I would like to thank both past and present members of the Chemla lab: Lance Min, Zhi Qi, Patrick Mears, Markita Landry, Vishal

Kottadiel, Kiran Girdhar, Kevin Whitley, Barbara Stekas, Tatyana Perlova, Ruopei Feng, Alice Troitskaia, and Roshni Bano. They unselfishly provided help, feedback, and assistance whenever I faced difficulties in my project. Their senses of humor also created a friendly and collaborative environment throughout my time here. I would also like to extend special thanks to Isaac Li, Alice Troitskaia, and Kevin Whitley for helping me proof-reading my thesis chapters.

I would like to thank the Development and Promotion of Science and Technology Talents Project (DPST) for supporting me since the beginning. The program prepared me through my high school year, trained me as a scientist, and finally gave me a huge opportunity I could have never afforded to study aboard. This opportunity completely change my life and my way of thinking.

I would like to thank the funding agencies including the Department of Physics, the Burroughs Wellcome Fund, and the Center for the Physics of Living Cells (CPLC). They provided funding to build an instrument, conduct researches, and support me throughout my graduate school.

I would like to thank my parents for being very supportive on everything I pursue. My dad's ambitious and hard-working instinct motivated me to be productive and relentless. My mom's creativity and thoughtful skill propelled me to be efficient and flexible. Without their care and encouragement I could never have achieve my goals. I would also like to thank my brother for taking care of our parents for all the time I spent studying in the US.

Lastly, I thank my wife and my best friend, Wanitchaya Suksombat with love. She sacrificed her career, and came to the US to stay with me as a family. She consoled me when I had difficulties or lacked motivation, and shared my happiness when I accomplished my goals no matter how small they are. Her unconditional love and emotional support cannot be described in words. Without her I could not have survived the graduate school.

Table of Contents

List of Tables

List of Figures

Chapter 1

Introduction

We begin this chapter by introducing the *Escherichia coli* (*E. coli*) single-stranded DNA binding (SSB) protein. A brief background of its interaction with nucleic acids and its importance to *E. coli*'s survival is given. We then present the specific goals of our study, and describe the tools and techniques we use to accomplish these goals. Lastly, we give an overview of all studies in this thesis.

1.1 Background

1.1.1 Single-stranded DNA Binding Proteins

During DNA replication, recombination and repair, single-stranded DNA (ssDNA) is inevitably exposed to the surrounding environment and becomes more prone to nucleolytic and chemical attacks. Cells evolve single-stranded DNA binding (SSB) proteins to bind, wrap, and protect specifically ssDNA in a sequence-independent manner [7]. Because of their importance for cell survival, SSB are found in almost all kingdoms of life. The first SSB, the T4 gene 32 protein, was discovered in T4 bacteriophage in 1970 [8], followed by a discovery of *E. coli* SSB soon after [9]. Since then, many prokaryotic SSBs have been identified in bacteria [10], plasmids [11], and bacteriophages [12, 13]. Recently, eukaryotic SSB (RPA or RFA) were classified in humans [14, 15], yeast [16], and fruit flies [17]. Mitochondrial SSBs [18, 19] and SSBs encoded by animal viruses [20] have also been characterized. Interestingly, these SSBs from different phylogenetic domains share very similar functions. They are essential for many DNA metabolic processes, and also interact specifically with other proteins involved in such processes [17, 21]. *E. coli* SSB has been chosen as a prototype for extensive biochemical and biophysical studies. Prior studies aimed to determine the role of SSB in various DNA metabolic processes [7, 22], but the detailed mechanisms remained poorly understood.

1.1.2 *E. coli* SSB and its Binding Configurations

The *E. coli* SSB protein is a homotetrameric protein, consisting of four subunits, 19 kDa each (Fig. 1.1(A)). Each subunit is comprised of two domains. The N-terminal domain (DNA-binding domain) is composed of 112 amino acid residues. It contains an oligonucleotide/oligosaccharide binding fold (OB fold) that binds to ssDNA (Fig. 1.1(B), red).

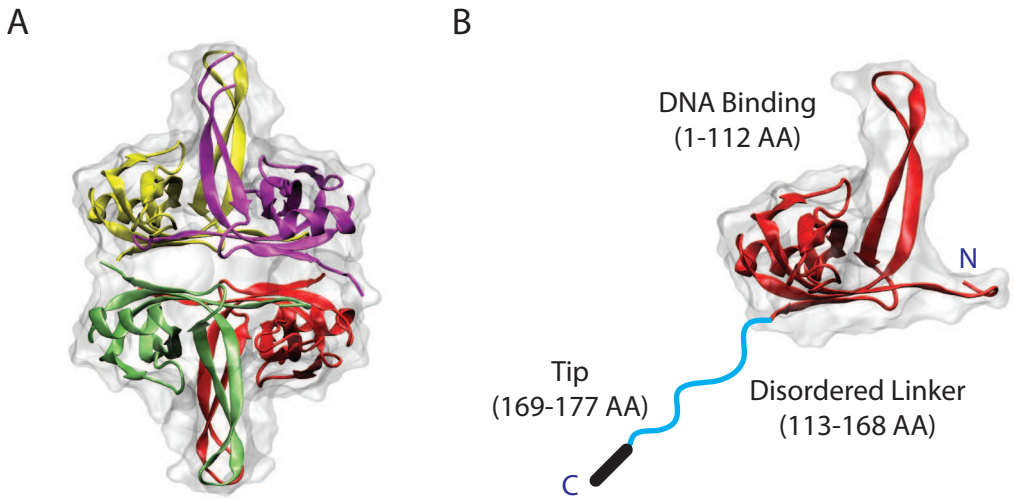

Figure 1.1: *E. coli* SSB. (**A**) Crystal structure of an *E. coli* SSB homotetramer [23]. Each color represents a single subunit of the SSB. (**B**) Crystal structure and schematic representation of *E. coli* SSB monomer. The N-terminal domain contains a DNA-binding fold (red), while the C-terminal domain is comprised of a disordered linker (cyan) and a negatively charged tip (black)

Some residues in the N-terminal domain interact strongly to the ssDNA than the other. Many chemical modification studies have suggested that tryptophan (Trp) is important for DNA binding [24]. Fluorescence quenching experiments showed that Trp-54 and Trp-88 might play major roles since the intrinsic fluorescence of these residues was partially quenched upon binding to ssDNA [25]. Trp-40 and Trp-54 are also believed to be necessary for high-affinity DNA binding. They form base- stacking interactions with the bases of the ssDNA [26]. The C-terminal domain, in contrast, is known to inhibit nucleic acid binding [27]. It consists of a flexible, intrinsically disordered linker (56 amino acids) and a negatively charged tip (9 amino acids) that is responsible for interacting with SSB interactin proteins (SIPs) (Fig. 1.1(B), [28, 29]). This tip can interact with the DNA binding site within the N-terminal domain, and compete for ssDNA binding [27]. The function of the linker is not well-understood, but previous studies have speculated that the linker may extend laterally

away from the DNA and facilitate interactions with other proteins [30].

Due to its stability as a tetramer over a wide range of solution conditions, *E. coli* SSB can wrap ssDNA in a variety of binding configurations that differ primarily in the number of OB folds interacting with the molecule [1]. The existence of these binding configurations or binding modes is supported by evidence obtained from experiments using various techniques [1, 3]. In 1984, Griffith et al. used an electron microscope to visualize distinct SSB-ssDNA configurations when different ratios of protein to DNA concentration were explored [3]. Under low protein to DNA ratio, SSBs formed clusters separated by SSB-free DNA linkers, resembling a beads-on-a-string structure found on nucleosome-DNA complexes (Fig. 1.2(A)). Increasing protein concentration above a certain threshold abruptly forced the nucleoprotein complex to acquire a smooth appearance (Fig. 1.2(B)).

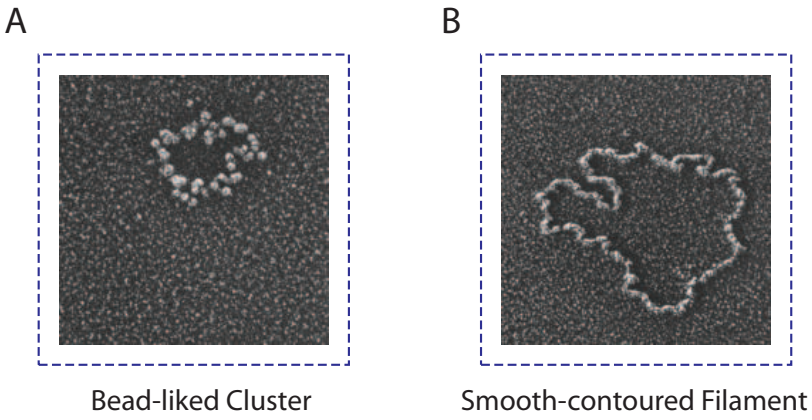

Figure 1.2: Configurations of the SSB-ssDNA complex. (**A**) An electron microscopy (EM) image of SSB binding to ssDNA under low SSB-to-DNA ratios. The complex has an appearance of a beads-on-a-string cluster. (**B**) An EM image of a high SSB-to-DNA ratios binding of SSB to ssDNA. Nucleoprotein demonstrates a smooth filament. Images are adapted from [3].

Independently of Griffith's , Lohman et al. studied SSB binding modes using intrinsic fluorescent property of Trp residues [1]. By varying salt conditions and protein concentrations, they discovered multiple binding modes of SSB. Under low salt ($<$ 10 mM NaCl) and high protein concentrations, SSB binds to ssDNA with high cooperativity, with an average of two subunits binding. Since approximately 35 $\pm$ 2 nt of ssDNA is wrapped, this binding mode is denoted as the $(SSB)_{35}$ binding mode. On the other hand, SSB exhibits an $(SSB)_{65}$ binding mode, wrapping 65 $\pm$ 3 nt ssDNA with all four subunits under high salt ($>$ 200 mM NaCl) conditions. These differences of site sizes and number of interacting subunits reflect different SSB configurations and compactions of the ssDNA. Combining the two independent results,

Lohman et al. concluded that SSBs in the $(SSB)_{35}$ mode exhibit 'unlimited' cooperativity where proteins associate with each other to form long protein filaments, and the $(SSB)_{65}$ mode shows 'limited' cooperativity where SSBs are limited to forming dimers of tetramers (octamers), and filaments are not created. Other binding modes, e.g. the $(SSB)_{56}$, have also been observed by this and other studies, using a variety of techniques, including circular dichroism [31] and electron spin resonance [32].

Several crystallographic studies of *E. coli* SSB have been reported [23, 33]. Most recently, Raghunathan et al., described a wrapping geometry of the $(SSB)_{65}$ mode using a structure of the C-terminal- truncated SSB tetramer (SSBc; 1-135 AA) with 2.8 Å resolution [23]. In this configuration, ~65 nt of ssDNA wrap around all four SSB subunits in a topology resembling the seams on a baseball (Fig. 1.3(A)). In this topology, ssDNA enters and exits the SSB tetramer around the same location. The structure of the $(SSB)_{35}$ is speculative, but evidence based on the symmetry of the SSBc complex and biochemical information provided a proposed structure as shown (Fig. 1.3(B)).

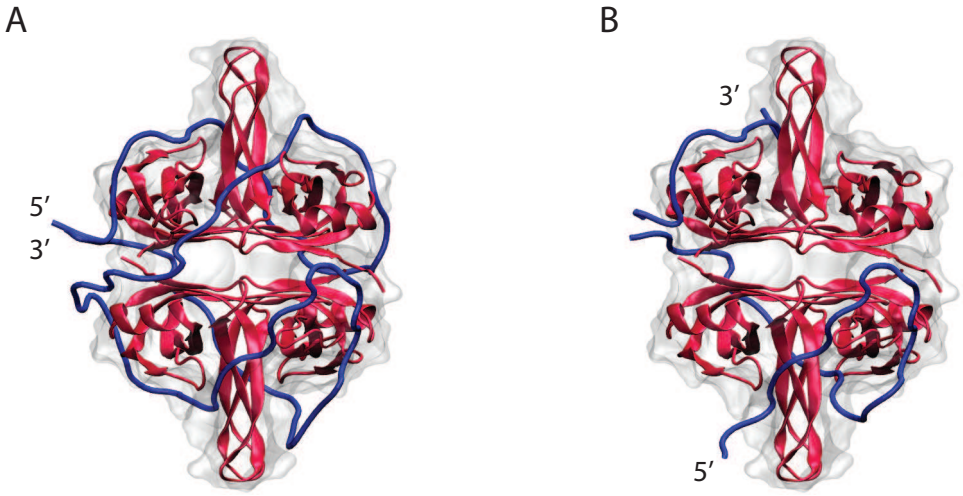

Figure 1.3: Binding modes of *E. coli* SSB. (**A**) Crystal structure of an *E. coli* SSB tetramer wrapped by 70 nt of ssDNA (blue) in the $(SSB)_{65}$ wrapping mode [23]. (**B**) Model of the $(SSB)_{35}$ wrapping mode based on the crystal structure in (A).

1.1.3 SSB Configurations and its Functionality

Various studies have shown that the properties of the SSB-ssDNA complex vary dramatically with the binding mode. It is interesting to consider whether any particular mode is associated with all DNA metabolic processes in *E. coli*. So far, no direct evidence has confirmed the link

between SSB binding modes and SSB's functions *in vivo*. *In vitro*, however, there are several hints indicating that it is unlikely that SSB modes function equivalently in all processes. For example, in homologous recombination – one of the *E. coli* DNA repair pathways – SSB has been shown to stimulate RecA filament formation under high salt (> 10 mM $MgCl_2$) conditions [34], while inhibiting the same process at low salt (~1 mM $MgCl_2$) [35]. This observation suggests the high salt SSB binding mode $(SSB)_{65}$ plays a role in helping RecA filament formation on ssDNA. Griffith et al. also consistently observed RecA filaments form more rapidly on ssDNA precoated with SSB in its beads-on-a-string $(SSB)_{65}$ mode, compared with ssDNA precoated with SSBs in a smooth-contoured $(SSB)_{35}$ mode [3]. The explanation could be simply that SSB in its beaded mode allows RecA to bind by leaving gaps of SSB-free ssDNA to which RecA can nucleate.

The $(SSB)_{35}$ mode, in contrast, is predicted to play a crucial role in the DNA replication process [2]. During replication, thousand nucleotides of ssDNA in the replication fork are exposed to environmental attacks. In order to protect these ssDNA strands in such a fast process, SSB needs to wrap and saturate the DNA very rapidly. Only SSBs in 'unlimited' - $(SSB)_{35}$ cooperativity can accomplish this task.

1.1.4 Interactions of *E. coli* SSB with Other Proteins

Beside protecting ssDNA from degradation, *E. coli* SSB also plays a role in controlling the accessibility of ssDNA to other proteins. In homologous recombination, for example, SSB allows recombinase RecA to access the ssDNA for the process to occur. To date, no direct interactions between SSB and RecA have been observed, although some interactions may occur when both are bound to ssDNA [36]. On the other hand, it has been shown that at least 14 other proteins (SIPs) interact directly with SSB, including DNA Polymerase II, III and V, RecQ, RecO, PriA, PriB and Exonuclease I [37]. SSB recruits SIPs to their functional sites.

1.1.5 Previous Studies and Open Questions

Tremendous progress has been made towards examining the interactions of *E. coli* SSB with ssDNA structurally, thermodynamically and kinetically. For example, crystal structure analysis by Matsumoto et al, revealed several pockets of positive electrostatic potential on

the SSB surface, which attract negatively-charged phosphates on the ssDNA to bind [33]. Investigating a structure of the full-length SSB tetramer, Savvides et al. confirmed the neccessity of the N-terminal domain for DNA binding, and proposed that the disordered linker in the C-terminal domain facilitates interaction between SSB and other proteins [30].

Several studies by Kozlov et al, showed that the binding of SSB to ssDNA is very fast ($10^8 - 10^9$ $M^{-1}s^{-1}$) and the wrapping rate is even faster ($k_{wrap} \gg k_{bind}$) [38]. In contrast, the SSB dissociation rate is extremely low at physiological conditions. High salt conditions (e.g. NaBr > 1 M) and high temperature were necessary to observe SSB dissociation from ssDNA [39].

Recently, several single-molecule techniques, including fluorescence resonance energy transfer (FRET) [4, 40], optical tweezers [41], and total internal reflection fluorescence microscopy (TIRF) [5] have been used to study SSB-ssDNA and SSB-ssDNA-RecA interactions. Using FRET, Roy et al., observed directly that SSB could undergo the transition between $(SSB)_{35}$ and $(SSB)_{65}$ binding modes without dissociating from ssDNA [40]. Other studies also showed that SSB is very dynamic, and can migrate along ssDNA by sliding [41] or hopping [42]. The ability of SSB to migrate to different locations on ssDNA allows it to facilitate interactions between ssDNA and various other proteins. Previous studies demonstrated that SSB diffusion melts short DNA hairpins transiently and stimulates RecA filament formation on ssDNA [4]. Yet other studies demonstrated that RecA is able to nucleate on transiently exposed ssDNA during SSB sliding or partial dissociation [5].

Despite extensive effort, the fundamental mechanisms of SSB interaction with ssDNA and other proteins remain unclear. One of the main reasons is an insufficiency of proper measurements and instrumentation. Bulk studies lack the ability to probe individual nucleoprotein complexes and extract mechanistic information. Single-molecule fluorescence alone is limited to qualitative information such as the presence (or absence) of a protein or a relative (rather than exact) location of the molecule of interest. Even optical tweezers are incapable of revealing the internal state of the system despite having the capability to observe system mechanics at high resolution. Hybrid instruments, on the other hand, provide a promising opportunity to study the system in detail. Through combining high-resolution optical tweezers with fluorescence microscopy [43], many interesting questions concerning protein-DNA interaction can be answered. Below are some of the questions we would like to address and answer in this thesis.

1. How does *E. coli* SSB wrap single-stranded DNA in different binding modes?
2. Can we detect other binding modes not previously observed?
3. How does SSB in the $(SSB)_{35}$ binding mode form a smooth-contoured filament, while SSB in the $(SSB)_{65}$ binding mode form a bead-liked cluster?
4. Do SSB binding modes affect interactions of other proteins with ssDNA differently?
5. How does SSB work with other proteins in DNA metabolic processes; for instance, with *E. coli* RecA in homologous recombination?

1.2 Goals

The primary goal of this thesis was to investigate the interactions between *E. coli* SSB, single-stranded DNA, and other proteins involved in DNA metabolic processes. The specific aims of this work were to:

1. Develop an experimental assay to observe *E. coli* SSB binding, wrapping, and interacting with ssDNA.
2. Analyze the DNA binding mechanism of individual SSB tetramers, and identify SSB wrapping intermediates not observed in previous studies.
3. Develop a detailed model to map the relationship between SSB wrapping intermediates and SSB binding configurations.
4. Explore the influence of SSB binding configurations on accessibility of ssDNA to other proteins.

In order to achieve these goals, we used high-resolution optical tweezers, fluorescence microscopy, mathematical models, and numerical simulations. Below, we describe the optical tweezers, the main instrument we used.

1.3 Tools

1.3.1 Optical Tweezers

In 1970, Ashkin et al. pioneered the field of laser-based optical trapping. They demonstrated that light carrying momentum could be used to manipulate the position of a micron-size dielectric particle in both water and air [44]. Soon after, a stable, three-dimensional optical trap based on counter-propagating laser beams was invented [45]. Over the next fifteen

years, tremendous efforts were made to develop a single-beam gradient force optical trap, or optical tweezers. This instrumentation was then used for the study of many systems, with applications ranging from trapping atoms to manipulating live cells, bacteria, and viruses [46, 47]. Today, optical tweezers are being used in many research areas including polymer physics [48, 49], condensed matter physics [50, 51], and biology [52–55] while innovation continues to flourish in all areas of instrumentation and technique. Theoretical and experimental studies, moreover, are being pursued to improve both temporal and spatial resolution of optical traps [56–59].

In this section, we briefly describe the basic principles of the operation of optical trapps and the studies of complex biological systems using optical tweezers.

Forming a Trap

An optical trap is formed by tightly focusing a laser beam with an objective lens. Near the focus, a dielectric particle feels a net force towards the focus due to momentum transfer from the scattering and refracting photons. This net force can generally be decomposed into two components; a scattering force and a gradient force. The principle of the optical scattering force can be explained using a simple ray optics diagram (Fig. 1.4). When incident light hits the bead, some photons will be absorbed and some will be scattered from the bead's surface (black). In the process, the momenta of the photons change. Through conservation of momentum, this results in momentum transfers (i.e., forces) to the bead. For isotropic scattering, the resulting forces cancel in all but the forward direction (blue). Increasing the intensity of light, increases the number of photons, which in turn results in more forces being transferred to the bead.

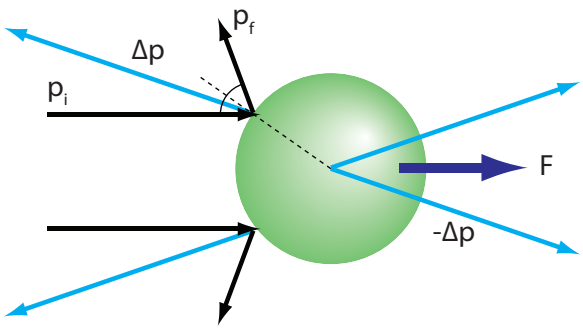

Figure 1.4: Scattering force. A transparent bead is illuminated by a trapping laser. Two representative rays of photons are shown scattering off the bead surface (black); the resulting change in photon momenta, Δp, is shown in cyan. The corresponding change of momentum of the bead results in a net force in the forward direction (blue).

The second component of the optical force is the gradient force. The gradient force can be further broken down into two components; a lateral and an axial gradient force; The lateral gradient force results from the Gaussian profile of the laser beam: if the bead is not at the center of the profile, the differential of intensity of the light refracting through the bead will result in a restoring force pulling it towards the center. This effect is diagrammatically shown below (1.5). Brighter light near the center of the profile is depicted by bold black lines, while dim light from the edge of the profile is depicted by thin lines. Upon entering the bead, both beams refract, undergoing changes in momentum and consequently exerting a force on the bead. The net resulting force (blue) directs the bead toward the area of light with higher intensity.

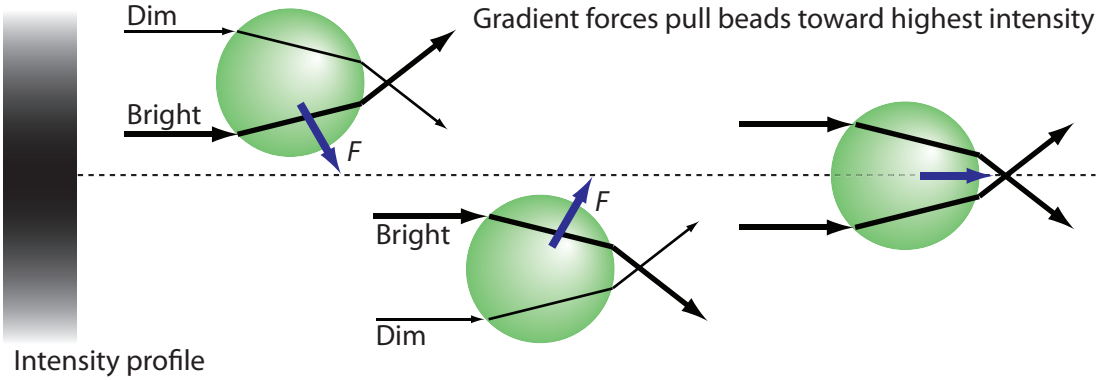

Figure 1.5: Lateral gradient force. A beam of light with an intensity gradient is projected asymmetrically on a bead. Two rays of light of different intensities (black, different thickness) are refracted from the bead, resulting in the momentum changes and forces. The net force directs the particle toward the area with higher intensity (blue).

For such a three-dimensional trap to be stable, there must be a force in the backward direction to compensate for the two forward forces previously described. This force arises through refraction of tightly focused light from a radial intensity beam through the bead. The change in momentum creates a net force toward the focal point, effectively pushing the bead backward (Fig. 1.6).

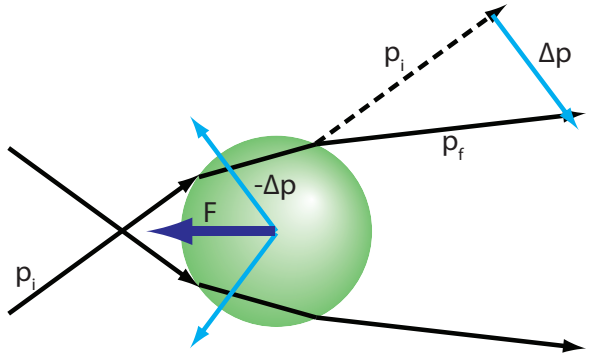

Figure 1.6: Axial gradient force. A bead is illuminated by a focused beam of light with a radial intensity gradient. Two rays of light are shown refracting through the bead (black), resulting in a momentum change or force which pushes the bead toward the focal point (blue).

When gradient forces pulling the bead towards the focus exceed scattering forces pushing it out, the bead is attracted to the point of highest intensity slightly beyond the focal point. If the bead is displaced from this spot by a distance x, the gradient restoring force, $F = -kx$, will pull the particle back to the equilibrium position. Effectively, the optical traps act as Hookean spring whose stiffness, k, is proportional to the light intensity.

Manipulation

The ability to manipulate the trap position provides immense advantages during experiments. One can align a trapped particle along a particular axis to accommodate the geometry of the sample plane. Two or more particles can also be trapped and controlled to create complex trapping setups. In addition to positioning the trap, the ability to move the trap locally around this position (scanning) greatly improves experimental assays where investigation of the dynamics of the sample can be examined.

The position of an optical trap can be controlled through two approaches; (i) directly displacing the trapping laser or (ii) moving the trapping chamber relative to the trap. Instrumentation commonly used to achieve such control includes the use of scanning mirrors,

acousto-optic deflectors (AOD), and electro-optic deflectors (EOD). If a scanning mirror is used, the position of the trap is limited by the mirror operating speed and the precision of the rotation angle (Fig. 1.7(A)). AODs and EODs, on the other hand, can operate at much higher speeds.

The crystal inside an AOD or EOD deflects light at different angles depending on the electric field of acoustic waves it is subject to; since the process is not based on mechanical movement of the components, it can change the deflection of light at frequencies on the order of 100 kHz (Fig. 1.7(A)). The main drawbacks of using these deflectors are loss of light intensity and a narrow deflection range.

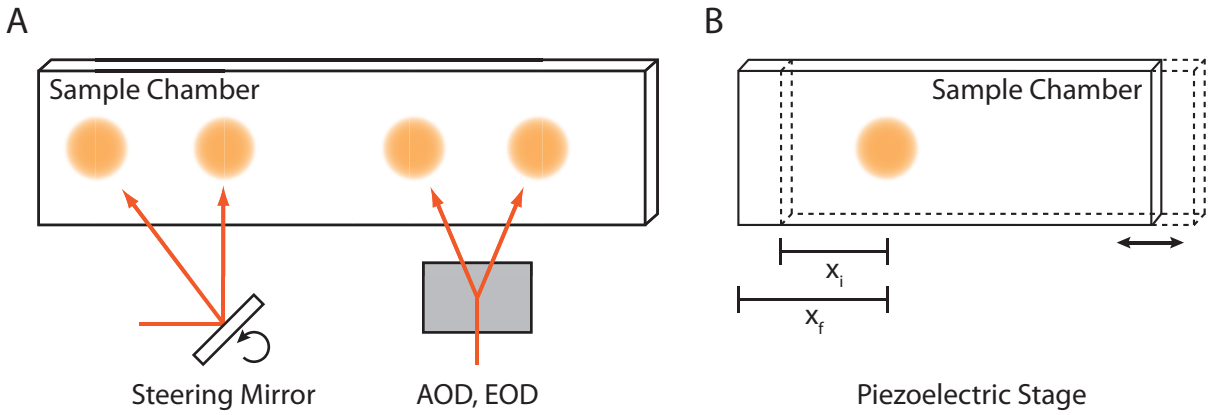

Figure 1.7: Manipulation of optical tweezers. (**A**) Cartoon representation of a direct beam-steering approach. A scanning mirror or an optical deflector guides the trapping light through a sample chamber. (**B**) Moving the sample chamber relative to the fixed trap indirectly controls the trap position. This approach provides a larger trap-manipulating range than a direct beam-steering approach.

The position of the trap in the chamber can also be changed by moving the chamber relative to the trap, (Fig. 1.7(B)), which is generally done by housing the chamber on a piezoelectric stage (PZ). Over the past several decades, PZ technology has been improved dramatically through the development of three-dimensional high-precision controllers and sensitive position sensors. The controllers allow a precise control over the movement in the axial dimension, which eliminates difficulties with focusing the objective lens. The position sensor is used to reduce drift in PZ devices through a feedback loop. To date, an absolute positional uncertainty of 1 nm has been achieved commercially. In this setup, the position of the trap is limited by the working range (~20 mm) of the stage.

Detection

Optical traps are not only used as a tool to manipulate dielectric particles, but also to make quantitative measurements. Since the optical trap acts like a Hookean spring, the force acting on a particle in the trap is directly proportional to its displacement from the focus. Consequently, sensitive detection of the particle position in the trap is necessary both for measuring the displacement and for calculating the force. Several methods for measuring the particle position have been studied, including video-based [60], laser-based [61, 62], and direct imaging detection [63]. One method which stands out and has become the standard in optical spectroscopy is back-focal plane interferometry [64, 65]. This method records the interference pattern produced by interference between (i) the laser light that is scattered from the particle and (ii) the laser light that does not interact with the particle. In the absence of an external force, the particle sits stably in the center of the trap, producing no change in the scattering pattern (Fig. 1.8, left). Force-inducd displacement from the center of the trap in any direction results in a change of the scattering pattern, which is reflected in the interference readout on the detector (Fig. 1.8, middle and right). Analysis of these interference patterns coupled with the calibration of the system allows the position and the subsequent force on the particle to be determined. It is possible to detect particle motion with a resolution as high as 1 Å on a millisecond timescale using this technique.

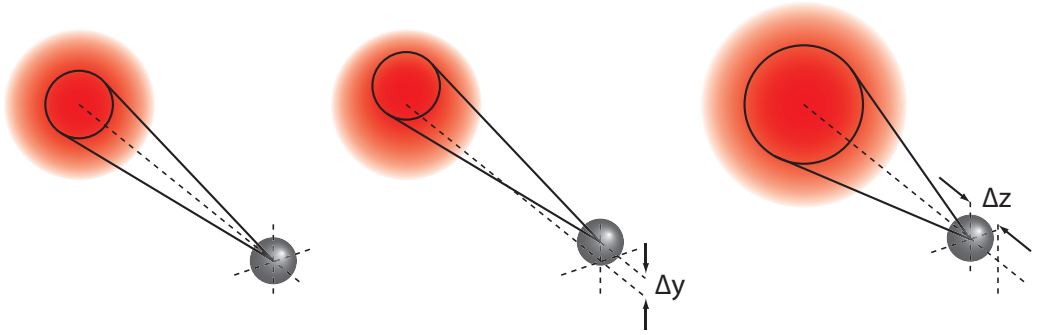

Figure 1.8: Back-focal plane interferometry. Interference patterns collected by the detector vary based on the location of the trapped dielectric particle. Changes in all three dimensions (x,y,z) can be detected.

Optical Tweezers in Biology

Optical tweezers have seen widespread use in molecular and cellular biology. At a molecular level, they have been especially used for measuring forces and displacements generated

by biological molecules. For instance, detailed mechanistic properties of various classes of proteins including cytoskeletal motors [66, 67], translocases [68], polymerases [69, 70], and ATPases [71, 72], have been studied. Mechanical properties of nucleic acids such as DNA and RNA have also been investigated [73, 74].

Optical tweezers have also been used to study living cells. Initially, they were employed as a positioning tool to hold single cells in place [46]. Later on, optical tweezers were used to transport [75], organize [76], and sort cells [77]. Not until recently were optical tweezers used for quantitative measurements. Mechanical characterization processes carried out by single cells including formation of membrane tethers [78, 79], deformation of red blood cells [80], and cell adhesion [81] have been investigated. Recent advances in optical tweezers and fluorescence microscopy enabled quantitative investigation of whole bacterial cells, in particular *E. coli* chemotaxis and its relationship to flagellar activity [82].

1.3.2 High-resolution Optical Tweezers

Recent advances in optical tweezers have enabled the application of optical trapping to biology, especially at the cellular level. Many fundamental processes inside the cell, including DNA metabolism, protein folding, and cellular transport, occur through motion between discrete states. Direct observation of these discrete steps requires high spatial sensitivity in the nanometer or sub-nanometer scale. Traditional optical tweezers, unfortunately, are unable to resolve these steps of a few nanometers with the necessary time resolution (as short as tens of milliseconds) due to external noise coupled to the instrument [83]. Noise can be classified as Brownian noise or experimental noise. The experimental noise can stem from fluctuations of the environment or components of the instrument such as a stage, a chamber or an optics table. Brownian noise, in contrast, stems from the fundamental thermal forces that generate fluctuation of the particle within the trap.

Improvements over Traditional Optical Tweezers

Improvements in the instrumentation have been made to reduce experimental noise at great effort. Sound isolation and temperature control of the setup room are used to overcome the acoustical and thermal noise, respectively. Vibrational noise is reduced by housing the instrument on a pressurized optical table in the basement. The sample chamber is

completely isolated from the instrument by using a dual-trap setup, eliminating the need for a micropipette or glass surface for tether formation and thereby getting rid of a source of drift.

Brownian noise, on the other hand, cannot be eliminated easily. Reducing this noise by decreasing the temperature is not feasible since most biological systems usually require room temperature to function. Recently, Chemla et al, has overcome this problem by developing dual, high-resolution optical tweezers [58]. Unlike the traditional setup with two traps, where fluctuations of the two traps are independent (anti-symmetric, out of phase) of each other (Fig. 1.9(A)), dual optical traps are generated by the same laser source. Any fluctuation of this laser will affect the trap identically (symmetric, in phase) (Fig. 1.9(B)). By measuring the difference of the positions of the traps, as opposed to the absolute position of the traps, the Brownian noise level is reduced, and the signal-to-noise ratio improves.

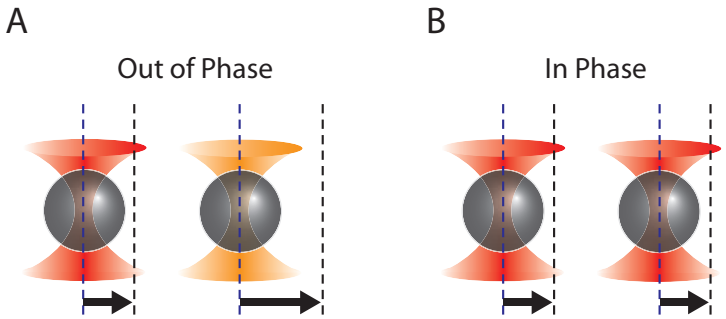

Figure 1.9: Fluctuation of the optical traps. (**A**) Two independent trapping lasers create anti-symmetric noise upon fluctuation. The relative positions of these traps change. (**B**) Optical traps generated by the same laser source experience symmetric shifts from fluctuations, resulting in no (or low) net position drift.

High-resolution Optical Tweezers in Biology

Providing exceptional benefits in sensitivity over traditional traps, high-resolution optical tweezers have led to many interesting findings in molecular machinery. For example, Qi et al. and Cheng et al. independently observed a DNA helicase unwinding DNA duplex one base pair at a time [84, 85]. Abbondanzieri et al. utilized Å-resolution dual traps to monitor RNA transcription, and revealed that RNA polymerase translocates along DNA in single base-pair steps, adding one nucleotide at a time to the nascent DNA [83]. Other APTase studies, including a study of DNA packaging mechanisms in bacteriophage ϕ29 [71] and studies of mechanical properties of ClpXP protease unfolding polypeptide [86] have also

been carried out.

Dual-trap Layout

The instrument (Fig. 1.10) involves a single, near infra-red laser that is used to form two optical traps. A single beam is generated at the laser source (DL - a 5-W, 1064-nm diode-pumped solid state laser), and directed through a polarized beam splitter (BS1) to separate into two orthogonally polarized beams. One of the beams can be controlled by a steering mirror mounted on a piezo-actuated stage (SM), while the other beam is fixed; this allows relative movement of the traps. The two beams are recombined (BS2) and guided toward the objectives. The front objective (FO) is used to focus the beams and form the traps. A second objective (BO) is used to collect and collimate the light from the sample chamber. Beams are split again at another beam splitter (BS3) and projected onto position detectors (QPD1 and QPD2). Half-wave plates (HWP) are used to control the light intensity, and thus the stiffness of two traps. In addition, a visible white light (LED) is used to illuminate the sample plane to facilitate trap visualization.

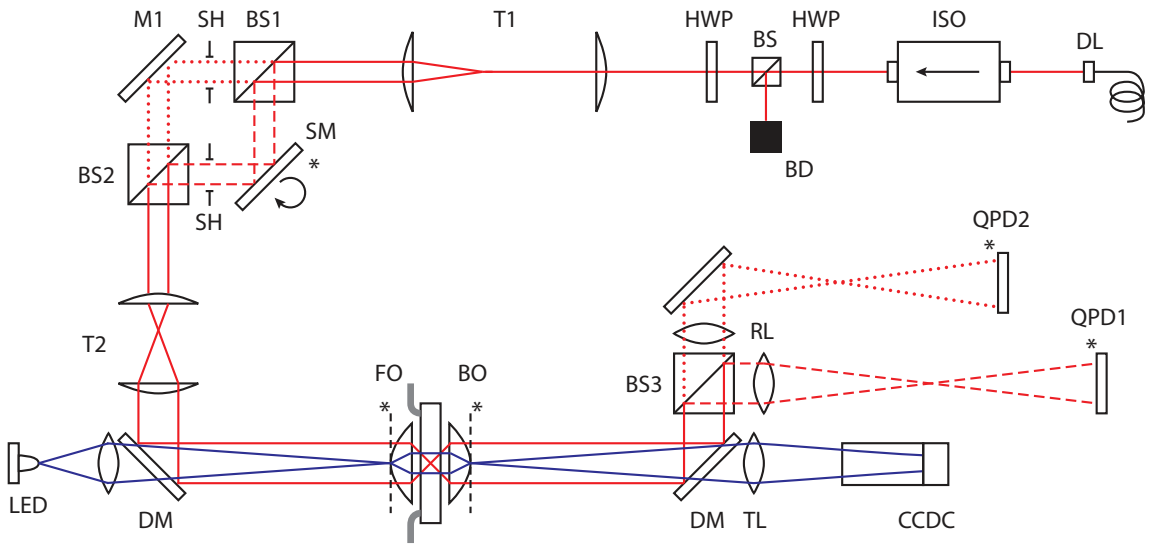

Figure 1.10: Dual-trap layout. A schematic of the high-resolution optical tweezers components. Light paths are indicated by red (1064-nm) and blue (white light from LED). Dashed and dotted red lines illustrate two orthogonal polarized beams. Components are labeled; DL - 1064-nm Laser source, ISO - Optical Isolator, HWP - Half-wave Plate, BS - Polarized Beam Splitter, BD - Beam Dump, T - Telescope, M - Mirror, SM - Steering Mirror, SH - Shutter, DM - Dichroic Mirror, FO - Front Objective, BO - Back Objective, TL - Tube Lens, RL - Relay Lens, CCDC - Camera, QPD - Quadrant Photodiode Detector.

1.3.3 Fleezers

As stated previously, both optical tweezers and fluorescence microscopy suffer from certain limitations. Optical tweezers provide high spatial resolution over long working distances, but cannot reveal the system's internal state (i.e. number of interacting proteins). Single-molecule fluorescence, in contrast, is capable of giving insight into conformational states, but has a much more limited spatial range. To overcome these difficulties, Comstock et al. developed a new instrument, named the *Fleezers* (*Fl*uorescence + T*weezers*) by combining high-resolution optical tweezers with a confocal fluorescence microscope [43]. The instrument has been demonstrated to have the ability to detect individual fluorophores and resolve sub-nanometer motion of several biological systems [43].

Photobleaching of fluorophores has proven to be a challenge in single-molecule fluorescence experiments. The near-infrared laser used to form optical traps also enhances photobleaching effect when it is focused on the fluorescent dye [87]. To minimize this effect, the Fleezers utilize an interlacing technique whereby the optical traps and confocal microscope are turned on and off sequentially [88]. Figure 1.11 illustrates the interlacing and time-sharing mechanism utilized by the Fleezers. To maintain sufficient trap stiffness and keep the beads trapped while interlacing, the traps must be turned on and off at rapid rates ($>$ 10 kHz) [88]. This is achievable by using an electronic device called the acousto-optic modulator (AOM) to manipulate the traps and the microscope at extremely fast speeds ($>$ 100 kHz). In this setup, two AOMs - one for the trapping laser, the other for the excitation laser - are used. The trap AOM controls the on-off state of the two optical traps by deflecting the laser away from the trap. The fluorescence AOM allows the excitation laser to illuminate the sample while the trapping laser is off.

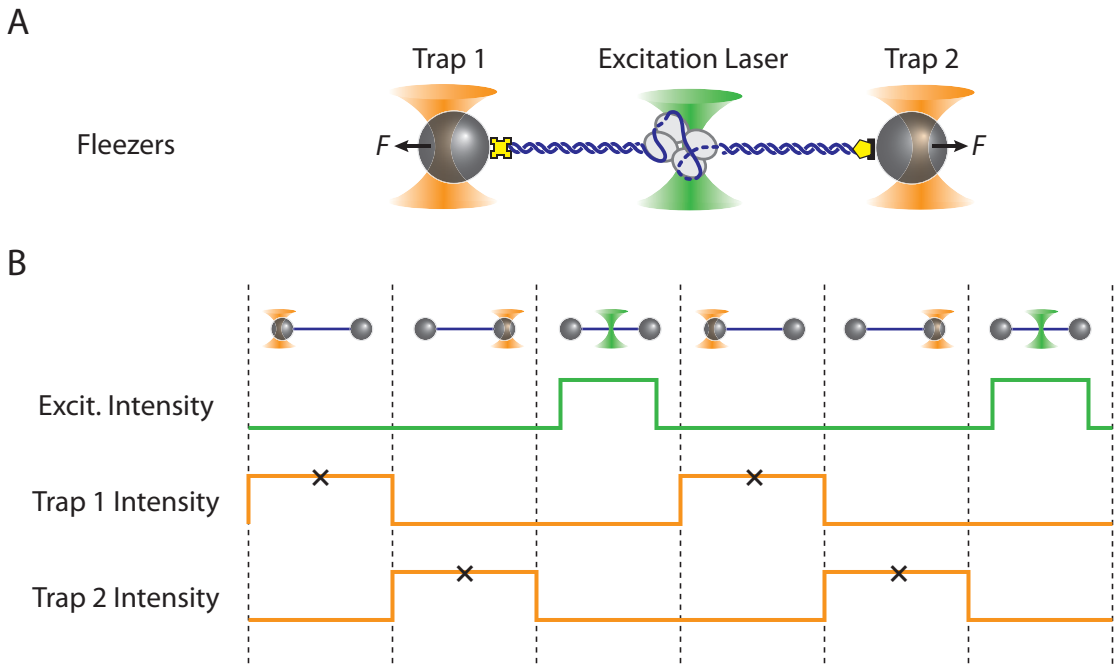

Figure 1.11: Interlacing and time-sharing of the Fleezers. (**A**) Schematic of the Fleezers setup showing optical tweezers (orange) trapping two beads with a nucleoprotein complex tethered between them. An excitation laser, located approximately at the center of two traps, is turned on while the traps are off and vice versa. (**B**) Two optical traps are created in sequence (orange), while the excitation laser is interlacing between them (green). The interlacing operates at a rate of 66 kHz, which is fast enough to hold two beads stably without having Brownian noise. Trap data aquisition occurs at time points indicated by '×', while the fluorescence is collected during the whole period of excitation.

1.4 Summary

Our goal was to investigate the interactions between *E. coli* SSB, single-stranded DNA, and other interacting proteins involved in DNA metabolic processes. Achieving these goals required developing new experimental assays, employing new tools, and improving current data analysis. The level of complexity in these biological systems will be presented in chronological order, ranging from studies of a single SSB, to multiple SSBs, to multiple proteins. Necessary background and introduction will be given at the beginning of each chapter. In chapter 2, we introduce standard procedures for optical trapping experiment, and describe the use of DNA substrate to study a single SSB binding. We also explore the effect of tension on the conformation of individual SSB-DNA complexes and their dissociation. Chapter 3 examines wrapping behavior of individual SSBs, and characterizes their intermediate conformational

states under tension. We utilize the SSB structural data, and develop a mathematical model to map SSB wrapping intermediates to binding configurations (binding modes) of the SSB in chapter 4. In chapter 5, we discuss dynamical behavior of the SSB, and investigate its diffusion mechanism under different binding modes. We extend our research from studying a single SSB to investigating multiple SSBs in chapter 6. Detailed oligomerization of SSB-DNA complexes under different binding configurations is described. Chapter 7 describes the addtion of recombinant protein, RecA, to the SSB-DNA complex. Competition between SSB and RecA for ssDNA is scrutinized and explained. We also discuss the influence of SSB binding configurations on ssDNA accessibility of other proteins.

Chapter 2

Observation of SSB Binding

In the previous chapter, we introduced the *E. coli* single-stranded binding (SSB) protein and its importance to DNA metabolism. We also described how optical tweezers work, and pointed out their advantages over other experimental techniques. In this chapter, we described the use of optical traps to investigate the interaction between SSB and ssDNA. The chapter begins by describing the procedures involved in conducting a trap experiment. Understanding of these procedures is essential for the comprehension of experiments in this and subsequent chapters. Next, we described studies of a single SSB binding to and unbinding from a ssDNA template. By applying a range of tensions to the SSB-ssDNA complex, we observed conformational changes of the nucleoprotein, and could consequently determine the tensions in which the complex was partially disrupted, and tensions where the complex was completely dissociated. In addition, we measured an estimated binding energy of each individual SSB on ssDNA in the same experiment. The results are as follow;

Unwrapping ssDNA from a single SSB requires 103 ± 8 pN·nm (25 ± 2 kT) of mechanical work. The ssDNA remains fully wrapped around SSB at tension < 1 pN. Beyond this force, ssDNA, on average, gradually unwraps from SSB, causing a conformational change of the complex. Once the force reaches ~10 pN, SSB dissociates from the ssDNA. However, when the unwrapping data for each SSB was analyzed separately, we observed detailed features that diverged from the average behavior. These features suggested that SSB might have several different unwrapping pathways, and might undergo transitions between hidden unwrapping states.

2.1 Introduction

As described in Chapter 1, *E. coli* SSB, under physiological conditions, is known to bind with highest affinity to ssDNA [2]. In order to understand the mechanism behind the SSB-ssDNA

interaction, the stability of the complex must be disrupted. Past studies have suggested that very high salt concentrations (NaBr > 0.8 M) can be used to lower this stability [39]. Doing so, however, will force the complex out of the biologically relevant conditions. To overcome this problem, we instead applied a mechanical force to destabilize the SSB-ssDNA complex using dual optical tweezers. This instrument allowed us to probe conformational changes of the nucleoprotein complex as well as complex dissociation.

2.2 Experimental Procedure

Successful optical trapping assays generally rely on three elements: stable optical tweezers, a well-prepared DNA construct, and a clean sample chamber. Due to recent advances in instrumentation, well-built optical tweezers attain high sensitivity in the Å-level and millisecond time scale. Once the instrument is built and calibrated, it can remain stable for several years. DNA constructs and sample chambers, in contrast, lose quality over much a shorter time period, and thus require a frequent preparation to obtain the best quality. Good quality of the DNA construct leads to a higher tether formation rate which in turn improves the trapping efficiency dramatically. It also reduces the DNA noise that can interfere with the actual dynamics of system interested. A well-made chamber results in more stable flow of the buffer streams, and reduces chances of buffer mixing.

Below, we describe our standard preparation and experimental techniques, including DNA construct preparation, chamber construction and DNA tether selection that are necessary for all experiments in this and subsequent chapters.

2.2.1 DNA Construct

The construct consists of three separate segments joined by DNA ligation (Fig. 2.1, Appendix A). The left handle (LH) and the right handle (RH) are double-stranded DNA (dsDNA) molecules of length 1,550 and 1,710 base pairs, respectively. They serve as functionalized linkers that connect the DNA construct to trapped beads, and distance the protein binding site from the trapping laser. The SSB binding site (BS) is a relatively short piece of single-stranded DNA. In this particular experiment, a 70-nt poly-dT ssDNA (dT70, Appendix A) is chosen to allow the wrapping of one SSB tetramer in the $(SSB)_{65}$ binding mode.

Figure 2.1: Standard single-stranded DNA construct. A DNA construct consists of two long dsDNA handles of length 1,550 and 1,710 bp (blue and green) and a short 70-nt ssDNA sequence (red). One end of the handles is covalently linked to a biotin (BIO), while the other end is functionalized with digoxygenin (DIG). These functional groups serve as a link, allowing attachment to particles coated with strepavidin and anti-digoxygenin.

2.2.2 Protein & Trapping Solution

Both wild-type and fluorescently labeled *E. coli* SSB (SSB and SSB_f) were expressed and purified as described [4, 89] with additional purification through a double-stranded DNA cellulose column to remove a minor exonuclease contaminant [90]. The labeled SSB was single-point mutated from Ala to Cys at position 122 (located in a C-terminus), and labeled with AlexaFluor555 maleimide with an efficiency of ~25 % (~1 dye per tetramer) [4].

In a typical experiment, two sets of trapping solution are prepared; one with and one without SSB. In the protein-free solution, a high concentration of monovalent salt (Na^+ and $Tris^+$) was used to favor SSB wrapping in the $(SSB)_{65}$ binding mode (Appendix A). The same buffer conditions were also used in the solution with SSB. To induce specifically the $(SSB)_{65}$ mode of SSB wrapping, a low concentration (0.5 nM) of SSB was used in this buffer. For experiments conducted with the Fleezer where fluorescence detection was needed, we substituted SSB_f for wild-type SSB, and modified the trapping solution slightly by adding an oxygen triplet-state quencher to the solution to prevent fluorophore blinking [91].

2.2.3 Microfluidic Chamber

To compare the behavior of the same DNA molecule in the presence and absence of SSB, we developed an experimental assay using a custom-built laminar flow chamber consisting of four channels that allows rapid exchange of buffers around the optical traps (Fig. 2.2, Appendix A, [92]). The chamber contains a central channel into which two separate buffer streams merge. One stream contains blank buffer only, while the other contains buffer plus SSB. Due to the laminar flow inside the channel, a stationary interface between the two streams is created with minimal mixing. The top and bottom channel are connected to the central channel through small glass capillaries. These capillaries are used to deliver anti-

digoxigenin beads and streptavidin beads plus DNA constructs to the central channel. To maintain the laminar flow, streams of buffer are injected continuously at a rate of 140 μm/s (100 μl/h) through syringe pumps.

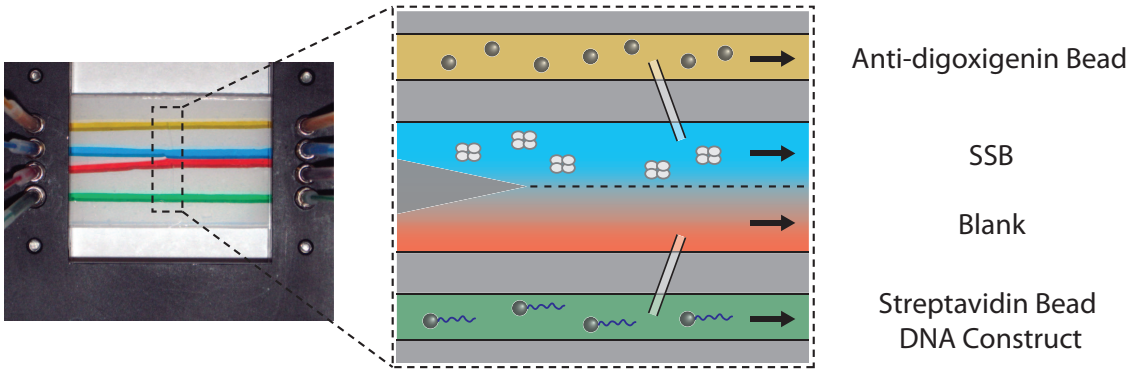

Figure 2.2: Microfluidic chamber. An experimental chamber consists of four separate channels. The top and bottom channels contain buffer with anti-digoxigenin and DNA-bound streptavidin coated beads, respectively. Two separate streams containing protein-free (red) and SSB buffer (blue) merge to form a single channel with laminar flow, allowing rapid exchange of buffer conditions during experiment. For the purpose of illustrating the separation of solutions during operation, food dye with different colors was pumped into the flow chamber.

2.2.4 Chamber Setup

Prior to the experiment, it was very important to correctly load the chamber. First, syringes equipped with 0.22-μm filters were used to fill the chamber with water and manually pulse water through to dislodge all air bubbles in the channels and tubing. Small bubbles near the capillaries are hard to remove. Flushing the chamber out with air and refilling the chamber with water usually fixed the problem.

Next, we carefully loaded beads and working buffer to the chamber with glass syringes mounted on syringe pumps. For consistency, the top channel was injected with anti-digoxigenin beads, while the bottom channel contained DNA-bound streptavidin beads.

2.2.5 Trapping Beads & Bead Calibration

To trap beads, a small flow (400 μl/h) was introduced to the top channel to push anti-digoxigenin beads through a glass capillary (Fig. 2.3). One trap was turned on, and moved to a location near the top capillary to trap a single anti-digoxigenin bead (Position 1). Once the bead was trapped, the chamber was moved to the other capillary from the bottom channel,

and the second trap was turned on (Position 2). Solution with DNA-coated streptavidin beads was injected at the same low rate in the bottom channel to deliver the beads. When a DNA-coated bead was captured in the second trap, the chamber was moved upstream to a location far away from the capillaries to avoid additional beads falling into the traps (Position 3).

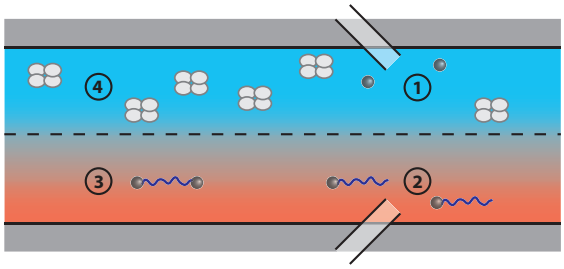

Figure 2.3: Beads trapping procedure. Two types of bead were delivered from the top and bottom channels through the capillaries. An anti-digoxigenin bead was trapped at position 1, and a DNA-coated streptavidin bead was then trapped at position 2. The beads were moved upstream to the position 3 for calibration.

The trap calibration was done by measuring the positions of the beads as they underwent Brownian fluctuations due to the thermal forces from the surrounding solvent. We saved the calibration data at a very high rate (62.5 kHz), and analyzed them to obtain a power spectrum of the fluctuations. Fitting the power spectrum allowed us to determine the trap stiffness.

2.2.6 DNA Tether Formation

Once the beads were trapped, it was necessary to bring them close enough to each other such that a DNA molecule attached to the streptavidin bead can attach with its other end to the other anti-digoxigenin bead, forming a tether. Tether formation was done by oscillating one bead in-and-out relative to the other bead (Fig. 2.4). Typically, the DNA-coated streptavidin bead was positioned upstream in a stationary trap, while the anti-digoxigenin located downstream in a steerable trap. When the flow was turned on, DNA molecules on the bead were pushed along the stream of buffer, effectively creating handles for the other bead to attach to. The formation of a tether resulted in a detectable force when the beads were next pulled away from each other; the oscillation was stopped as soon as the tether was detected. During this process, it was important to find the optimal distance between

the beads at closest approach for tether formation: bringing the bead too close to each other would result in the formation of multiple tethers, and not bringing them close enough would result in a lack of any tether formation. The process therefore involved iteratively changing the oscillation amplitudes (dashed lines) until the optimal distance for single tether formation could be found.

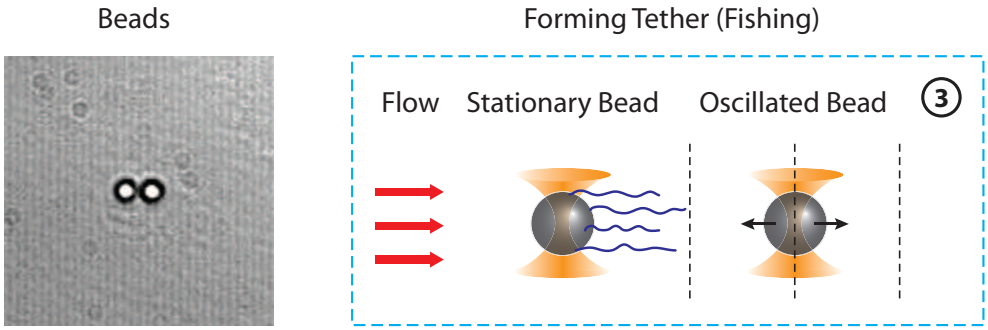

Figure 2.4: Tether formation. A DNA-coated streptavidin bead is positioned upstream to allow the flow to drive DNA molecules away from the bead. An anti-digoxigenin bead is placed downstream and oscillated until the tether is formed.

2.2.7 DNA Tether Qualification

Before any experiment involving SSB was conducted, the quality of the DNA tether was tested by determining whether its behavior agreed with predictions of established theoretical models of DNA elasticity. To achieve this, an external force was applied to stretch the molecule, and total extension was measured as a function of force. Next, the resulting force-extension curve (FEC) of each DNA molecule was analyzed and compared against theoretical models.

The extension of a bare DNA molecule, x_{bare}, involves a contribution from the dsDNA handles and from the ssDNA binding site:

$$x_{bare} = \xi_{ss}(F) \cdot N_{ss} + \xi_{ds}(F) \cdot N_{ds} \tag{2.1}$$

where $\xi_{ds}(F)$ and $\xi_{ss}(F)$ are the extension of one dsDNA base pair and one ssDNA nucleotide at a tension F, respectively, and $N_{ds} = 3{,}260$ bp is the total length of the dsDNA handles, while $N_{ss} = 70$ nt is that of the ssDNA loading site. We used the extensible worm-like chain model [93] for the dsDNA handles and found that the ssDNA component was best fit to a snake-like chain elasticity model [94]. Force-extension curves (FEC) of many DNA molecules

(Fig. 2.5, green) are in excellent agreement with the model (black).

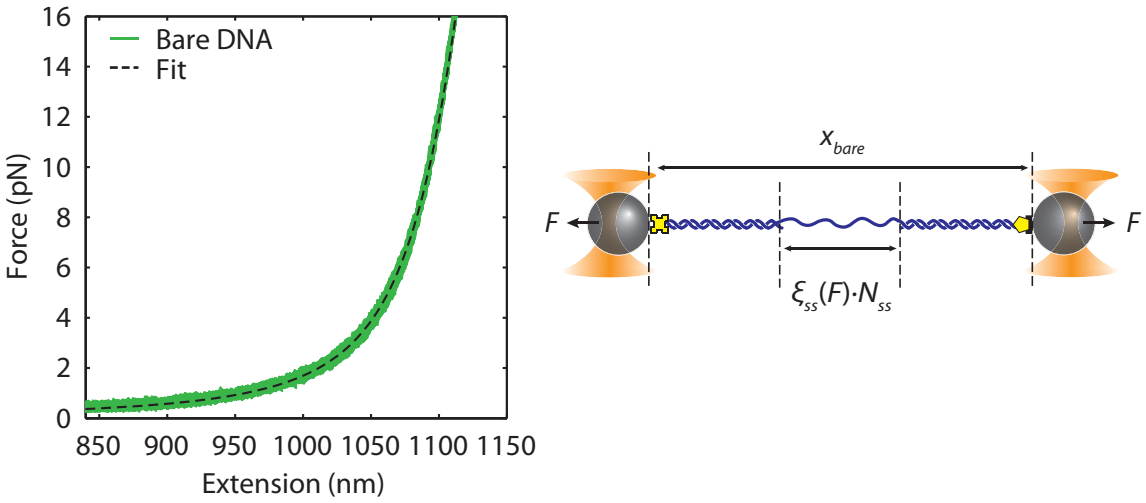

Figure 2.5: Bare single-stranded DNA polymer modeling. Representative force-extension curves (FEC) measured while stretching and relaxing a bare DNA construct containing 3,260-bp long dsDNA handles and 70 nt of ssDNA (green). The total extension of the tether, x_{bare}, is modeled by the sum of dsDNA and ssDNA extensions ($\xi_{ds}(F)\cdot N_{ds}$ and $\xi_{ss}(F)\cdot N_{ss}$, respectively). The dsDNA segment is modeled using the extensible worm-liked chain [74], while the ssDNA segment is fit with the extensible snake-like chain [94]. A black dashed line is the fit to the construct.

2.3 Gradual Unwrapping of SSB under Tension

To observe the nucleoprotein complex, the qualified tether was moved into the buffer stream containing SSB (Fig. 2.3, Position 4) for a short period of incubation, allowing a single SSB to bind the 70-nt ssDNA, and moved out of the SSB stream back to the blank stream (Position 3). This procedure allowed us to exert force on the nucleoprotein complex in the absence of proteins in solution that may interfere. The applied force of 0-25 pN was ramped from 0-25 pN to stretch the DNA molecule, and then ramped back down to 0 pN.

FECs of stretching and relaxing many molecules are shown in Figure 2.6. During stretching (blue), the increasing force disrupted the interactions between ssDNA and the single SSB loaded on it. After stretching the molecule to a force > 20 pN and allowing it to relax, FECs of the relaxation (red) were clearly distinguishable from the FECs of the stretching. The relaxing FECs matched those measured in the absence of protein (Fig. 2.6, right: green), indicating that the SSB had dissociated during the stretching of the DNA (Fig. 2.6, left: schematic).

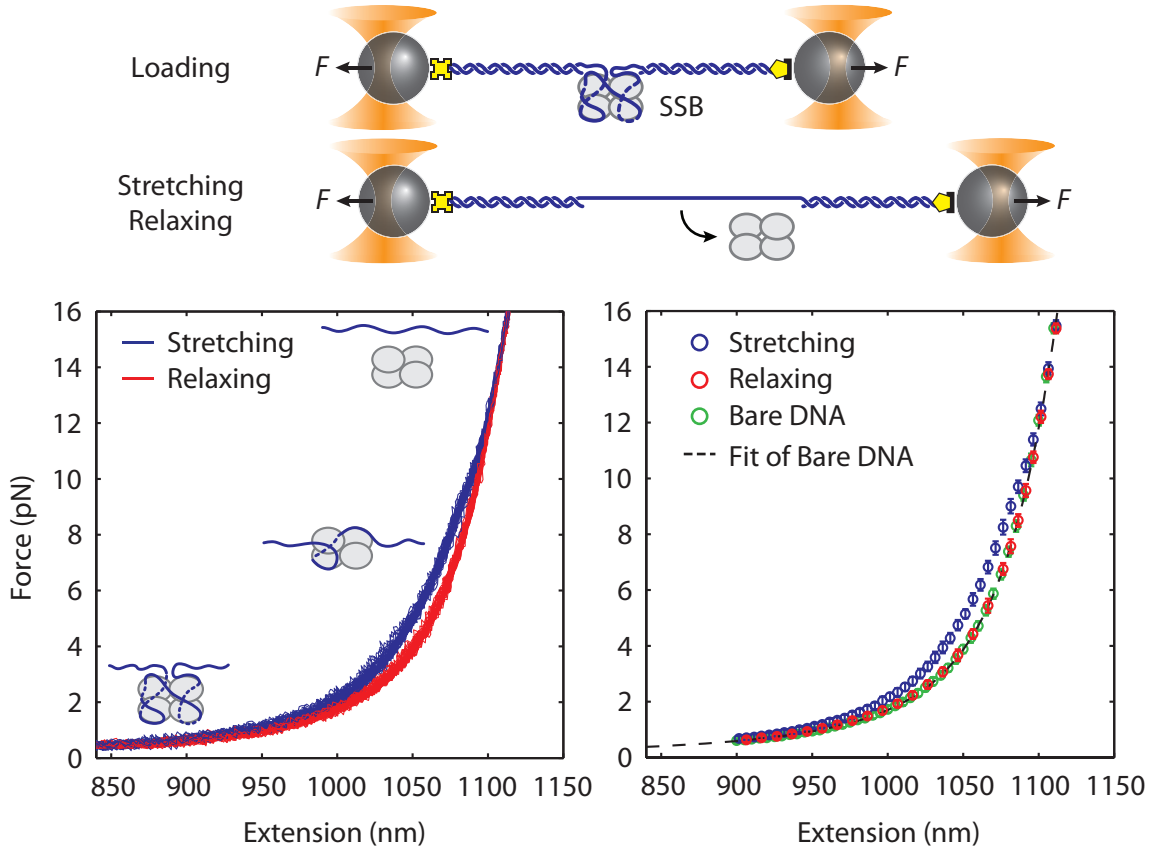

Figure 2.6: Dissociation of SSB upon stretching DNA molecule. Representative force-extension curves (FEC) of stretching (blue) and relaxing (red) DNA molecule are distinct, indicating that the nucleoprotein complex undergoes a conformational change. Averaged relaxing (red circle) FECs and bare DNA (green circle) FECs are fit to the same polymer elasticity model in Figure 2.5. The resulting fits are consistent with each other, demonstrating that SSB has dissociated during stretching.

The offset in extension between stretching and relaxing FECs represents the ssDNA condensed by SSB wrapping. This extension change provides information on the SSB-ssDNA wrapping state as a function of force. We compared both curves to theoretical predictions based on models of DNA elasticity (Appendix B). First, the relaxing FECs were compared with the bare DNA previously described in Eq. (2.1)

$$x_{bare} = \xi_{ss}(F) \cdot N_{ss} + \xi_{ds}(F) \cdot N_{ds}$$

The model agreed well with the relaxing FECs (Fig. 2.7, black dotted line).

For SSB-bound DNA, we hypothesized that SSB wrapped $N_w = 65$ nt of ssDNA according

to the canonical $(SSB)_{65}$ structure during the entirety of the stretching curve;

$$x_{bound} = \xi_{ss}(F) \cdot (N_{ss} - N_w) + \xi_{ds}(F) \cdot N_{ds} \tag{2.2}$$

Interestingly, the stretching FECs (blue) diverged significantly from the predictions of this theoretical model (Fig. 2.7, black dashed line), indicating that the SSB did not fully wrap 65 nt throughout the stretching cycles.

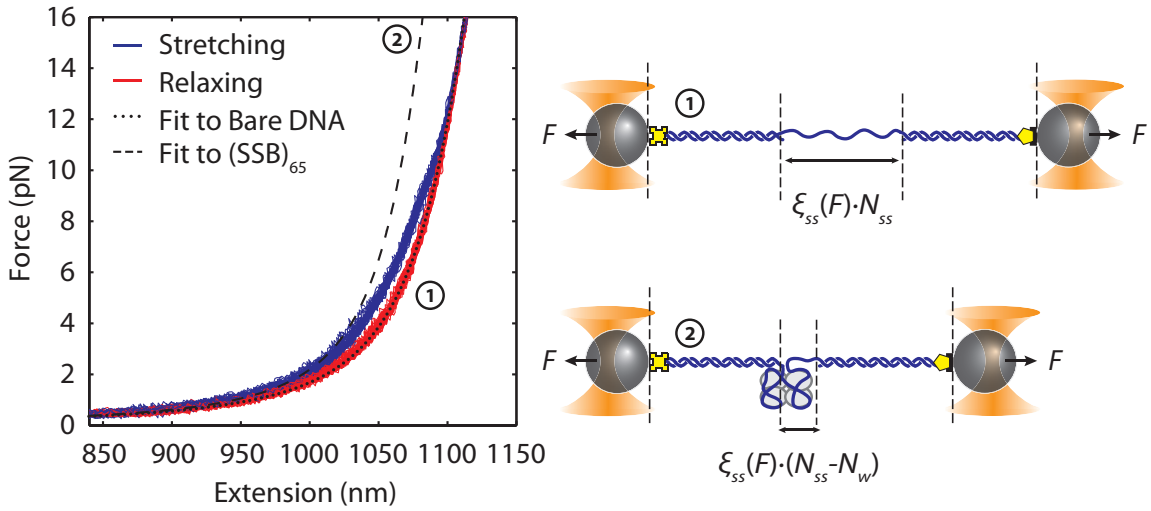

Figure 2.7: Unwrapping of SSB under force. Relaxing curves (red) are obtained after SSB dissociation, and are well fit with a polymer model of bare DNA (black dotted line). Stretching curves (blue) of the SSB-ssDNA complex deviate from the model which assumes that the protein adopts the $(SSB)_{65}$ wrapping mode at all forces (black dashed line).

We calculated the difference in extension, Δx, between the stretching and corresponding relaxing curves, averaged over many molecules (Fig. 2.8, black circles), and compared with the predictions of $x_{bare} - x_{bound}$ of the theoretical model (black dashed line). The agreement between model and data at tensions < 1 pN was consistent with ssDNA remaining fully wrapped around SSB at low forces. Beyond this force, Δx was consistently less than the prediction, indicating that the SSB wrapped less than 65 nt of ssDNA. The ssDNA unwrapped gradually for forces > 1 pN, in agreement with the earlier observations based on single-molecule FRET combined with optical tweezers [41].

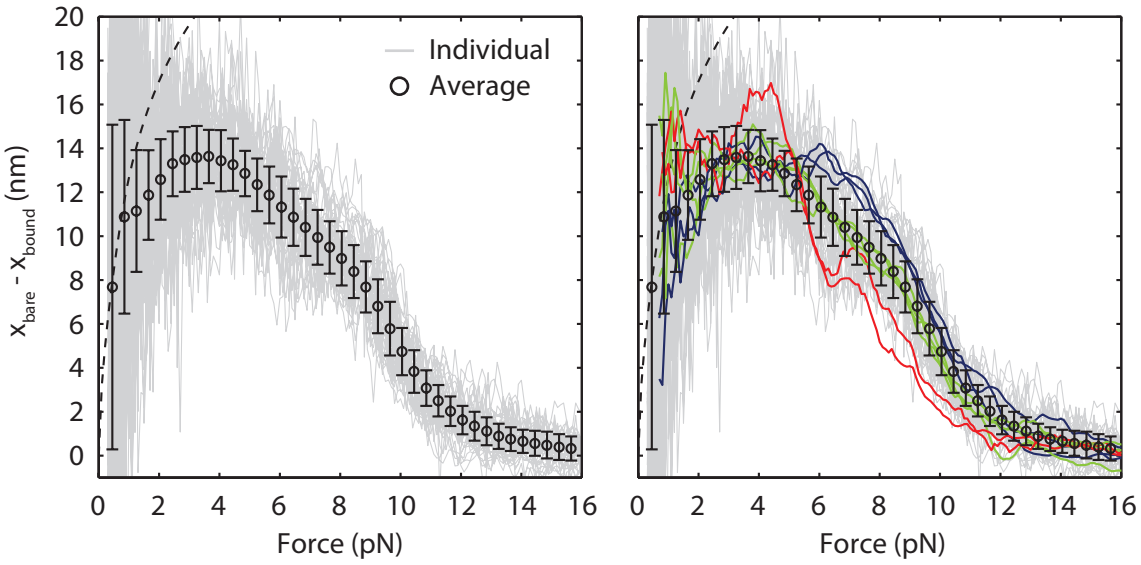

Figure 2.8: Change in extension upon SSB wrapping vs. applied force. Individual traces (gray) are binned and averaged to yield a mean change in extension (black circle). The data deviates from the model (dashed line, determined from the difference between the dashed and dotted lines in Fig. 2.7) at forces > 1 pN. Representative traces (red, green, and blue) display discrepancy between the individual and averaged traces.

Interestingly, neither the data in Figure 2.8 (black circles) nor in the previous studies [41] provide evidence for the discrete wrapping morphologies such as $(SSB)_{56}$ and $(SSB)_{35}$ which have been observed in ensemble assays. If different SSB modes are stable and interconvertable, discrete transitions in the extension would have been expected in the stretching-relaxing experiment. However, detecting intermediates would depend on the rate at which the force was ramped. Moreover, averaging over multiple molecules would likely conceal transitions between SSB-ssDNA wrapping intermediates. Example individual traces (Fig. 2.8, blue, red, and green curves) support this view by illustrating the variability between different FECs and their divergence from the average behavior (black circles). These traces suggest that SSB may take different unwrapping pathways and may undergo fast transitions between different wrapping states.

2.4 Dissociation Force & Wrapping Energy of SSB

2.4.1 SSB Dissociation Force

In addition to providing insight into the SSB unwrapping, FECs can be used to calculate the force required to dissociate the SSB from ssDNA, F_d. By observing the tension at which stretching and relaxing FECs merged (Fig. 2.6), we estimated an average dissociation force of 10.3 ± 0.9 pN, consistent with previous reports [41]. To ensure that the SSB indeed dissociated at the F_d, we verified this result with measurements of fluorescently labeled SSB, SSB_f. Using the Fleezers to conduct a force-ramp experiment (Fig. 2.9, right), we were able to observe stretching and relaxing time traces simultaneously with fluorescence from SSB_f.

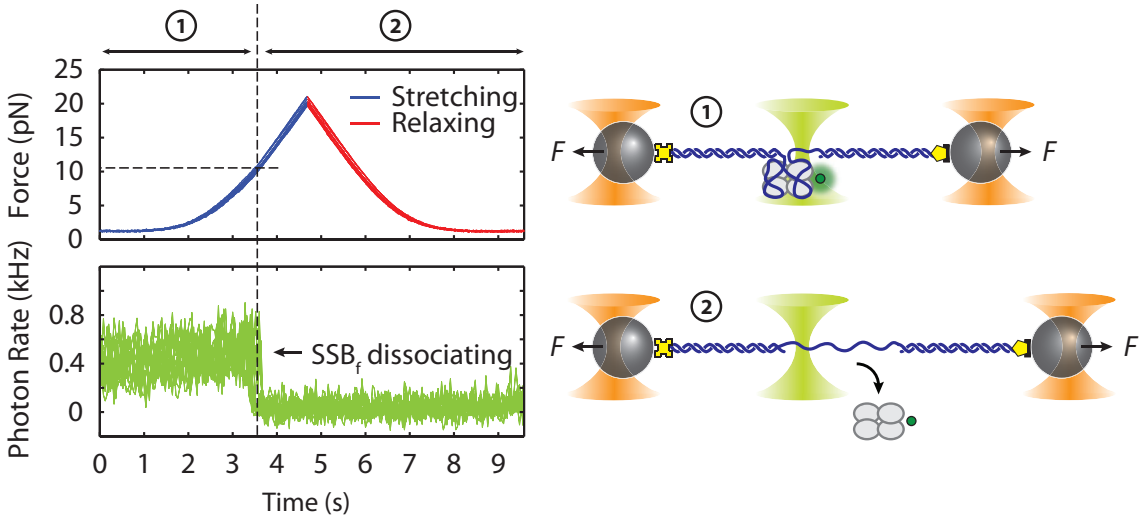

Figure 2.9: Dissociation force of SSB. A DNA construct bound by fluorescently labeled SSB, SSB_f, is stretched (blue) and relaxed (red) by mechanical force. Upon reaching > 10 pN force, SSB_f dissociates from the DNA as indicated by the decrease in fluorescence

Initially at low tension (~0 pN), SSB_f bound to a DNA construct. Fluorescence readout at $t = 0$ confirmed the presence of the SSB_f (Fig. 2.9, left). Slowly increasing tension to ~9 pN unwrapped ssDNA, but did not remove the SSB_f. As tension was raised to the dissociation force (~10 pN), the loss of fluorescence was observed (dashed line), indicating that SSB_f dissociated from the DNA molecule.

2.4.2 SSB Wrapping Energy

We estimated the energy of SSB wrapping to ssDNA by comparing the mechanical work required to stretch bare DNA to that of SSB-bound DNA. Upon stretching bare DNA molecule, work was done upon the molecule, transferring energy to it. The area under the FECs of the bare DNA (Fig. 2.10, pink) was calculated to obtain G_{DNA}, the average energy transferred. In comparison, stretching an SSB-bound DNA requires more work. The area under the FECs of the bound DNA (cyan) consists of energy stored in the DNA and energy used in disrupting the SSB-DNA interaction, G_{bound}. Since the energy stored in the DNA in both cases is approximately the same, the estimated wrapping energy of a single SSB wrapping 65 nt ssDNA is simply the difference between these two (orange), $G_{SSB} = G_{bound} - G_{DNA} = 103 \pm 8$ pN·nm (25 ± 2 kT). Our result are consistent with the previous studies showing that the SSB wrapping energy consists of the ssDNA unraveling energy and the dissociation energy of the SSB [41].

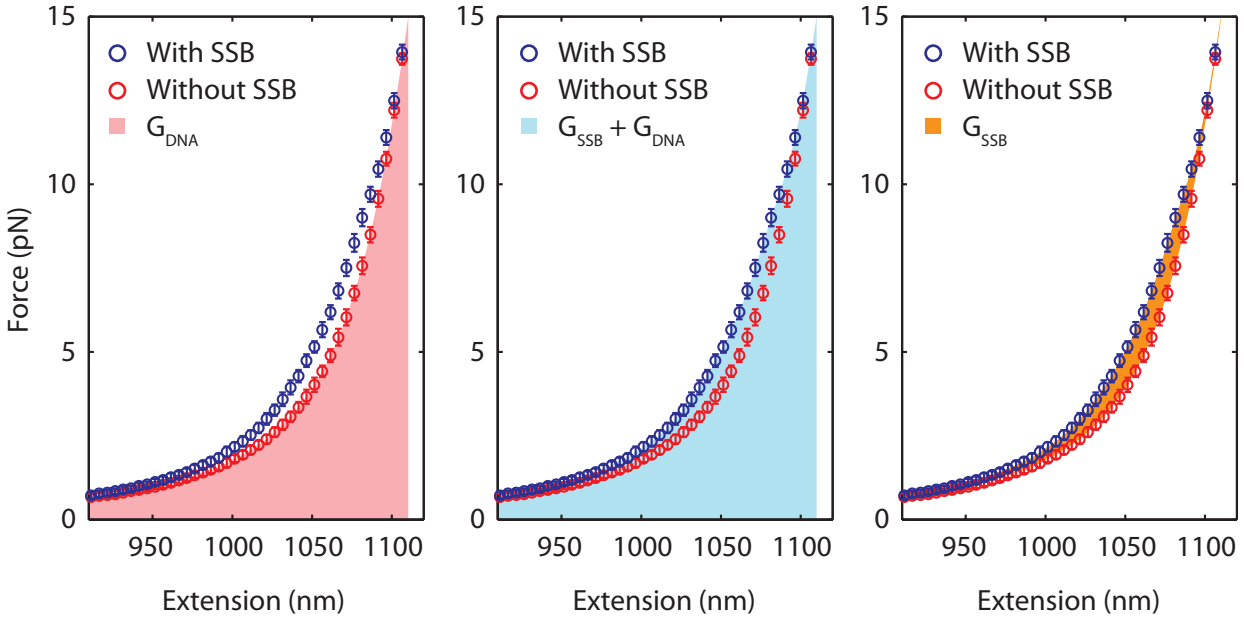

Figure 2.10: Binding energy of SSB. Areas under averaged force-extension curves of stretching SSB-bound DNA (cyan) and bare DNA (pink) are used to estimate the SSB binding energy. Stretching an the SSB-bound DNA requires more work than that of the bare DNA. The difference of these works represents the binding energy of the SSB (orange).

Chapter 3

Intermediate Wrapping States of SSB

In the previous chapter, we used optical tweezers to detect the presence of an individual SSB on a DNA construct and apply mechanical forces to study a conformational change of the nucleoprotein, a dissociation force of the nucleoprotein complex, as well as an estimated binding energy of each individual SSB. We also discovered that precise measurements describing individual SSB behaviors were likely concealed by averaging data during the analysis. This results in a loss of important information of intermediate wrapping states of SSB. To bypass the problem, this chapter develops a new experimental assay where individual SSBs binding to ssDNA were observed under a constant tension. The technique provides us with the ability to measure the behavior of nucleoprotein complexes at desired tensions precisely and for a very long period of time.

We discovered that an individual SSB wraps ssDNA in discrete steps. Many intermediate wrapping states were observed across all ranges of tension. Fleezers experiments with fluorescently labeled SSB confirmed that a single protein was responsible for the observed intermediate wrapping-unwrapping dynamics, and not multiple SSBs wrapping the same DNA construct.

3.1 Introduction

E. coli SSB is a functional homotetramer protein. Each monomer contains an OB fold that binds ssDNA. This results in a variety of binding configurations (binding modes) that differ in the number of OB folds interacting with the DNA. Three different binding modes, $(SSB)_{65}$, $(SSB)_{56}$ and $(SSB)_{35}$, which wrap 65, 56, and 35 nt of ssDNA respectively, have been found *in vitro* [1].

Interestingly, neither the data from Chapter 2, nor the recent study [41] provide evidence for discrete wrapping morphologies such as $(SSB)_{56}$ and $(SSB)_{35}$ observed in the past [1].

If different SSB modes are stable and interchangeable, discrete transitions in the extension would be expected. To investigate this inconsistency, we operated optical tweezers in a force-clamp, which allowed us to measure individual SSB binding to the ssDNA at constant tension. The technique also provided the capability to observe nucleoprotein complexes at particular forces for a very long time.

3.2 Experimental Procedure

The experimental setup was prepared in the same way as in Chapter 2. Briefly, a custom-built microfluidic chamber was assembled and setup on an experimental stage. Buffers containing beads and SSB were injected into the chamber. We trapped the beads, performed a bead calibration, and formed a DNA tether. The tether was stretched to measure its extension as a function of force, and compared to theoretical models of polymer elasticity.

3.3 Intermediate Wrapping States of a Single SSB

Following the basic preparation for trapping, we operated a force-clamp to hold a DNA construct at desired constant tensions of 2-10 pN in the absence of protein (Fig. 3.1). The tethered construct was moved into the buffer stream containing SSB, maintaining a constant tension throughout. After a short time, SSB bound and compacted DNA. At the end of each observation, the tension was increased to a value (~25 pN) at which SSB cannot remain stably bound to the protein. This cycle allowed the measurement to be repeated numerous times with new protein on the same DNA construct.

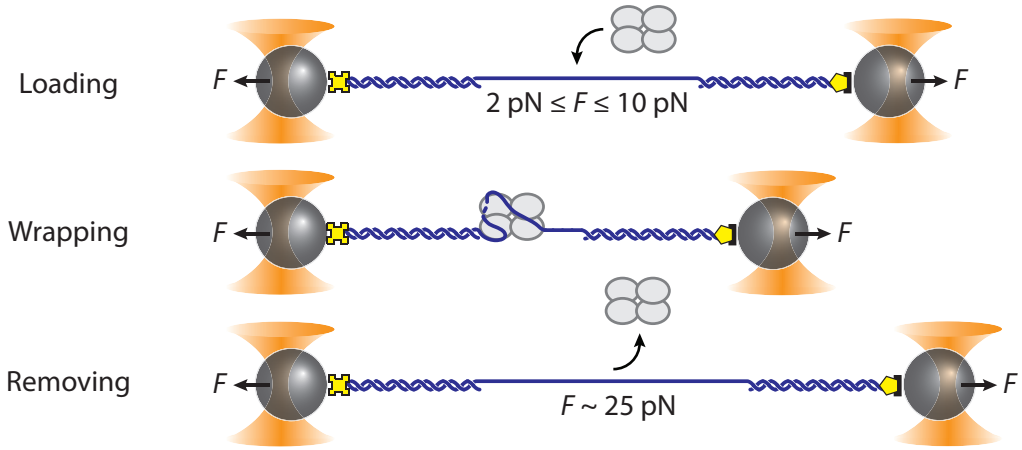

Figure 3.1: Constant force (force-clamp) experiment. A DNA construct is held between two optical traps under a constant tension between 2-10 pN in the presence of protein. Maintaining a constant tension throughout, SSB binds and condenses DNA. At the end of each observation, SSB is removed by stretching the DNA construct to high force (> 25 pN)

The change in DNA end-to-end extension between bare DNA and SSB-wrapped DNA, $\Delta x = x_{bare} - x_{bound}$, was measured as a function of force (Fig. 3.2). Using bare DNA as a reference (set to 0 nm), negative extension changes correspond to SSB wrapping (becoming shorter), and positive changes to release of wrapped DNA (becoming longer).

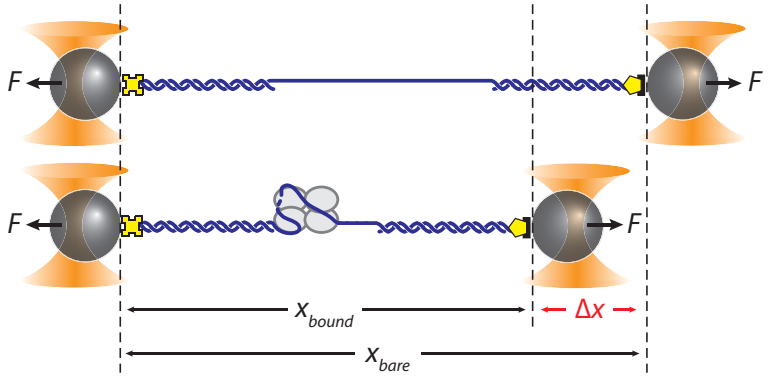

Figure 3.2: Change in DNA extension upon SSB wrapping. An extension change, $\Delta x = x_{bare} - x_{bound}$ is measured upon SSB binding, wrapping or unwrapping ssDNA.

At low tensions (< 3 pN), we observed individual SSBs to bind and condense ssDNA in a single step (Fig. 3.3; red). SSBs remained bound to the ssDNA indefinitely under these tensions.

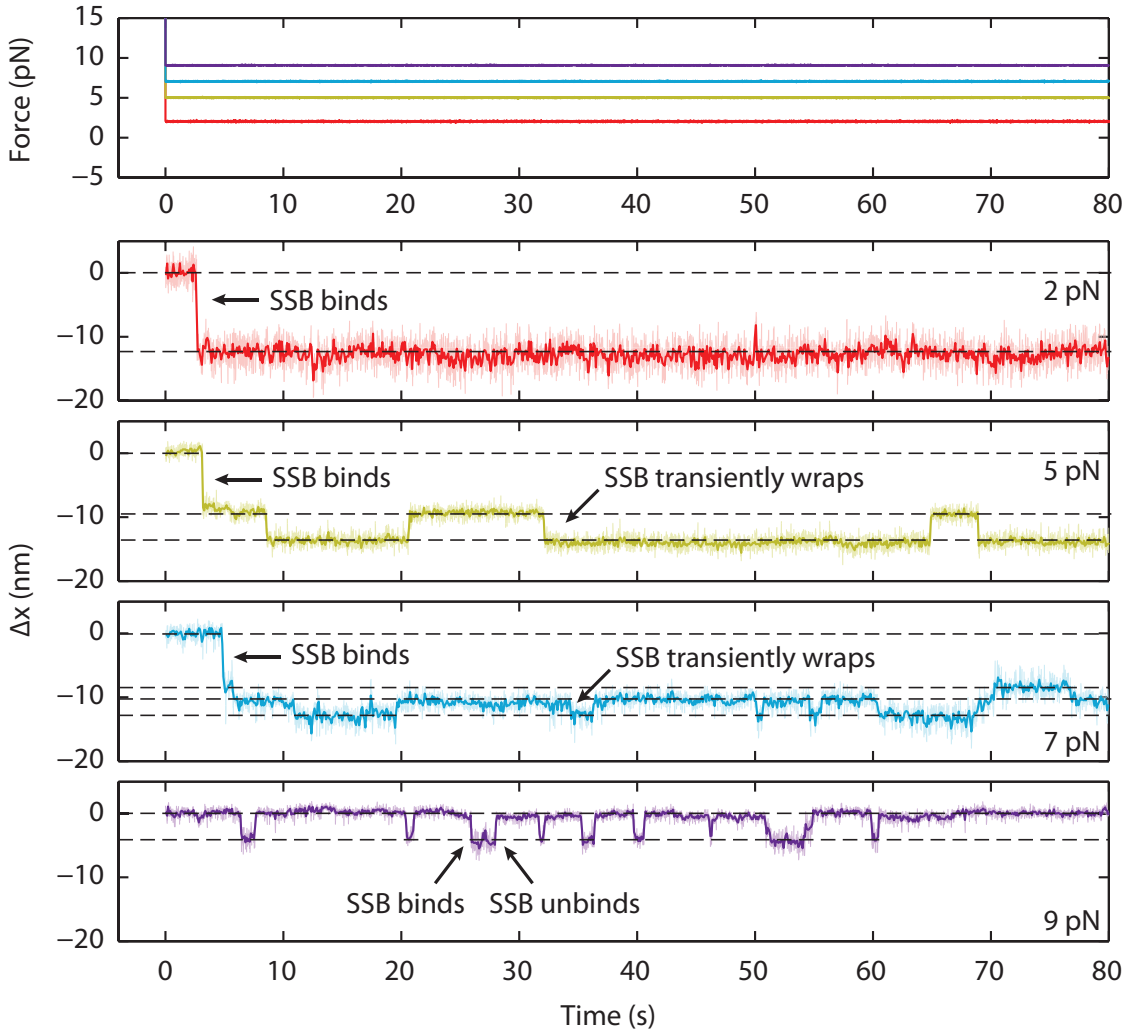

Figure 3.3: Intermediate wrapping states of SSB under tension. Representative time traces of SSB wrapping at 2, 5, 7, and 9 pN (red, green, blue, and purple, respectively). Extension change data were acquired at 66 kHz (light color) and boxcar averaged to 10 Hz (dark color). In all traces, SSB first binds and contracts ssDNA as indicated by an extension decrease. Depending on tension, SSB displays several intermediate wrapping states. Black dashed lines represent the mean extension change of each particular wrapping state.

In contrast, at higher tensions, (3-8 pN; green and cyan), we observed multiple steps upon SSB binding, with dynamic transitions between 2 to 3 distinct states (dashed lines) depending on tensions. Despite these transitions, SSBs did not dissociate at these forces. We interpreted these dynamic changes in extension as wrapping and unwrapping transitions between transient intermediate conformations of a single ssDNA-SSB complex. Near the dissociation force (9-10 pN; purple), we observed multiple instances of one-step wrapping followed by complete release of ssDNA. At these forces, SSB is unable to bind the DNA

tether stably, and the observed transitions correspond to protein binding and unbinding.

To ensure that multiple SSBs were unlikely responsible for causing transient intermediates during one cycle, we performed experiment at low SSB concentration (0.5 nM). In addition, we corroborated this interpretation with measurements of fluorescently labeled SSB. Using an instrument combining optical traps with a single-molecule fluorescence confocal microscope (Fleezers), we measured DNA wrapping simultaneously with fluorescence from protein site-specifically labeled with an average of one AlexaFluor555 dye per protein, SSB_f (Fig. 3.4).

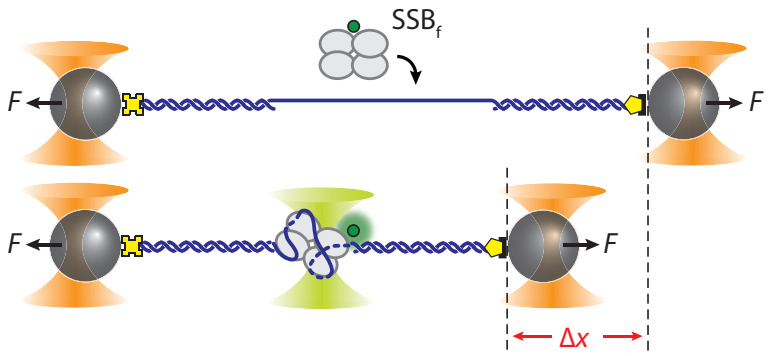

Figure 3.4: Fluorescently labeled SSB wrapping experiment. A DNA construct is held between two optical traps under constant tension of 2, 5, and 9 pN. Extension change, Δx, is measured upon a fluorescently labeled SSB (SSB_f) binding.

Examples of data from the Fleezers measurement under 2, 5, and 9 pN are shown in Figure 3.5. At 2 pN (left), a single protein bound to the DNA as indicated by a negative change in extension. Simultaneous with the trap signal, an increase in fluorescence from the SSB_f was observed (lower panel). Under 5 pN (middle), fluorescence signal was observed at the same time as the SSB binding. No further gain of fluorescence was detected when the second extension change occurred. This implied that the second extension change did not come from a second SSB. Instead, the first and only SSB wrapped more ssDNA. On the right, the observed binding and unbinding events of multiple SSBs under high tensions (9 pN) correlated with the gain and loss of fluorescence, respectively.

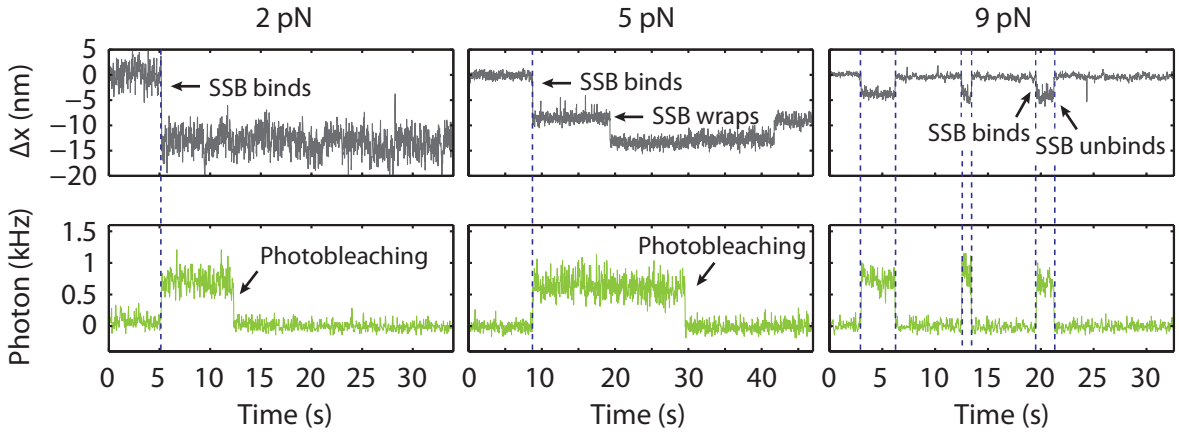

Figure 3.5: Single SSB binding. Upon SSB_f binding, a decrease in extension (gray) and increase in fluorescence (green) are observed simultaneously (all panels). Further decrease in extension (middle panels) does not result in further increase in fluorescence, indicating that only one SSB binds to the construct. At high forces (right panels) extension increases correspond to SSB dissociation.

To characterize SSB wrapping states at any particular tension, we aligned the unbound states of all SSB binding events (0 nm), and constructed a distribution representing SSB wrapping dynamics. An example of five aligned SSB binding events at 5 pN is shown (Fig. 3.6).

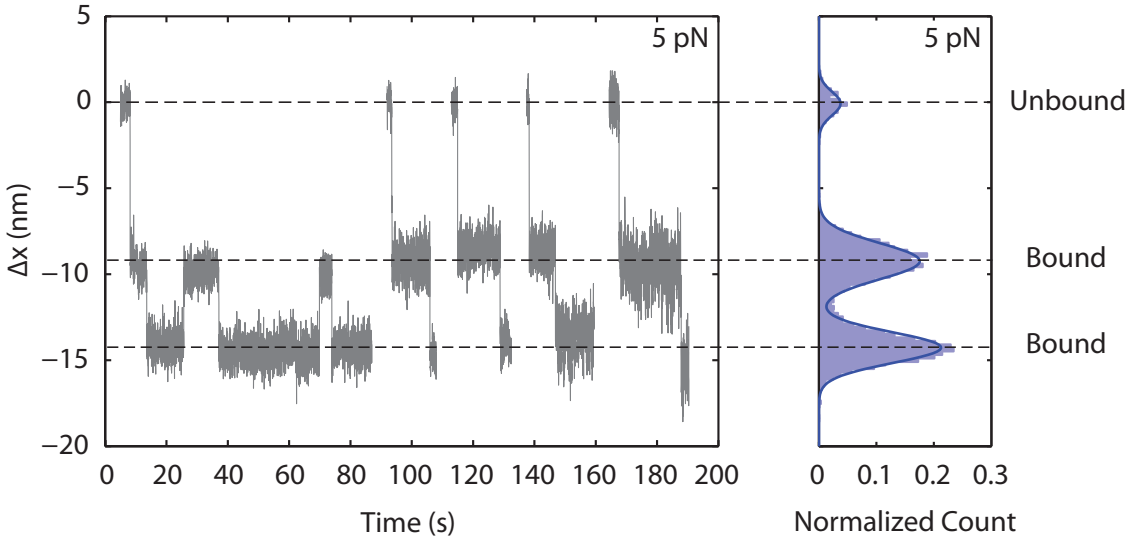

Figure 3.6: Analysis of SSB wrapping states. Representative extension change traces of individual SSB wrapping events at 5 pN are aligned at the unbound state ($\Delta x = 0$ nm). The change in extension distribution illustrates the preferred wrapping states of SSB.

Repeating this procedure for all tensions (2-10 pN), we demonstrated extension change distributions from many individual SSBs (Fig. 3.7(A)). Similar to the force-ramp results in

Chapter 2, Δx decreases as tension increases, indicating that the amount of ssDNA wrapped by SSB decreases. However, in contrast to the force-ramp experiment, the constant force experiment provided evidence for intermediate wrapping conformations of SSB, since multiple states are observed at many tensions. The areas under the peaks in the distributions indicate that SSB spends different amount of time in these particular states. As tension is increased, it disrupts the SSB-ssDNA interaction and shifts the equilibrium to states with smaller Δx, corresponding to less ssDNA wrapped. The widths of the peaks also suggest that rapid protein-ssDNA dynamics occur at certain forces, since they exceed those for bare ssDNA at the same tension.

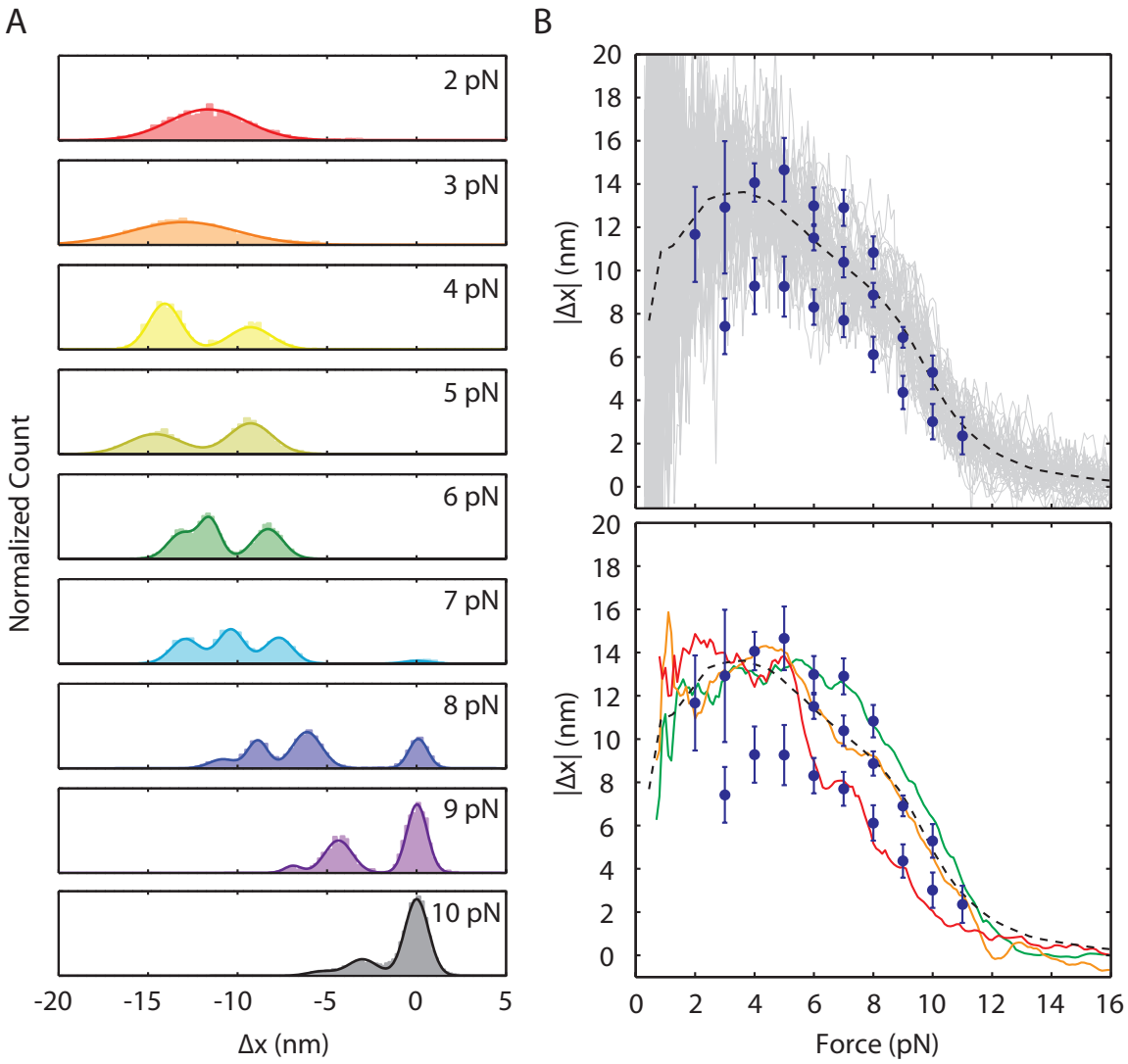

Figure 3.7: SSB wrapping intermediates. (**A**) Extension change distributions of many SSB wrapping events at a constant tension between 2-10 pN. Solid lines are multi-Gaussian fits to the distributions. (**B**) Mean extension change of SSB wrapping states. SSB wrapping intermediates (blue dots) exhibit a clear discrepancy from the population-averaged extension change (dashed line) obtained from the force-ramp experiment in Chapter 2 (top). Representative traces (red, green, and orange) display consistency between the individual traces and the wrapping intermediates (bottom).

We analyzed the peaks of the distributions, and compared them against the population-averaged extension changes in Chapter 2 (Fig. 3.7(B)). It is clear that the average unwrapping behavior (black dashed line) is missing many detailed features of SSB-ssDNA wrapping intermediates (blue dots). Example traces (red, green, and orange) obtained from examining individual SSBs separately corroborated this result, suggesting that SSB may take different unwrapping pathways and may undergo fast transitions between different wrapping

intermediates.

Chapter 4

Model of SSB Wrapping Modes

The previous chapter showed how a single SSB wrapped ssDNA under tension. Multiple SSB wrapping states at many tensions were observed in the optical tweezers experiment. The data analysis further provided the possibility that these intermediate states correspond to different SSB binding modes previously reported [1, 3]. In this chapter we present a detailed model that maps SSB wrapping intermediates to SSB wrapping configurations (SSB wrapping modes). First, we develop the model using a simple approximation based on geometry and statistical mechanics. Later, we refine these approximations using SSB structural data [23] and information previously reported [95–98]. Finally, we perform a control experiment using an SSB mutant, SSB_m, to confirm our analysis. All together, the model demonstrates four SSB wrapping modes: $(SSB)_{65}$, $(SSB)_{56}$, $(SSB)_{35}$, and $(SSB)_{17}$, which wrap 65, 56, 35 and 17 nt of ssDNA, respectively. The first three correspond well with the known $(SSB)_{65}$, $(SSB)_{56}$, and $(SSB)_{35}$ wrapping conformations [1].

4.1 Introduction

E. coli SSB functions as a homotetramer, with each monomer consisting of an OB fold that contains the ssDNA binding site [23]. The tetramer binds and wraps ssDNA in a variety of binding modes that differ primarily in the number of OB folds interacting with the DNA [2]. Three different binding modes have been identified *in vitro*, termed $(SSB)_{65}$, $(SSB)_{56}$, and $(SSB)_{35}$, which wrap 65, 56, and 35 nt per tetramer, respectively [1]. These modes can reversibly interconvert, with the transitions influenced primarily by salt concentration and type as well as protein density on the DNA.

Our result in Chapter 3 suggested the possibility that SSB wrapping intermediates correspond to these different SSB binding modes. To investigate this prediction further, we developed a detailed model utilizing the crystal structure of SSB [23], and refined it succes-

sively to obtain the best approximation explaining how SSB wraps ssDNA.

4.2 Modeling

4.2.1 The Basics

Interpreting the changes in extension, Δx, observed in Chapter 3 and attributing these to binding modes requires a detailed model. As shown in Figure 4.1 (top), the extension of the bare molecule before SSB binding, x_{bare}, is given by Eq. (2.1):

$$x_{bare} = \xi_{ss}(F) \cdot N_{ss} + \xi_{ds}(F) \cdot N_{ds}$$

Wrapping by SSB contributes two changes to the extension of the DNA tether: (i) the loss of N_w ssDNA nucleotides wrapped by the SSB, and (ii) the addition of its length due to the physical size of the SSB-ssDNA complex, x_{SSB}^{eff}. The extension of the wrapped DNA molecule, x_{wrap} is thus (Fig. 4.1, bottom):

$$x_{wrap} = \xi_{ss}(F) \cdot (N_{ss} - N_w) + \xi_{ds}(F) \cdot N_{ds} + x_{SSB}^{eff}(N_w, F) \tag{4.1}$$

The extension change upon wrapping, Δx, is simply the difference between x_{wrap} and x_{bare}:

$$\Delta x = \xi_{ss}(F) \cdot N_w - x_{SSB}^{eff}(N_w, F) \tag{4.2}$$

x_{SSB}^{eff} accounts for the distance between the two ends of the wrapped ssDNA on the SSB. This geometrical term depends on the size of the SSB and the geometry of wrapped ssDNA around the protein, and is thus a function of N_w (and F). For example, according to the $(SSB)_{65}$ structure, $x_{SSB}^{eff}(N_w = 65) < 2.2$ nm since the ends of the wrapped ssDNA exit at the same point on the protein (Fig. 1.3). By contrast, in the $(SSB)_{35}$ structural model, the ssDNA strand exits at opposite ends of the protein and $x_{SSB}^{eff}(N_w = 35)$ would be predicted to be ~5.5 nm.

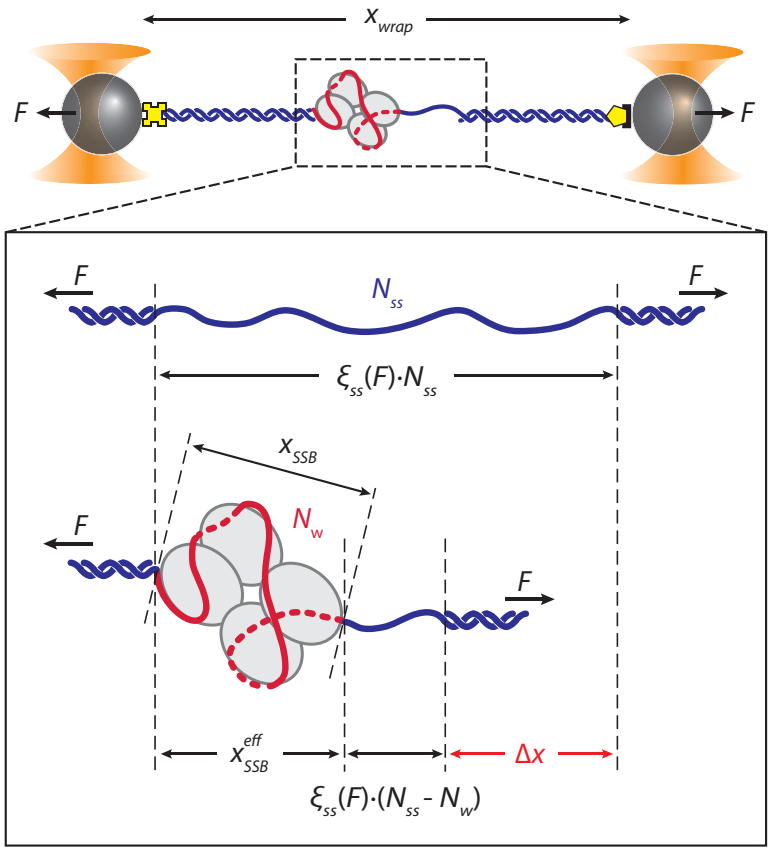

Figure 4.1: Representation of change in extension, Δx. Top: Bare ssDNA (with N_{ss} = 70 nt) and its extension, x_{bare}, based on a polymer elasticity model. Bottom: SSB-wrapped ssDNA showing the number of wrapped nucleotides, ($N_w < 70$, red) and the remaining unwrapped nucleotides ($N_{ss} - N_w$, blue). The extension of wrapped DNA, x_{wrap} is calculated from the elasticity model and the effective physical size of the SSB-ssDNA complex, x_{SSB}^{eff}. Δx is the difference between x_{wrap} and x_{bare}.

x_{SSB}^{eff} must also account for the fact that the nucleoprotein complex can diffuse rotationally, and only the projection along the direction of the applied force contributes to the extension of the DNA tether. At very low tensions, we expect that the contribution of the SSB-ssDNA complex size will be negligible because the complex can reorient itself completely by thermal fluctuations. As force F is exerted, a torque is applied on the complex, orienting it along the direction of tension. This effect can be modeled by writing:

$$x_{SSB}^{eff}(N_w, F) = x_{SSB}(N_w) \cdot L\left(\frac{F x_{SSB}}{k_B T}\right) \tag{4.3}$$

where x_{SSB} is the distance between wrapped ssDNA ends in the protein's frame of reference (Fig. 4.1) and $L(z) \equiv coth(z) - 1/z$ is the orientational factor, derived from the alignment

of a particle undergoing Brownian rotational motion to an external torque. Substituting Eq. (4.3) into (4.2) yields a grand equation that relates N_w, x_{SSB}, F, and Δx:

$$\Delta x = \xi_{ss}(F) \cdot N_w - x_{SSB}(N_w) \cdot \left(coth(\frac{F x_{SSB}}{k_B T}) - \frac{k_B T}{F x_{SSB}} \right) \tag{4.4}$$

Experimental data from Chapter 3 already provided us with a relationship between Δx and F (Fig. 3.7(B)). To determine N_w properly, x_{SSB} must be accounted for with care. Below, we develop three successive levels of approximation to estimate the values of x_{SSB}, and refine the model to obtain the best values of N_w explaining how SSB wraps ssDNA in different modes.

4.2.2 First-leveled Approximation: The Size

The first-leveled approximation takes into account the fact that x_{SSB} can be no greater than the size of the SSB. We measured the longest distance using the SSB structural data [23] and imposed the limit $x_{SSB} < 6.5$ nm. Next, we used this x_{SSB} and Eq. (4.4) to calculate a range of possible N_w for every measured (Δx,F) data pair obtained from the previous chapter (Fig. 3.7(B)). Figure 4.2 demonstrates examples of this approximation procedure at four different forces. Given a range of 0 nm $< x_{SSB} <$ 6.5 nm, estimated ranges of N_w could be determined (solid lines). Dotted lines represent upper and lower bounds for each particular example. Our results are in agreement with the previous finding in Chapter 2 and 3, where ssDNA remains fully wrapped around SSB (N_w ~65 nt) at low tension (0.5 pN; purple). As tension increases, SSB partially unwraps from ssDNA, wrapping less nucleotides (blue, green, and red).

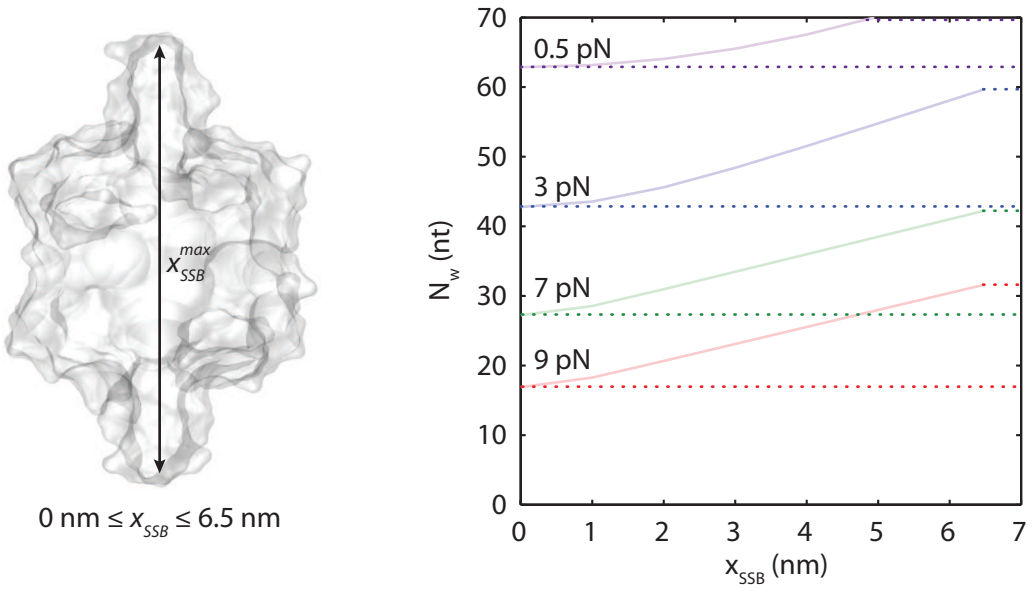

Figure 4.2: Approximation I: The Size. (**A**) Crystal structure of SSB showing the largest value possible for x_{SSB} [23]. (**B**) Representative traces (purple, blue, green, and red) display estimated number of nucleotides being wrapped by the SSB under different tensions. Dotted lines represent the maximum possible range of N_w at each tension.

4.2.3 Second-leveled Approximation: The Structure

We limited the range of N_w further by utilizing the $(SSB)_{65}$ structure to restrict the potential geometries of any intermediate wrapping states. By measuring end-to-end distance, x_{SSB}, between every pair of nucleotides separated by N_w nt along the ssDNA in the structural model (Fig. 4.3(A), red), we imposed upper and lower bounds on x_{SSB} at each force F (Fig. 4.3(B), gray). Interestingly, this refined range of possible N_w (Fig. 4.3(B), dashed lines) restricts our observed wrapping intermediates to four bands centered around N_w = ~65, 50-60, 30-40, and 10-20 nt. The first three correspond well with the known $(SSB)_{65}$, $(SSB)_{56}$, and $(SSB)_{35}$ wrapping conformations [1].

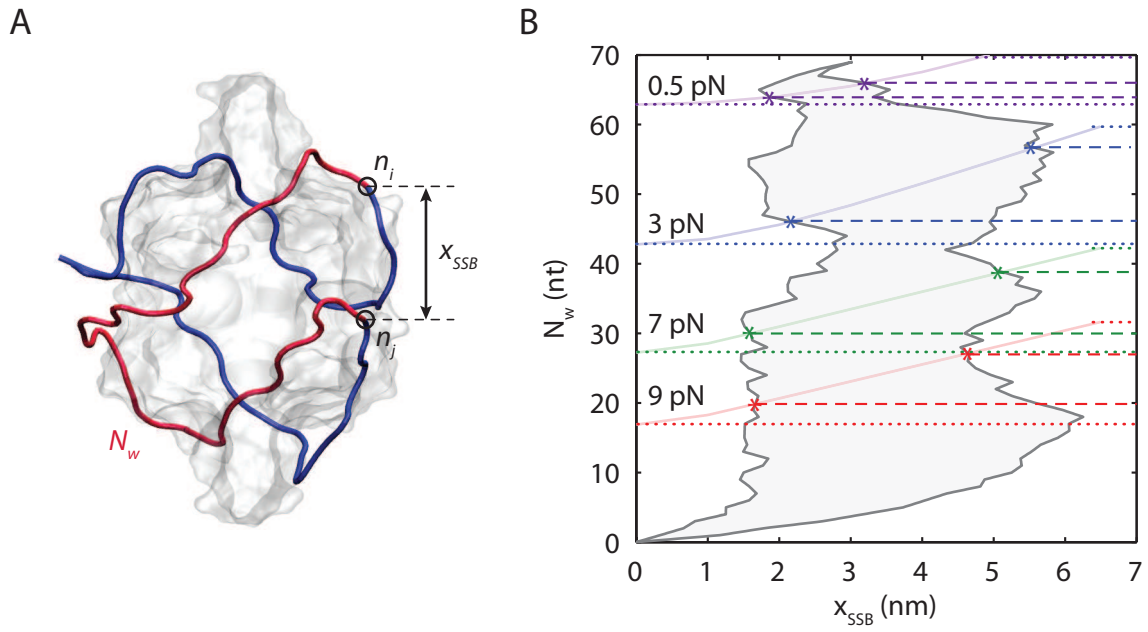

Figure 4.3: Approximation II: The Structure. (**A**) Crystal structure of SSB displaying a pair of nucleotides separated by N_w nt along the ssDNA and end-to-end distance x_{SSB}. Measuring x_{SSB} between every pair of nucleotides (n_i, n_j where $i, j = 0 \rightarrow 70$) limits the range of possible N_w. (**B**) Imposed lower and upper bounds (gray) further refined the range of possible N_w at each tension (stars, dashed lines).

4.2.4 Third-leveled Approximation: The Hotspots

The above model implicitly makes the assumption that all nucleotides of the ssDNA interact equally with the SSB. However, past studies have shown that ssDNA wraps preferentially and makes contact to specific residues of the protein. Trp-40, Trp-54, Trp-88, and Phe-60 are known to play an important role in maintaining protein-DNA stability [95–97]. Crystal structure analysis also implicates Trp-54 and Arg-56 as important in creating pockets of positive electrostatic potential on the SSB surface for ssDNA to bind [23]. In addition, the binding affinity of the nucleoprotein complex is estimated to drop 2,000 fold when His-55 is replaced by Tyr-55 [95]. Site-specific mutagenesis also shows that His-55 is important for SSB tetramerization [98]. Based on this, we identified the (Trp-54, His-55, Arg-56) cluster as a 'hotspot' on each SSB monomer with which nucleotides interact most strongly (Fig. 4.4; green). These four hotspots on the SSB tetramer serve as anchor points along the DNA wrapping path.

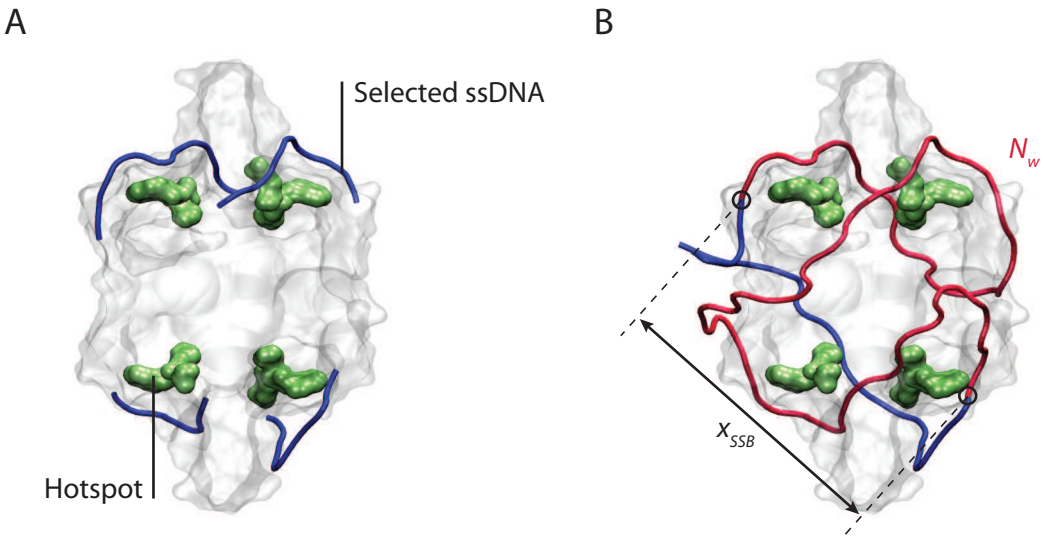

Figure 4.4: Hotspot selection (**A**) Crystal structure of SSB illustrating four clusters (hotspots) of Trp-54, His-55, and Arg-56 residue (green) and selected segments of ssDNA predicted to interact strongly with the hotspots (blue). (**B**) Measuring x_{SSB} from every pair of selected nucleotides limits the range of possible N_w.

To apply these hotspots to our approximation, we first made an assumption that nucleotides near hotspots interact with SSB better than nucleotides further away. Following this hypothesis, we selected nucleotides that only reside within ~5-6 Å of the hotspots, yielding ~6-7 nucleotides each (Fig. 4.4(A), blue). Next, we measured x_{SSB} for every nucleotide pair between four hotspots, and counted the number of nucleotides N_w between them (Fig. 4.4(B)). Since each group contains ~6-7 nucleotides, we expected ~36-49 pairs of (x_{SSB},N_w) in any combination of two hotspots. These pairs are illustrated as a bound area (black) in Figure 4.5. The 'best' estimated values for x_{SSB} and N_w (colored dots) were determined by imposing our approximation (black) to optical tweezers data (solid lines).

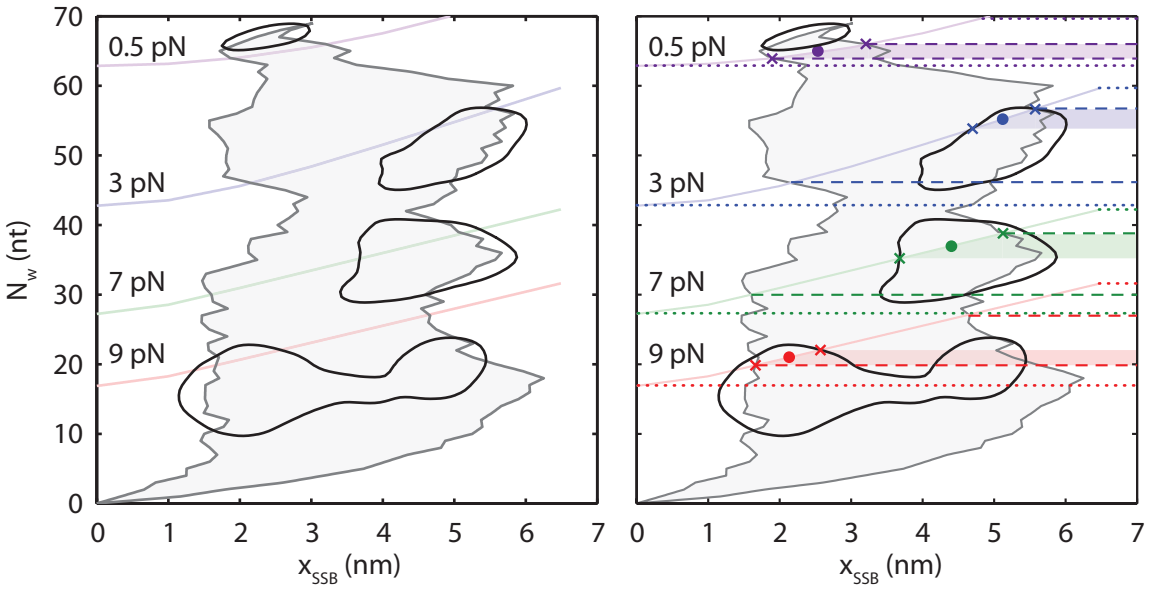

Figure 4.5: Approximation III: The Hotspots. Possible relationships between x_{SSB} and N_w (bound areas in black lines) are derived from the location of selected nucleotides interacting with the hotspots. Best estimated values of N_w (colored dots) are determined by correlating experimental data at different tensions (colored thick lines) with these bound areas . Corresponding shaded areas (purple, blue, green, and red) represent the errors for these estimations.

4.2.5 Interpretation

By applying three levels of approximation on all intermediate wrapping data previously obtained (Fig. 4.6(A)), we yielded best estimates of N_w under tensions (Fig. 4.6(B)). To our surprise, the model consistently demonstrated that SSB unwraps ssDNA in discrete steps as tension increases. This result contradicts the observation previously reported, where SSB gradually unravels ssDNA [41]. As tension increases from 0-8 pN, the number of wrapped nucleotides, N_w, decreases from 65 to 56 to ~35 nt (purple, blue, green points, respectively). The corresponding x_{SSB} values for these wrapping intermediates were consistent with the structural [23] and binding site data [1] for the $(SSB)_{65}$, $(SSB)_{56}$, and $(SSB)_{35}$ modes. For instance, site size studies showed that all four monomers interacted with ssDNA in both $(SSB)_{65}$ and $(SSB)_{56}$ modes [1], consistent with our model of $N_w = 65$ and 56 nt states in which all four hotspots bound ssDNA (Fig. 4.6(C)).

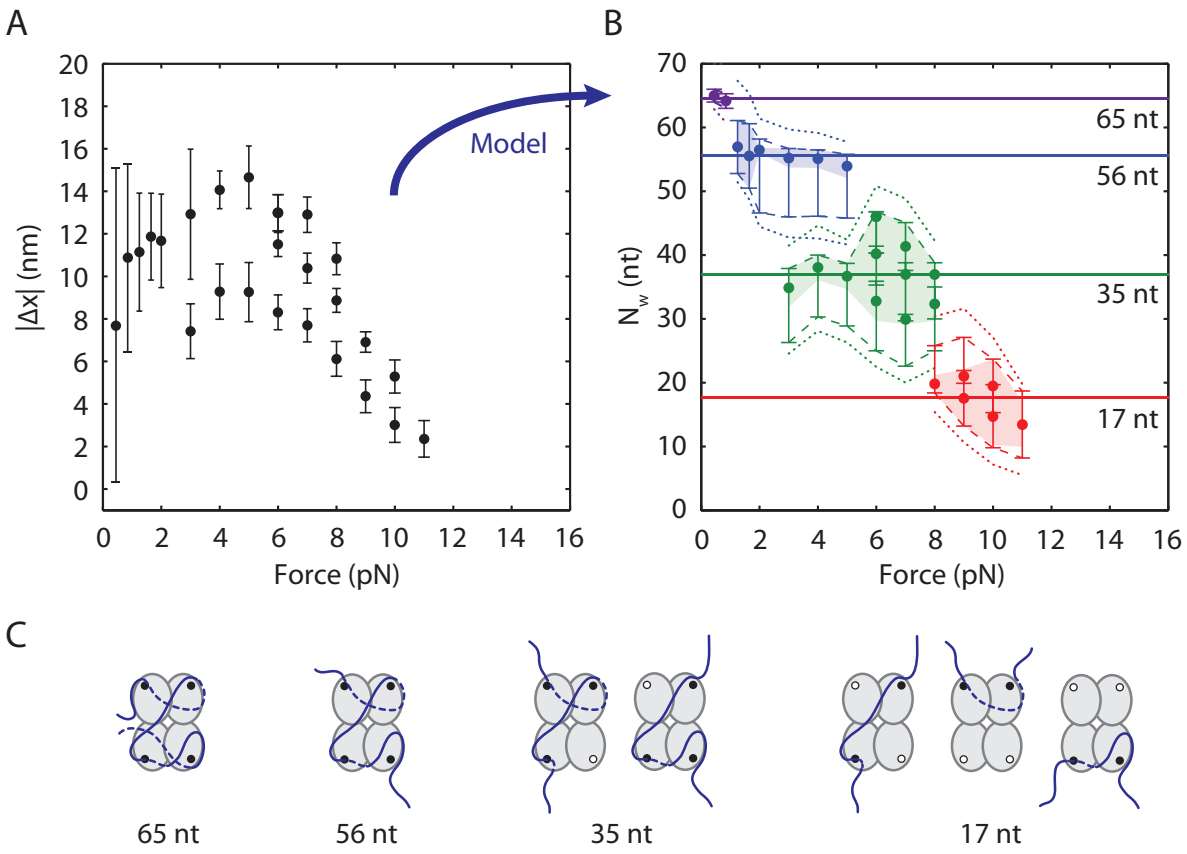

Figure 4.6: SSB wrapping modes. (**A**) Mean Δx for each wrapping state derived from the peaks of the distributions in 3.7(A) vs. tension. Error bars were obtained from the widths of the distributions. (**B**) Number of wrapped nucleotides vs. tension. Each data point (filled circle) corresponds to one in (A), and is determined by Eq. (4.4)plus three levels of approximation. The average N_w for each group (solid lines; purple, blue, green, and red) and the corresponding shaded areas give the best estimate of N_w. (**C**) Cartoon schematic of SSB wrapping modes. Black dots represent SSB subunits that interact with the ssDNA, while white dots depict those that do not.

In the 30-40 nt band, we observed 1-3 separate wrapping states. Our data and analysis were not sensitive enough to ascribe specific wrapping conformations to each. We believed at least two conformations wrapping ~35 nt were consistent with observed extension changes (Fig. 4.6(C)), one of which was nearly identical to the proposed $(SSB)_{35}$ structure ([23], Fig. 1.3). Interestingly, prior studies [40] have suggested the existence of an alternate $(SSB)_{35}$* mode that occludes 35 nt but is structurally distinct from the $(SSB)_{35}$ binding mode.

As tension is increased from 8 to 11 pN, SSBs wrap between 15-20 nt before dissociating. A multitude of wrapping conformations were consistent with the data, and there was no known distinct structural state wrapping 15-20 nt. It is likely that near dissociation, wrapping geometries are more heterogeneous. We therefore proposed three distinct wrapping

configurations of $(SSB)_{17}$ that interact with two hotspots and wrapped an average of 17 nt.

Combining our results, analysis, and previous studies [1, 99], we proposed a complete unwrapping pathway of SSB as a function of tension. As tension increases, SSB unwraps ssDNA in discrete steps: $(SSB)_{65}$, $(SSB)_{56}$, $(SSB)_{35}$, and $(SSB)_{17}$, which correspond to 4, 4, 3, and 2 subunits interacting with ssDNA, respectively. The illustration accompanying our model is shown (Fig. 4.7).

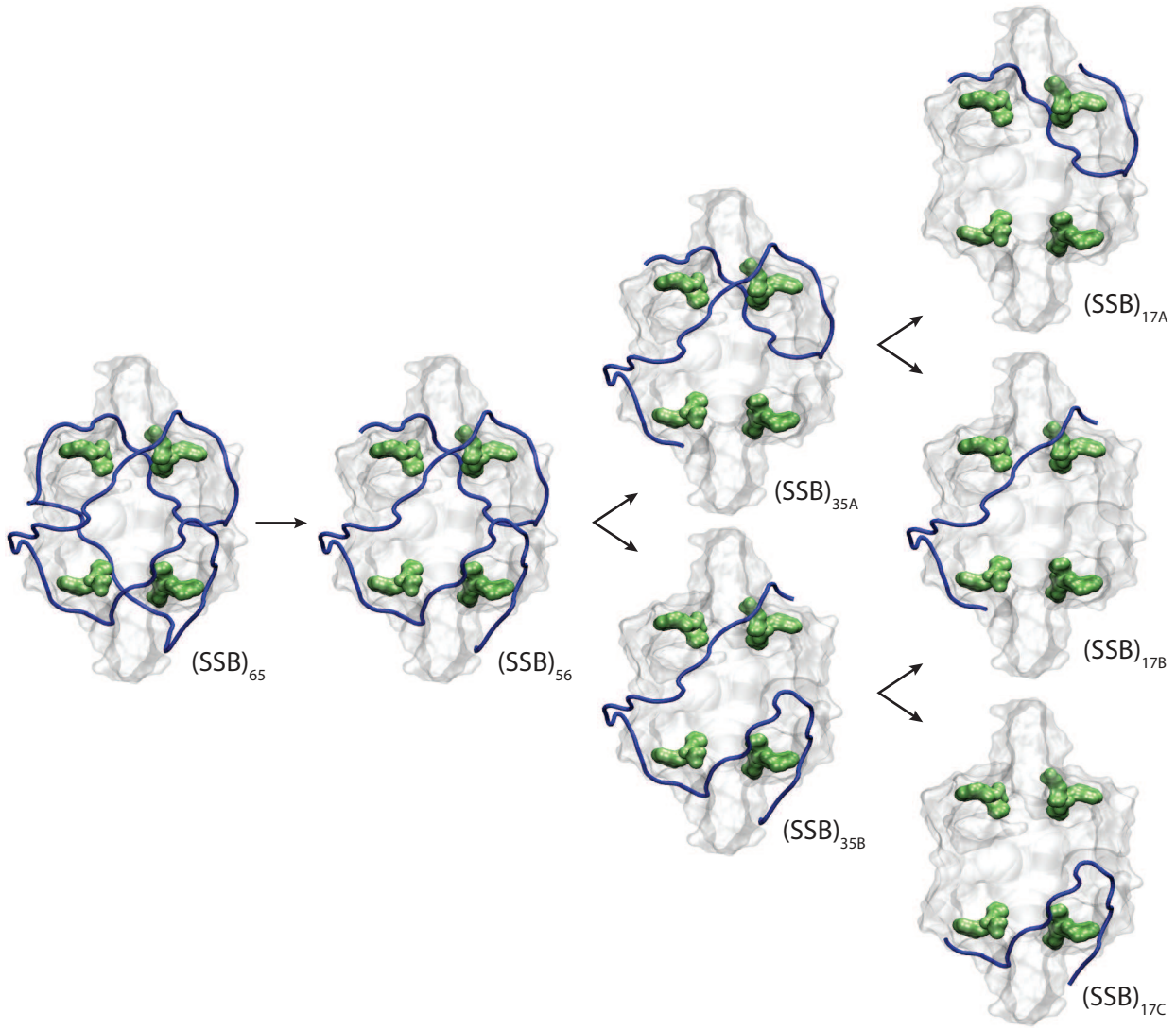

Figure 4.7: SSB unwrapping pathway. Crystal structures of SSB wrapping ssDNA (blue) in different configurations. As tension increases (from left to right), SSB wraps less ssDNA, and the number of interacting subunits (green) decreases.

Control experiments using an SSB mutant (SSB_m, Appendix A) confirmed our analysis. Mutation of Trp-54 to Ser-54 was previously shown to disrupt the protein's interaction with

ssDNA, and led to preferential wrapping in $(SSB)_{35}$ mode [95]. We similarly found that the number of nucleotides wrapped by the mutant was lower than that of the wild type SSB under the same tension (Fig. 4.8). The most probable wrapping conformation in the range of tensions is N_w ~35 nt.

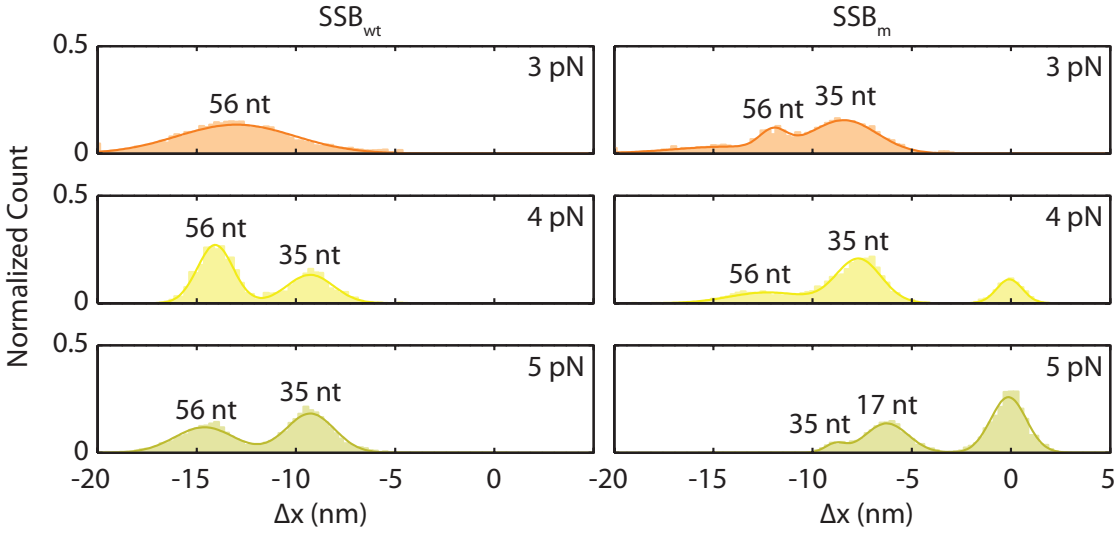

Figure 4.8: Wrapping intermediates of SSB mutant. Comparison of extension change distributions between wild-type SSB (left) and SSB mutant, SSB_m (right). At the same tensions (3-5 pN), SSB_m wraps less ssDNA than wild-type SSB, and is more likely to wrap ~35 nt.

Chapter 5

SSB Diffusion

Previous chapters described how a single SSB wrapped ssDNA in different binding modes: $(SSB)_{65}$, $(SSB)_{56}$, $(SSB)_{35}$, and $(SSB)_{17}$, which wrap 65, 56, 35 and 17 nt of ssDNA, respectively. The same experiments also showed that tension could be used to control these SSB binding modes. For example, applying a constant force of 2 pN to a DNA tether allowed SSB to wrap in the $(SSB)_{56}$ binding mode only. Increasing the tension to 5 pN, in contrast, let the SSB to wrap alternatively between two transient intermediates of $(SSB)_{35}$ and $(SSB)_{56}$ binding modes. This discovery provides us the excellent capability to investigate SSB binding modes in a solution condition that is normally unfavorable. In this chapter we examine whether these different wrapping modes of SSB affect its behavior on ssDNA, in particular its ability to diffuse. Using a combined optical tweezers and a confocal microscope, we observe simultaneously the SSB wrapping mode and its position on ssDNA. The results show that SSB is capable of diffusing along ssDNA in both $(SSB)_{35}$ and $(SSB)_{56}$ binding modes using a sliding mechanism. Rolling mechanism of diffusion is also ruled out by the experiment.

5.1 Introduction

During DNA metabolic processes in *E. coli*, a lot of proteins compete for access to single-stranded DNA (ssDNA). Due to its high affinity and no sequence specificity, *E. coli* single-stranded binding (SSB) protein has advantage over the other. SSB binds and wraps ssDNA strands, protecting them from degradation. Previous studies have shown that SSB can wrap ssDNA in a variety of binding configurations including the $(SSB)_{65}$, $(SSB)_{56}$, and $(SSB)_{35}$ binding mode [1]. It is interesting to consider whether any of these modes are responsible for any DNA metabolism. In DNA replication, for example, thousand of nucleotides of ssDNA at the replication fork are generated and exposed to environmental attacks. To protect these ssDNA rapidly, SSB in the 'unlimited' - $(SSB)_{35}$ cooperativity, is predicted to be responsible

for the task. On the other hand, the $(SSB)_{65}$ binding mode has been demonstrated to regulate other DNA metabolic processes such as DNA recombination [3, 4]. In order for these processes to function, SSB directly interacts with other proteins, recruiting them to specific functional sites [37]. In some cases, SSB also indirectly helps other proteins by preparing access to ssDNA [4]. We considered the possibility that SSB has to travel along ssDNA to facilitate these tasks. Roy et al. used single-molecule FRET (smFRET) to show that SSB can diffuse on ssDNA which in turn, melts DNA secondary structure and stimulates RecA filament formation [4]. Another smFRET study by Zhou et al. demonstrated the SSB sliding mechanism which can carry SSB interacting proteins (SIP) along ssDNA for use in DNA metabolic processes [41]. Despite immense effort, the role of SSB binding modes in DNA metabolism, and their mechanistic properties on other proteins remains obscure. Here, we combine optical force spectroscopy and smFRET to simultaneously monitor SSB wrapping modes and their behaviors on ssDNA.

5.2 Experimental Procedure

We selected AlexaFluor555 and Cy5 fluorophore as a donor-acceptor pair in our smFRET experiment (Appendix A). The AlexaFluor555 donor is chemically linked to SSB at one dye per one SSB tetramer ratio, while the Cy5 acceptor is attached to the 5' ss-dsDNA junction of our standard 70-nt poly-dT ssDNA (Fig. 5.2). In a typical experiment, two $(SSB)_{65}$ trapping buffers (Appendix A) containing 0.5 nM SSB_f and no protein were prepared. To these buffers, an oxygen triplet-state quencher was added to prevent fluorophores blinking [91]. Following the same experimental procedure described in Chapter 2, we trapped the beads, formed a DNA tether in a stream containing no protein, and checked the quality of the DNA.

A constant force of 5 pN was chosen and maintained throughout this chapter for two reasons. First, we previously observed solely both $(SSB)_{56}$ and $(SSB)_{35}$ binding modes at this force. This allowed us to identify SSB wrapping states easily. Moreover, under this force, ssDNA was stretched such that the distance between the donor on the SSB and the acceptor at the ss-dsDNA junction is suitable for the FRET measurement (Fig. 5.1).

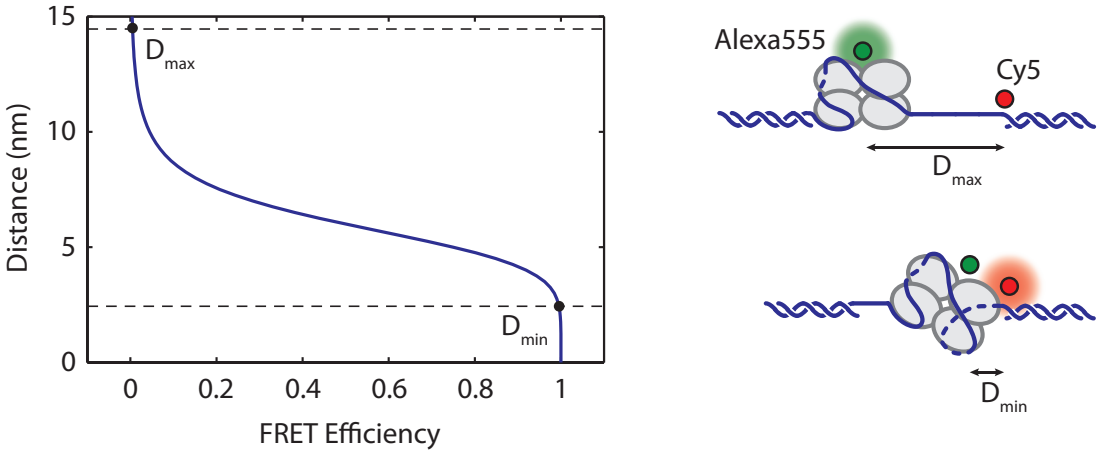

Figure 5.1: Geometry of FRET-extension assay. Single-stranded DNA construct and the force (5 pN) applied to it were designed to suit the FRET measurement. The minimum FRET (E ~0) is achievable when SSB binds in $(SSB)_{35}$ binding mode, and resides on the other side of the Cy5-labeled DNA. The maximum FRET (E ~1) is obtainable if SSB binds in $(SSB)_{56}$ binding mode, and stays right where the Cy5 does.

5.3 SSB Wrapping Behavior

The experiment was performed using a similar technique previously described in Chapter 3. Briefly, the construct was held at a constant force of 5 pN in the protein-free solution. While the construct was being moved into the buffer stream containing SSB_f, the excitation laser was turned on. After a short incubation time, SSB_f bound to ssDNA. We monitored simultaneously the change in extension and fluorescence energy transfer.

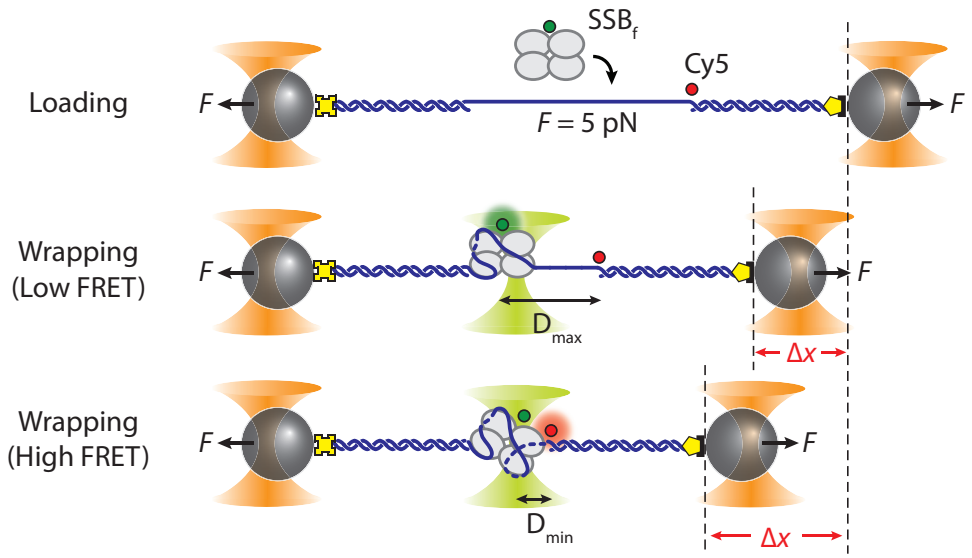

Figure 5.2: Combined optical tweezers and smFRET measurement. A Cy5-labeled DNA construct is tethered between two optical traps under a constant tension of 5 pN. Upon binding of an Alexa555-labeled SSB, SSB_f, both DNA extension change, Δx, and smFRET are measured simultaneously.

Upon SSB_f binding to ssDNA, we observed transitions between the two wrapping states with $N_w = 35$ and 56 nt, based on the analysis from the previous chapter. We also observed transitions between two FRET states with high (E ~0.5) and low (E ~0) FRET efficiencies corresponding to SSB_f positioned at the 5' ss-dsDNA junction vs. the 3' end, respectively (Fig. 5.3, colored dots). All four combined extension-FRET states were detected and characterized; *'1'* – 35 nt wrapping and low FRET (red), *'2'* – 35 nt wrapping and high FRET (blue), *'3'* – 56 nt wrapping and high FRET (black), and *'4'* – 56 nt wrapping and low FRET (green). Corresponding schematic of our combined extension-FRET states were shown (Fig. 5.3, schematic).

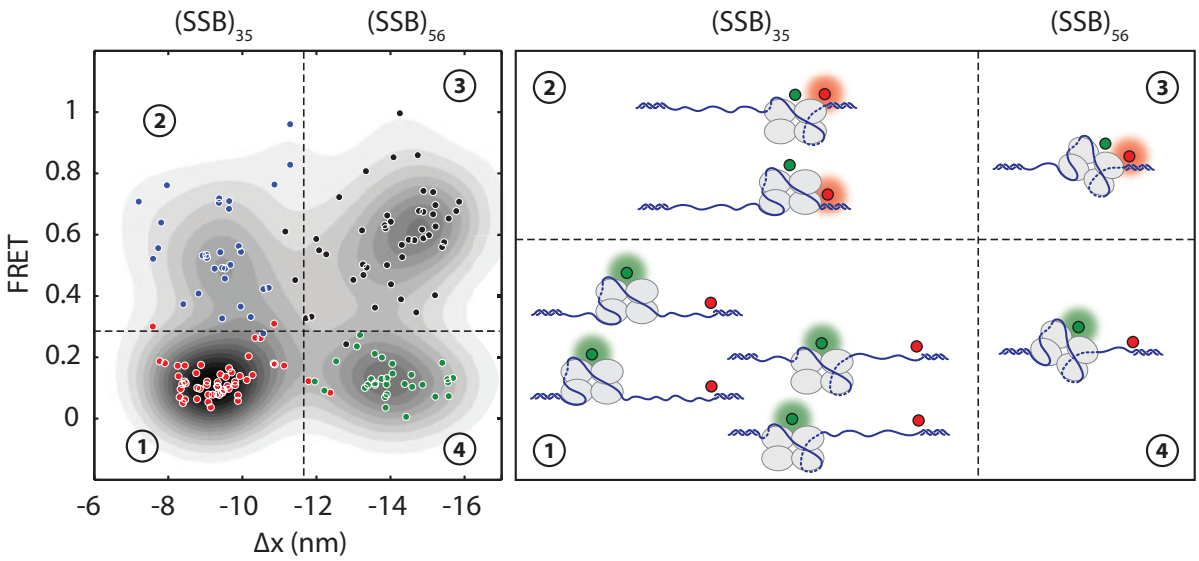

Figure 5.3: FRET-extension states. Scatter plot of FRET efficiency and Δx displaying data (circles) assigned into four states (red (1), blue (2), black (3), and green (4)) based on the value of FRET and Δx. A density map of the combined FRET-extension states overlaid with the scatter plot confirms that the data can be separated into four states. Cartoon illustrations of nucleoprotein complexes demonstrate possible SSB wrapping configurations corresponding to the four assigned states.

Inspection of individual time traces revealed cases in which transitions in extension and FRET were correlated. Figure 5.4 showed such an example of a transition from state *1* $\rightarrow$ *3* $\rightarrow$ *1*, in which an SSB in $(SSB)_{35}$ mode wrapped an additional ~20 nt of ssDNA from the 5' end into $(SSB)_{56}$ mode, then released the same end of DNA. We defined this behavior as 'grabbing'. Grabbing confirms our interpretation that these change in extension represent transitions between SSB binding modes.

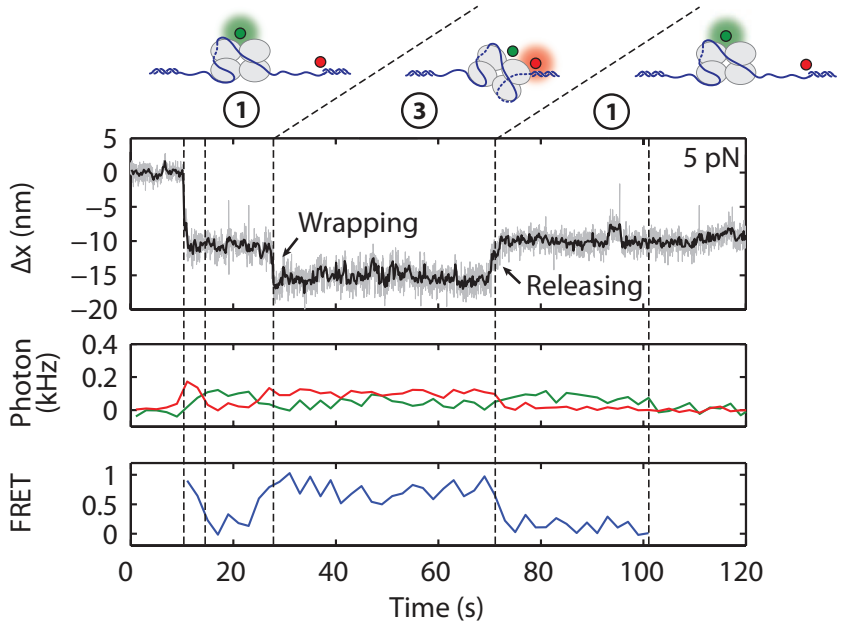

Figure 5.4: SSB grabbing. A representative time trace of combined fluorescence and DNA extension measurement revealing SSB dynamics on ssDNA. Change in extension (gray) and fluorescence of donor (SSB_f, green) and acceptor (Cy5, red) are measured simultaneously. Together, FRET efficiency (blue) and extension change (black) reveal the SSB 'grabbing' (wrapping-releasing) ssDNA.

Alternatively, we observed cases in which FRET transitions occurred independently of changes in wrapping state. These events supported a 'sliding' diffusion mechanism for SSB, as previously proposed [41]. Sliding of SSB occurred in both $(SSB)_{35}$ (*1* $\rightarrow$ *2* or *2* $\rightarrow$ *1*), and $(SSB)_{56}$ (*3* $\rightarrow$ *4*) wrapping modes (Fig. 5.5).

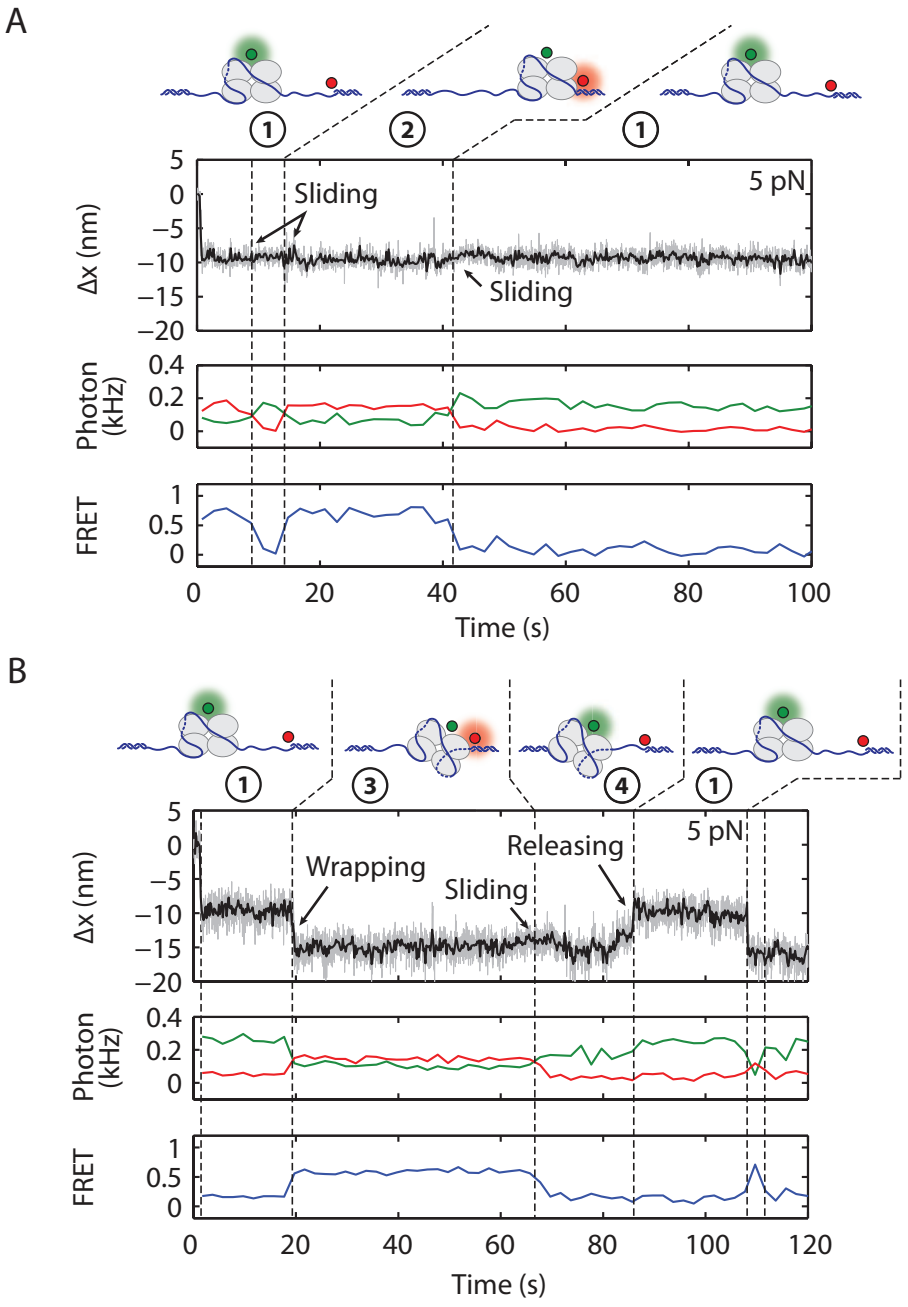

Figure 5.5: SSB sliding. Representative time traces of combined fluorescence and DNA extension measurement showing dynamics of SSB on ssDNA. (**A**) FRET transitions (blue) occurring independently of changes in extension (black) illustrate SSB sliding in $(SSB)_{35}$ binding mode (*1* $\rightarrow$ *2* or *2* $\rightarrow$ *1*). (**B**) SSB sliding in $(SSB)_{56}$ binding mode occurs at the *'3'* $\rightarrow$ *'4'* transition.

In contrast, we observed no examples (0 of N=82) of transitions from state *1* $\rightarrow$ *3* $\rightarrow$ *2* or *2* $\rightarrow$ *3* $\rightarrow$ *1* (i.e. wrapping one end of DNA and releasing the other) providing no support

for a 'rolling' mechanism of diffusion.

All three consecutive states representing different behaviors of nucleoprotein complexes, for example *1* → *4* → *1*, were characterized and illustrated (Fig. 5.6).

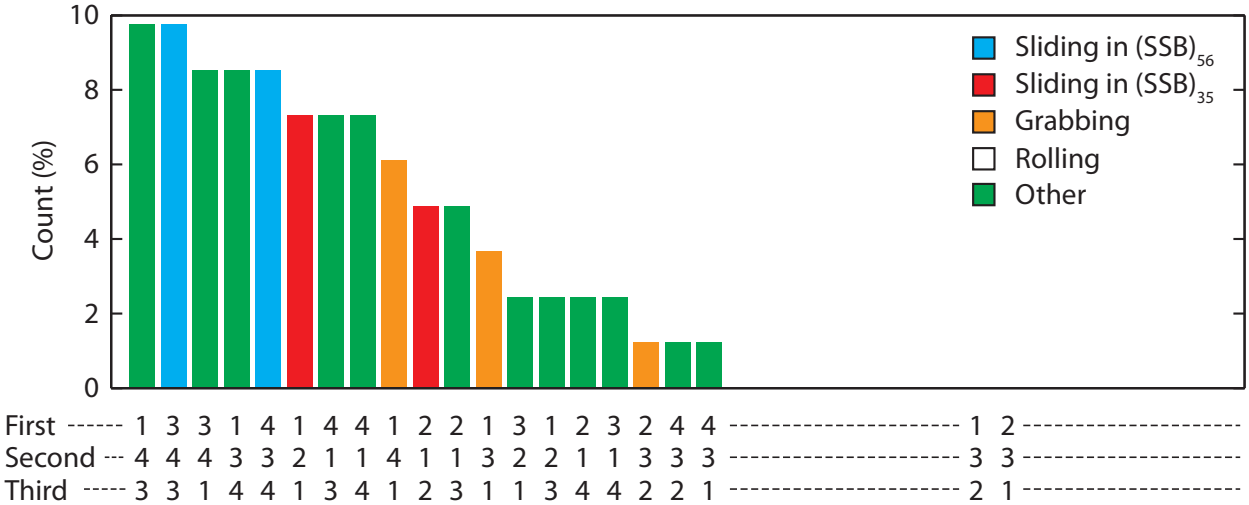

Figure 5.6: SSB wrapping behaviors. Three consecutive FRET-extension states are categorized into groups. These groups represent distinct behaviors of the SSB on ssDNA (color bars). Rolling mechanism (*1* → *3* → *2* or *2* → *3* → *1*, white) is not observed.

Chapter 6

Oligomerization of SSB

Experiments in previous chapters demonstrate how a single *E. coli* SSB wraps ssDNA in four different binding modes. The experiments also show that these SSB modes, in particular $(SSB)_{65}$, $(SSB)_{56}$ and $(SSB)_{35}$, have the ability to translocate along ssDNA without dissociation. In this chapter, we hypothesize that multiple SSBs use this mechanism to distribute and rearrange themselves to form isolated clusters or long filaments during DNA metabolism. To test this hypothesis, we designed and constructed ssDNA of various lengths to allow us to load different number of SSBs. We investigated the SSB oligomerization, conformation, and stability under different SSB binding configurations by using a combined optical tweezers and confocal microscopy.

Our results revealed two distinct conformations of SSBs-DNA complexes. In conditions that favor the $(SSB)_{35}$ binding mode, SSBs oligomerize into a long and stable filaments. On the other hand, in conditions that favor the $(SSB)_{65}$ binding mode, SSBs form isolated clusters. Each of these clusters exhibits wrapping-unwrapping dynamics the two SSB states, indicating an instability of the SSBs-DNA conformation.

6.1 Introduction

E. coli SSB is capable of binding to ssDNA in distinct modes [1]. In $(SSB)_{65}$ binding mode, SSB wraps ~65 nt ssDNA with all four subunits. It displays a limited type of cooperativity where multiple SSB tetramers pair up and form bead-liked clusters along ssDNA [3]. In contrast, in the $(SSB)_{35}$ binding mode, SSB wraps ~35 nt using approximately two subunits, and exhibits an unlimited cooperativity forming smooth long filaments. Previous studies have proposed that these different cooperativities may be utilized selectively in different DNA metabolic processes [2]. During homologous recombination, for example, RecA filament forms on ssDNA wrapped by SSB in the $(SSB)_{65}$ binding mode. $(SSB)_{35}$, in comparison, is

predicted to function during the DNA replication where rapid saturation of SSB on ssDNA is needed [2].

Here, we used a combined optical tweezers and single-molecule fluorescence microscopy to dissect the binding mode and cooperativity of multipe SSBs on ssDNA. Detailed conformations and stabilities of these SSBs-DNA complexes were also examined.

6.2 Experimental Procedure

In Chapter 2, we designed a DNA construct containing two functionalized dsDNA handles linked to a 70-nt ssDNA binding site. The size of this binding site was chosen to accommodate a single SSB tetramer wrapping in the $(SSB)_{65}$ binding mode or two SSB tetramers wrapping in the $(SSB)_{35}$ binding mode. Longer ssDNA binding site is required to investigate SSB oligomerization. With the flexibility to interchange the protein binding site fragment, we engineered three additional ssDNA of different lengths: 105, 140, and 175 nt, which can presumably accommodate 3, 4, and 5 SSBs in the $(SSB)_{35}$ mode, respectively.

In addition to our standard solution condition - $(SSB)_{65}$ trapping buffer (Appendix A) used in previous chapters - we prepared solution containing low monovalent salt and high SSB concentration to favor the $(SSB)_{35}$ wrapping mode, $(SSB)_{35}$ trapping buffer (Appendix A). These solutions were used interchangeably among experiments throughout this chapter.

Standard preparations were performed prior to experiments similarly to that in Chapter 2. Briefly, we loaded buffer containing beads and SSB into the sample chamber. Beads were trapped and calibrated. Next, we formed the DNA tether and checked its quality by comparing to theoretical models of elasticity. Force-extension curves (FEC) of many DNA molecules containing various lengths of ssDNA (Fig. 6.1; red, green, orange, and blue) are in excellent agreement with the models (black).

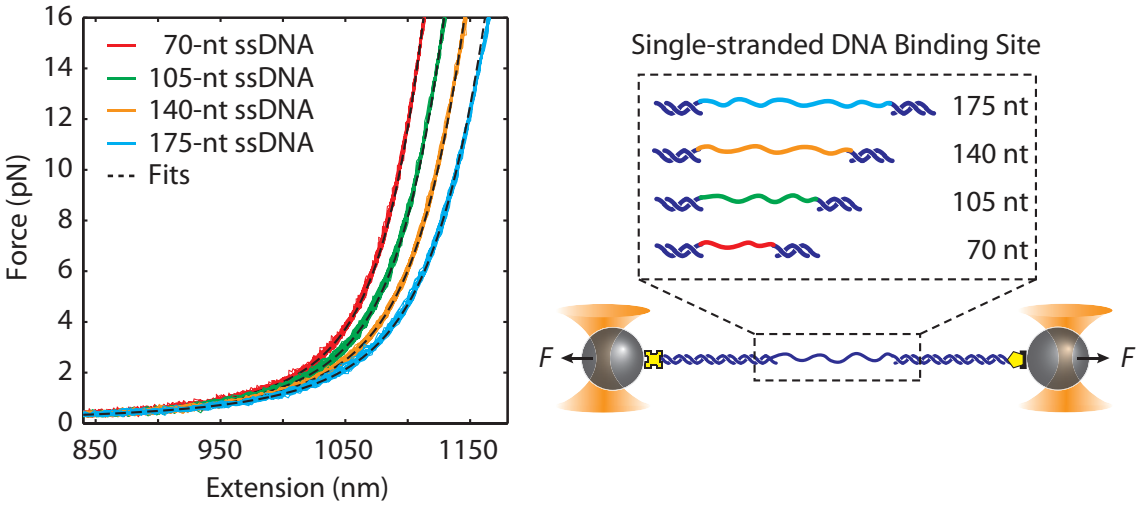

Figure 6.1: Polymer modeling of single-stranded DNA segments. Representative force-extension curves (FEC) of stretching and relaxing bare DNA constructs containing 3,260-bp dsDNA handles and various lengths of ssDNA (red, green, orange, and blue) designed to accommodate different numbers of SSB. The total extension of the tether is modeled of by the sum of dsDNA and ssDNA extensions. The dsDNA segment is modeled using the extensible worm-liked chain [93], while the ssDNA segment is fitted to the extensible snake-liked chain [94]. Black dashed lines are fits to the constructs.

6.3 SSB Oligomerization and its stability

6.3.1 SSB Oligomerization

To investigate oligomerization of SSB in both $(SSB)_{65}$ and $(SSB)_{35}$ binding modes, we performed a force-clamp experiment holding a construct containing 140-nt poly-dT ssDNA binding site at a constant force of 5 pN (Fig. 6.2). Maintaining this force throughout, we exposed ssDNA to SSB in two different buffer conditions, and observed many SSB binding (or wrapping) events. Changes in DNA end-to-end extension, $\Delta x = x_{wrap} - x_{bare}$, upon wrapping by multiple SSBs were measured. Using bare DNA as a reference (set to 0 nm), negative extension change corresponds to SSB binding to ssDNA.

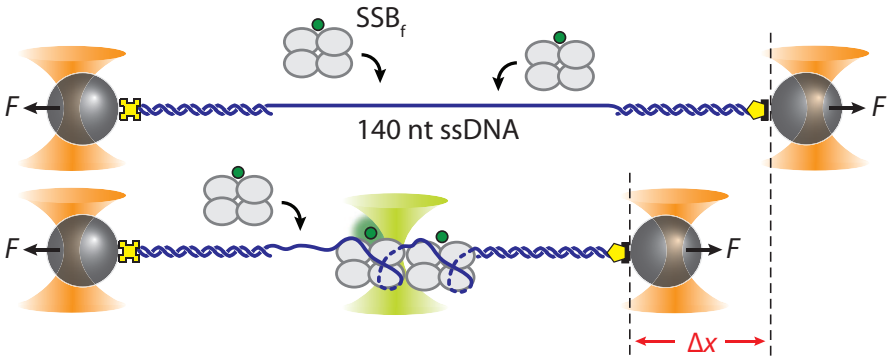

Figure 6.2: Multiple SSBs wrapping experiment. A DNA construct containing 140 nt poly-dT ssDNA segment is held between two optical traps under a constant tension of 5 pN. Extension change, Δx, is measured upon SSB_f(s) binding to ssDNA.

Interestingly, we observed distinct SSB wrapping states in different buffer conditions. In $(SSB)_{35}$ trapping buffer, three consecutive steps were frequently observed (Fig. 6.3(A)). Since these steps had almost identical stepping sizes, we hypothesized that three SSB proteins were bound to the 140-nt ssDNA. Our interpretation were corroborated with measurements of fluorescence from fluorescently labeled SSB, SSB_f, using the Fleezers. Appearances of a single step fluorescent signal occurred simultaneously with the negative extension changes from the trap signal were observed, confirming that three SSBs indeed wrapped ssDNA.

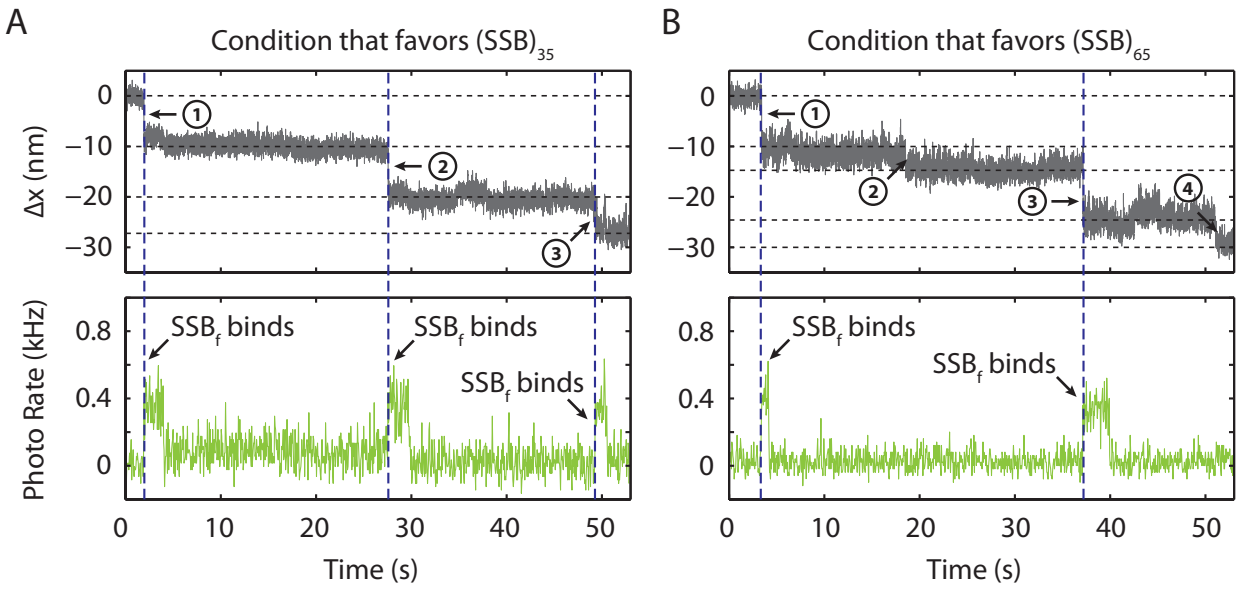

Figure 6.3: Multiple SSBs wrapping. (**A**) Upon SSB_f binding in a condition that favors $(SSB)_{35}$ binding mode, decreases in extension (gray) and increases in fluorescence (green) are observed simultaneously. Three SSBs are shown to bind 140 nt ssDNA in this condition. (**B**) In a condition that favors $(SSB)_{65}$ binding mode, some decreases in extension are observed at the same time with increases in fluorescence (*'1'* and *'3'*), indicating SSB binding. Decreases in extension that do not correlate with the change in fluorescence (*'2'* and *'4'*) demonstrate additional wrappings by the bound SSB, and not from additional SSBs binding. Only two SSB are observed to bind 140 nt ssDNA in this case.

On the other hand, in the presence of solution that favors the $(SSB)_{65}$ binding mode, we observed four shortening steps (Fig. 6.3(B)). The step size were generally bimodal (-5 or -10 nm) at 5 pN. In this particular example, a sequence of -10, -5, -10, and -5 nm stepping occurred. We also observed other stepping sequences, including a frequent [-10, -10, -5, -5] and a rare [-10, -10, -10] step. Simultaneous fluorescence data revealed a striking revelation. Increase in fluorescence (due to the binding of SSB_f) only correlates to extension change of -10 nm, but not -5 nm. This observation is consistent with the result from Chapter 4 where a single SSB exhibits a transient wrapping between the $(SSB)_{35}$ and $(SSB)_{56}$ binding mode, we hypothesize that two SSBs bound to 140-nt ssDNA and exhibited transient wrapping states between stable intermediates.

To test our hypothesize, we characterized SSB wrapping states by aligning all binding events at the unbound state (0 nm), and constructed a distribution representing a population of SSB wrapping dynamics (Fig. 6.4). In both solution conditions, peaks were clearly recognized. In conditions that favor the $(SSB)_{35}$ binding mode, populations of SSB illustrated

that three SSBs bound to ssDNA successively (Fig. 6.4(A)). Majority of SSBs in the $(SSB)_{65}$ buffer, in contrast, exhibited two SSBs binding in a bind-bind-wrap-wrap [-10, -10, -5, -5] pattern (Fig. 6.4(B)).

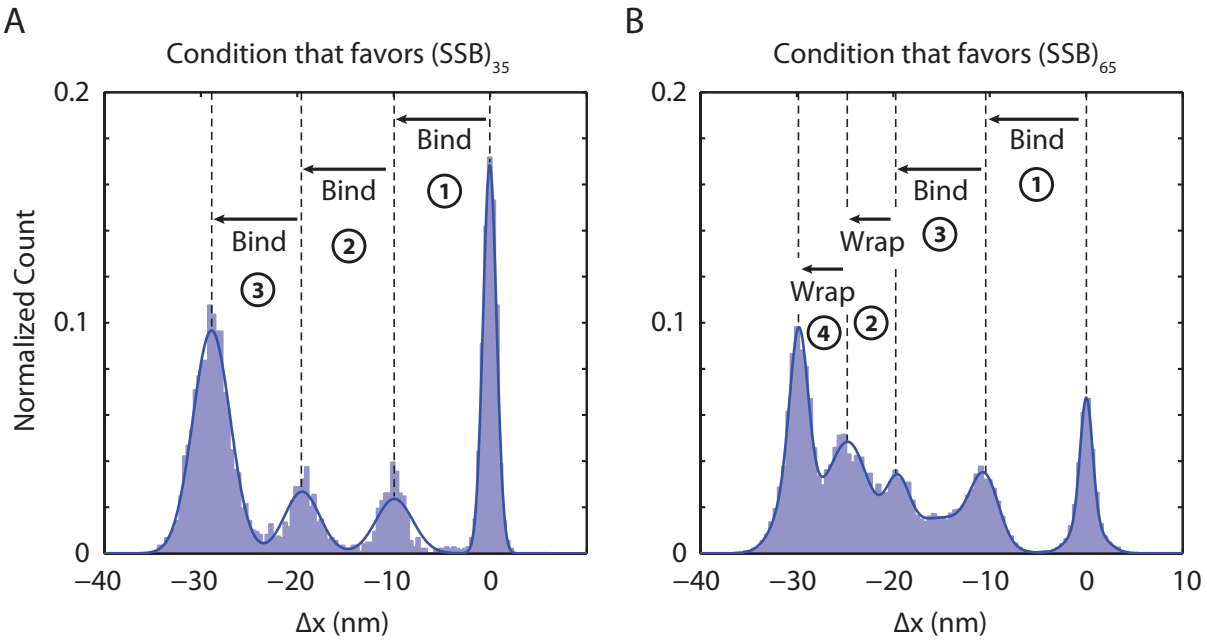

Figure 6.4: Multiple SSBs wrapping characteristic. Extension change distributions of many SSB wrapping events in a condition that favors $(SSB)_{35}$ (**A**) and $(SSB)_{65}$ (**B**) binding mode. Solid lines are multi-Gaussian fits to the distributions. Predictions of the wrapping characteristic in each condition is presented (arrow and text).

In order to characterize the binding configuration of each SSB in the complex, we tested our result against the model established in Chapter 4. The change in extension, Δx, for a single SSB wrapping was denoted by (4.4):

$$\Delta x = \xi_{ss}(F) \cdot (N_w) - x_{SSB}(N_w) \cdot \left(coth(\frac{F x_{SSB}}{k_B T}) - \frac{k_B T}{F x_{SSB}} \right) \tag{6.1}$$

where $\xi_{ss}(F)$ is the extension of one ssDNA nucleotide at a tension F, and x_{SSB} is the distance between wrapped ssDNA ends in the protein's frame of reference. Since the elasticity of ssDNA is very sensitive to monovalent ions in the solution [70, 100, 101], we modified $\xi_{ss}(F)$ based on the nonlinear low-force elasticity model accordingly (Appendix B). We also made an assumption that the change in extension due to multiple SSB wrapping, Δx_M, should be

proportional to the number of SSB bound, M:

$$\Delta x_M = M \cdot \Delta x \tag{6.2}$$

Applying extension changes, Δx_M, using the peaks in the distributions to Eqn. (6.2), we obtained a relationship between change in extension, Δx_M, and number of nucleotides wrapped by SSBs, N_w (Fig. 6.5).

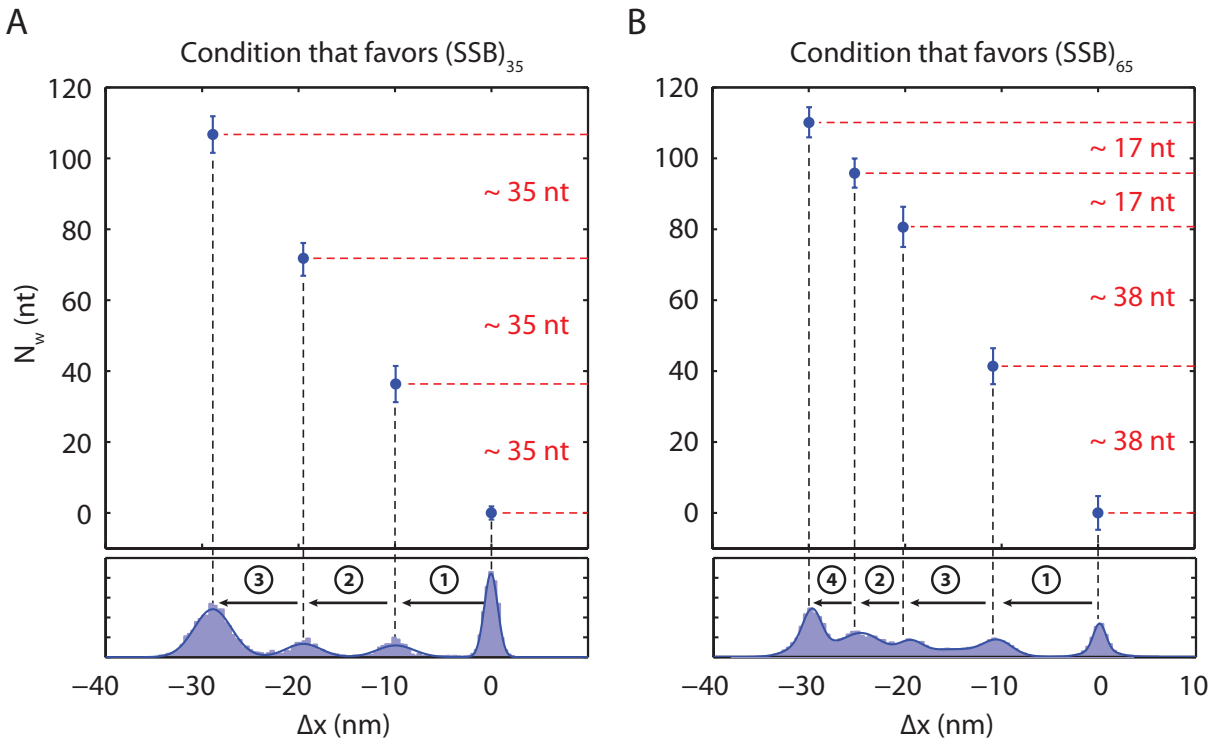

Figure 6.5: Wrapping modes of multiple SSBs. Utilizing an established model from Chapter 4, changes in extension of multiple SSB wrapping states (black dashed lines) are converted to the number of wrapped nucleotides (red dashed lines). Horizontal differences between adjacent red lines indicate additional number of nucleotides being wrapped between states.

In conditions that favor the $(SSB)_{35}$ binding mode, three individual SSBs wrapped ~35 nt of ssDNA consecutively (Fig. 6.5(A)). To our knowledge, this was the first time that the oligomerization (or filament formation) of the SSB in $(SSB)_{35}$ mode was observed in real-time. In contrast, in conditions that favor the $(SSB)_{65}$ binding mode, we consistently observed two SSBs wrapping ~38 nt ssDNA each, followed by additional wrappings of ~17 nt and ~17 nt ssDNA (Fig. 6.5(B)). This result could be pictured as two SSBs first wrap ssDNA in $(SSB)_{35}$ mode and switch to $(SSB)_{56}$ mode by wrapping more DNA. Schematics

representing these wrapping dynamics are shown accordingly (Fig. 6.6).

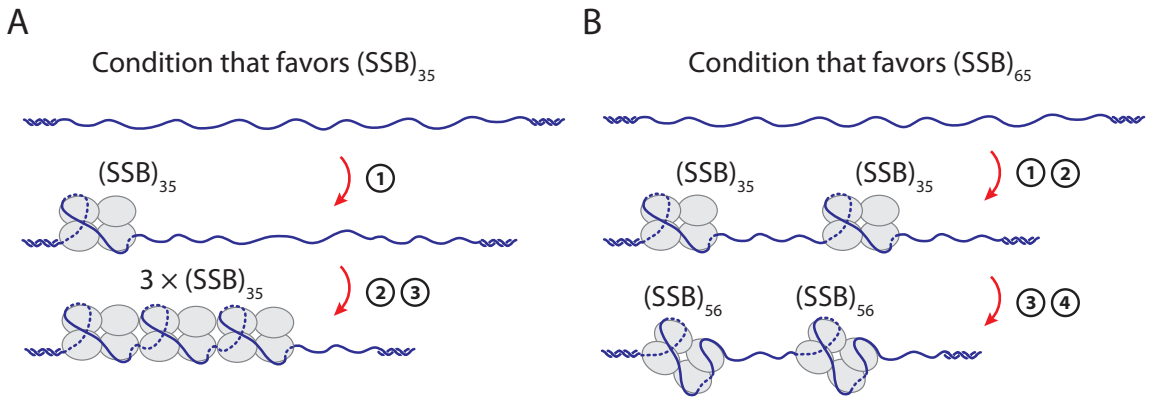

Figure 6.6: SSB oligomerization. Schematic representation of multiple SSB wrapping pathways in different solution conditions. (**A**) Three SSBs consecutively wrap ~35 nt and form long filaments of $(SSB)_{35}$ in a condition that favors $(SSB)_{35}$ binding mode. (**B**) Two SSBs wrap ~38 nt each, followed by additional ~17 nt wrappings to form isolate clusters of $(SSB)_{56}$ in a condition that favors $(SSB)_{65}$ binding mode.

We further confirmed our interpretation by performing a force-tramp experiment previously used in Chapter 2. Briefly, a 140-nt poly-dT ssDNA construct was incubated in a stream containing SSB for a short period, allowing several SSBs to bind, and moved out of the SSB stream to a blank stream. A ramping force of 0-25 pN was applied to stretch and subsequently relax the nucleoprotein complex.

Force-extension curves (FEC) of stretching and relaxing many protein-bound DNA molecules in two solution conditions are shown (Fig. 6.7, gray). Unlike the result from Chapter 2 where a single SSB dissociated upon stretching to a very high force (> 20 pN), multiple SSBs generally did not dissociate at once. Cycles of stretching and relaxing were performed to remove SSBs from the DNA. Here, blue lines represent FECs of a DNA construct occupying at least one SSB, while black dashed lines depict that of a bare DNA. Jumping from one line to the next line on the right indicates the dissociation of a single SSB. In the $(SSB)_{65}$ trapping solution, two cycles of stretching and relaxing were usually enough to remove two SSBs consecutively (Fig. 6.7(B)). In $(SSB)_{35}$ trapping buffer, on the other hand, many stretching cycles were required to disrupt the nucleoprotein filament (Fig. 6.7(A)). Once disrupted, observation of three SSBs binding to ssDNA was possible through a series of dissociation. Our results were consistent with the constant-force results where three and two SSBs bound to 140-nt ssDNA in a condition that favor $(SSB)_{35}$ and $(SSB)_{65}$, respectively.

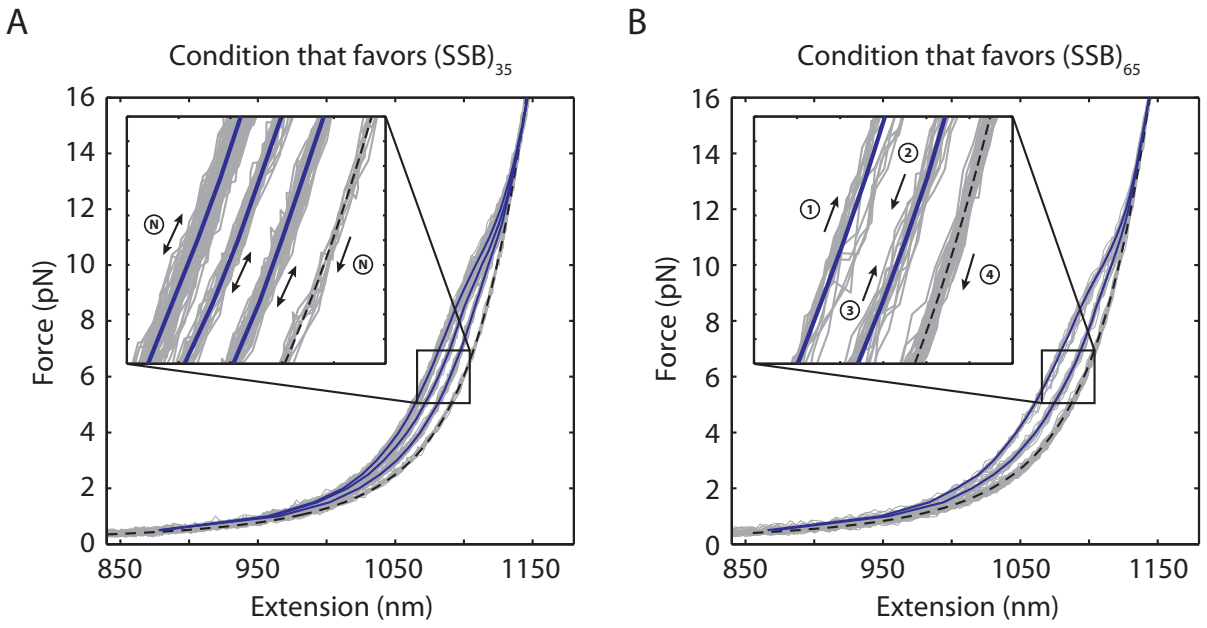

Figure 6.7: Dissociation of multiple SSBs. Representative force-extension curves (FEC) of stretching and relaxing (gray) DNA molecule in a condition that favors $(SSB)_{35}$ (**A**) and $(SSB)_{65}$ (**B**) binding modes are distinct, indicating the difference in SSB wrapping configuration. Three SSB dissociation steps are observed in a condition that favors $(SSB)_{35}$ binding mode, while only two SSB dissociation steps are seen in a condition that favors $(SSB)_{65}$ binding mode. Black dashed lines are fits to the bare DNA, demonstrating that all SSBs have dissociated after many cycles of stretching.

6.3.2 Stability of SSB Filament

As mentioned earlier in Chapter 1, electron microscopy has revealed two distinct binding configurations of SSB on the ssDNA. In the conditions that favor the $(SSB)_{35}$ binding mode, SSBs form smooth-contoured filaments. On the contrary, in the conditions that favor the $(SSB)_{65}$ binding mode, SSBs form isolated clusters resembling a bead-on-string structure. We considered the possibility that our results represented these observations. To investigate this matter, we conducted an experiment to observe the behavior of bound SSBs after the formation of filaments or clusters. The force-clamp assay previously described in Chapter 2 was modified to achieve this goal (Fig. 6.8). Briefly, a 140-nt ssDNA construct was held at a constant force of 5 pN in the presence of SSB (Position 2). Instead of staying in the SSB stream, the SSB-bound construct was moved to the protein-free stream for observation (Position 1). This enabled monitoring of only the behavior of the ssDNA bound SSB without interference of SSB in solution.

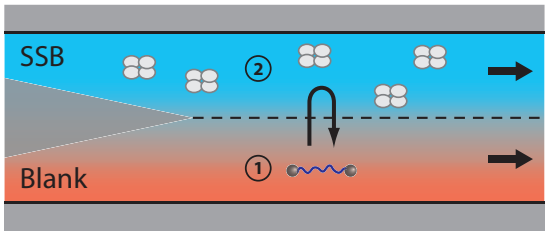

Figure 6.8: Stability of SSB filament assay. Two separate streams containing experimental buffer only (red, Position 1) and buffer plus SSB (blue, Position 2) form a laminar interface. Observation was done at Position 1 to avoid interference from excess proteins.

Time traces representing the extension change of nucleoprotein complexes were shown (Fig. 6.9). In the presence of excess proteins (blue), changes in extension data fluctuated stochastically. We believe these dynamics came from excess SSB in solution competing against bound SSBs for the ssDNA space. Upon entering protein-free stream (red), bound SSBs in two different solution conditions exhibited distinct behaviors. In the solution that favors the $(SSB)_{65}$ binding mode, two SSBs, both initially in the $(SSB)_{56}$ mode, began to partially unwrap ssDNA and switched their wrapping states (Fig. 6.9(B)). We matched these states to the SSB binding configuration previously characterized (Chapter 4), leading to three combinations: (i) two SSBs in the $(SSB)_{56}$ mode, (ii) two SSBs in the $(SSB)_{35}$ mode, and (iii) one SSB in each mode. On the contrary, we observed three SSBs wrapped ssDNA stably and uniformly in the $(SSB)_{35}$ mode over a long period of time (Fig. 6.9(A)).

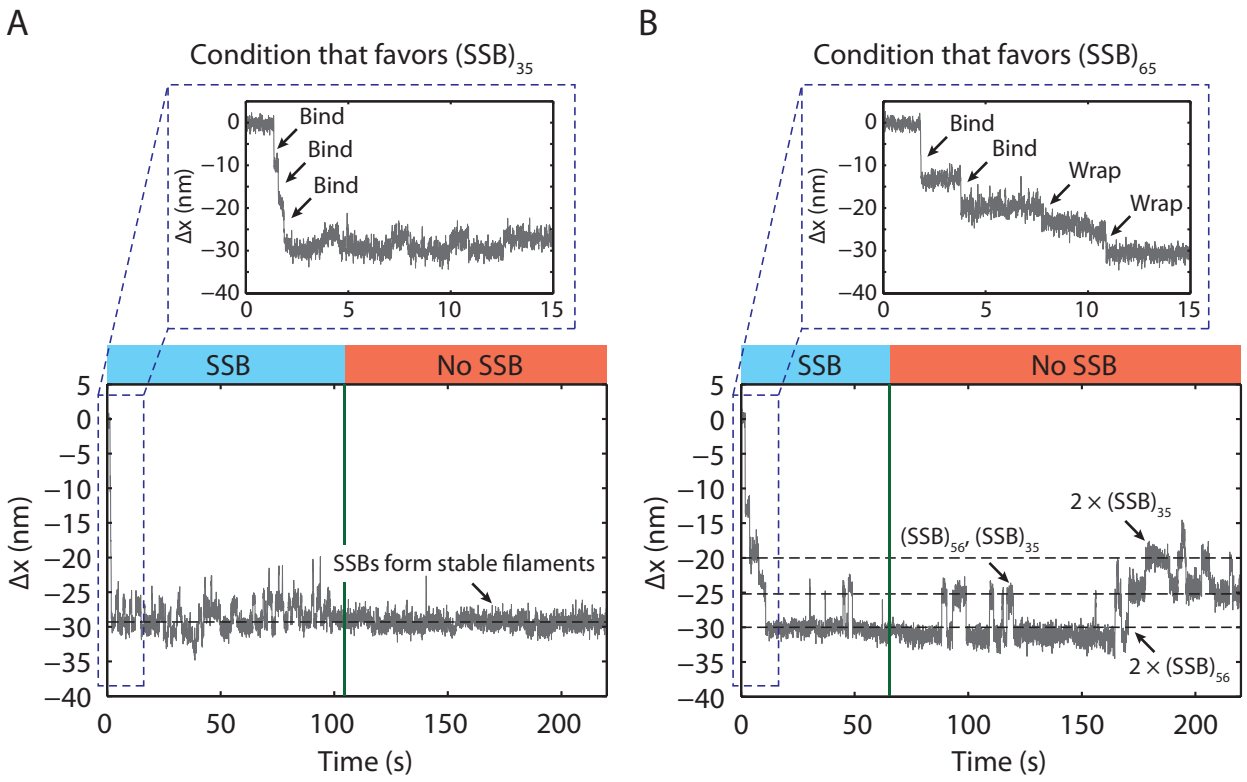

Figure 6.9: SSB assembly dynamics. Representative change in extension time traces of multiple SSBs wrapping in a condition that favors $(SSB)_{35}$ (**A**) and $(SSB)_{65}$ (**B**) binding mode. In the presence of SSB (blue interval), multiple SSBs bound to ssDNA under their preferred configurations (insets). Distinguished behaviors of the preformed SSB-DNA complexes are observed upon entering the SSB-free channel (red interval). In a condition that favors $(SSB)_{35}$, no change in extension is observed, indicating that SSB warps ssDNA stably. Transient wrapping between SSB intermediates, however, is shown in a condition that favors $(SSB)_{65}$.

Interestingly, neither data from the $(SSB)_{65}$ nor $(SSB)_{35}$ trapping buffer provided a reasonable explanation for the inconsistency of the number of nucleotides wrapped by SSBs and the number of available nucleotides on the ssDNA. In conditions that favor the $(SSB)_{65}$ binding mode, the maximum number of nucleotides wrapped by SSB is $56 \times 2 = 112$ nt. Since our construct had 140 nt of ssDNA available, there should be 28 nt left for an additional SSB to partially bind. Furthermore, the maximum number of nucleotides spent by wrapping three SSBs in the $(SSB)_{35}$ condition is $35 \times 3 = 105$ nt. One more SSB in the $(SSB)_{35}$ binding mode should be able to fit into this space.

We believe this inconsistency came from a non-compact arrangement of the SSBs. ssDNA gaps exist between adjacent SSBs leading to this non-perfect utilization of ssDNA.

6.4 Conformation of SSBs-ssDNA Filament

Previous section demonstrated two distinct types of SSB oligomerization, and posted an interesting concern on the arrangement of the SSB where numbers of bound SSB were lower than expected. To clarify the compactness of SSB binding on limited ssDNA space, we carried out a force-clamp experiment on various lengths of the DNA binding site including 70, 105, 140, and 175 nt ssDNA. The DNA end-to-end extension, Δx_M, was measured with multiple SSBs wrapped in the solution that favors the $(SSB)_{35}$ binding mode. Numbers of SSB binding to these ssDNA constructs were counted and investigated.

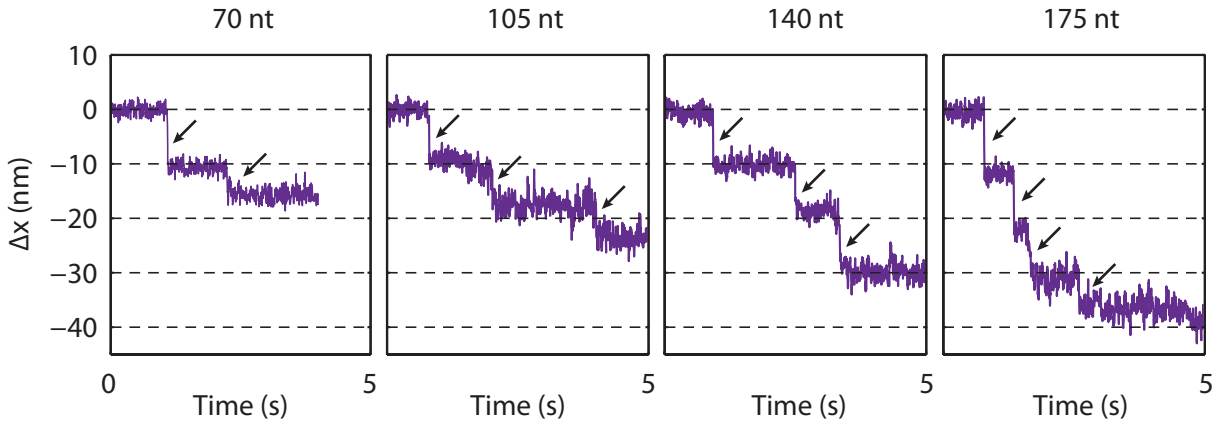

Figure 6.10: Multiple SSB bindings. Representative time traces of multiple SSBs wrapping on different lengths of ssDNA. Arrows indicate SSB binding event.

In comparison with the case where three SSBs bound to 140-nt ssDNA with identical ~10 nm step sizes, we observed multiple SSB binding events with steps of ~10 nm as well as smaller steps of various sizes (Fig. 6.10, arrow). Combined extension change distributions from many SSB binding events confirmed our observation. Given enough exposed nucleotides, individual SSBs bind and wrap ssDNA in the $(SSB)_{35}$ binding mode (Fig. 6.11; blue, arrowed lines). Excess nucleotides are occupied by additional SSBs partially wrapping ssDNA. These additional SSBs did not necessarily wrap the same amount of ssDNA (red), leading to smaller steps of various sizes.

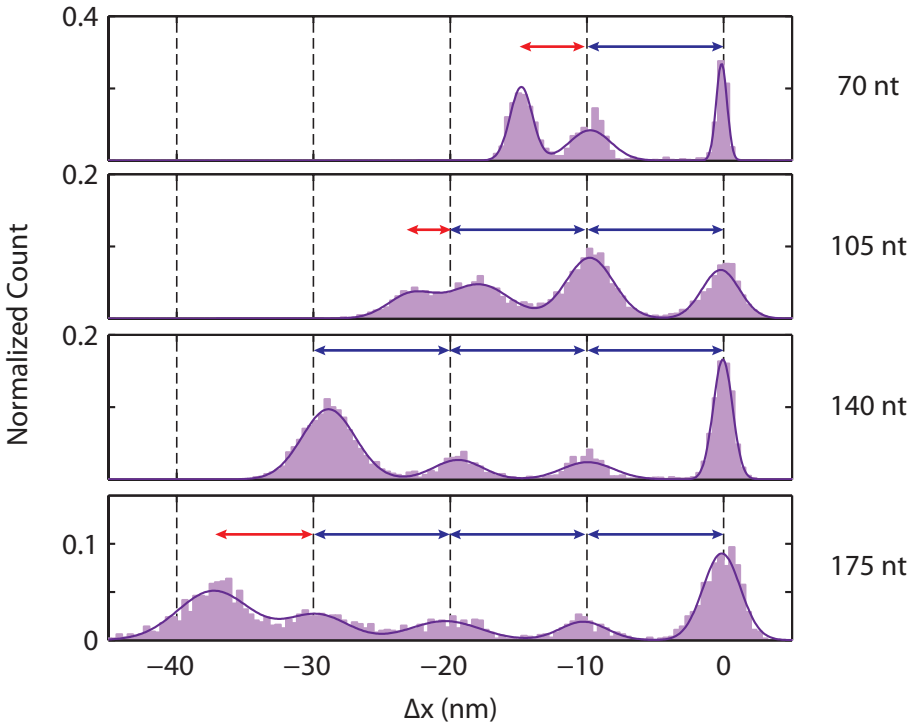

Figure 6.11: Multiple SSB wrapping characteristic. Extension change distributions of many SSB wrapping events on different lengths of ssDNA. Each blue line indicates a single SSB wrapping in $(SSB)_{35}$ binding mode. Red lines represent partial wrappings of additional SSBs. A constant tension of 5 pN is maintained in all constructs.

We further analyzed the extension change from all peaks in the distribution, and plotted them against the number of nucleotides available (Fig. 6.12, black circle). Using equation (4.4) previously described, these changes in extension were converted to the number of nucleotides wrapped by SSBs. On average, a single SSB binding in $(SSB)_{35}$ mode wrapped ~36 nt of ssDNA (red, dashed lines). It was important to note that some SSBs, especially the last one that binds, are not completely wrapped in the $(SSB)_{35}$ binding mode. In the case of 175-nt ssDNA, for example, three SSBs wrapped ssDNA in the $(SSB)_{35}$ binding mode, while the forth SSB only wrapped ~26 nt.

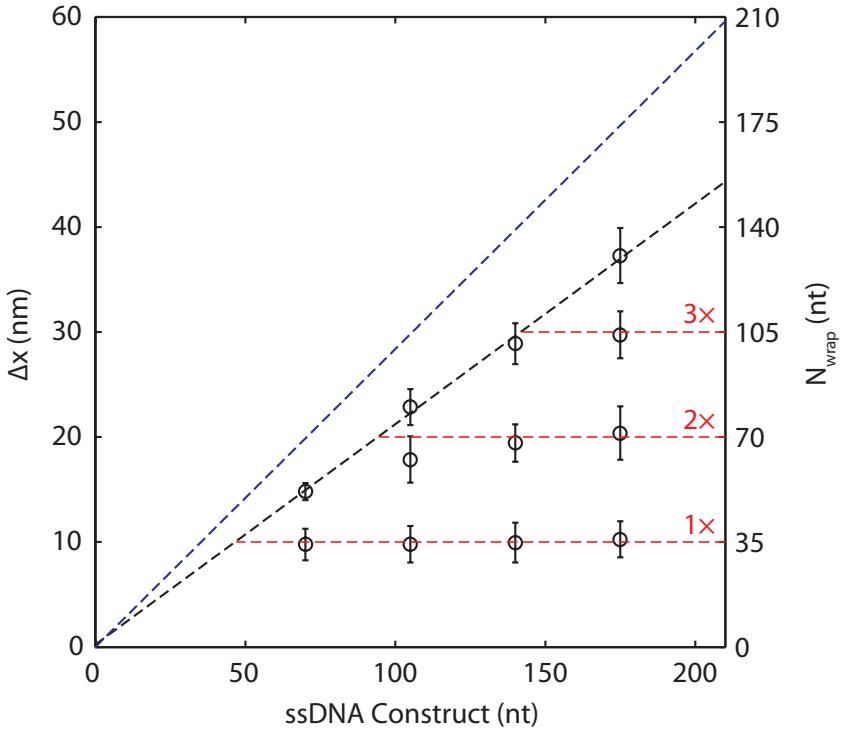

Figure 6.12: Multiple SSB wrapping. Mean extension change of multiple SSB wrapping (black circles) demonstrates an incompetency of SSBs to wrap all available nucleotides across all lengths of ssDNA. Extension change, Δx, is converted to a number of wrapped nucleotides, N_w, using a previously established model in Chapter 4. The conversion rate goes as follow; Δx of ~10 nm $\leftrightarrow$ N_w of ~36 nt $\leftrightarrow$ 1 SSB binding in $(SSB)_{35}$ binding mode (red dashed lines). A black dashed line represents a maximum number of nucleotides actually wrapped by SSBs for each ssDNA construct, while a blue dashed line depicts a total number of ssDNA available for binding.

We also observed another astonishing behavior of SSB oligomerization. In every ssDNA construct, SSBs wrapped less nucleotides (black, dashed line) than the number of nucleotides actually available (blue, dashed line). The difference between the blue and the black line illustrates the number of nucleotides 'abandoned' by SSBs. We hypothesize that these abandoned nucleotides act as a DNA linker that bridges adjacent SSBs.

To investigate this circumstance further, we derived a model describing arrangements of multiple SSBs on a ssDNA. First, we considered a relationship between number of abandoned nucleotides and number of SSBs fully wrapping ssDNA in $(SSB)_{35}$ binding mode. However, the partial bindings of SSB makes modeling difficult. To cope with this problem, we extrapolated our result to find the DNA constructs that could accommodate exactly 1, 2, 3, or 4 SSBs wrapping in $(SSB)_{35}$ (Fig. 6.13(A)). Since a single SSB binding in $(SSB)_{35}$ mode wrapped ~36 nt of ssDNA, it would require ~36, 72, 108 and 144 nt to wrap 1, 2, 3,

and 4 SSBs respectively (green, dashed lines). Extrapolating along the black dashed line, we found that DNA constructs containing ~47, 94, 142, and 190 nt ssDNA were required to achieve the required binding number of SSB (green asterisks). At these particular lengths of ssDNA, exactly 1, 2, 3, and 4 SSBs wrapped 36, 72, 108, and 144 nt. Number of abandoned nucleotides of each extrapolated DNA construct (Fig. 6.13(B), filled circles) was simply the difference between available nucleotides and wrapped nucleotides (Fig. 6.13(A); red, arrowed lines).

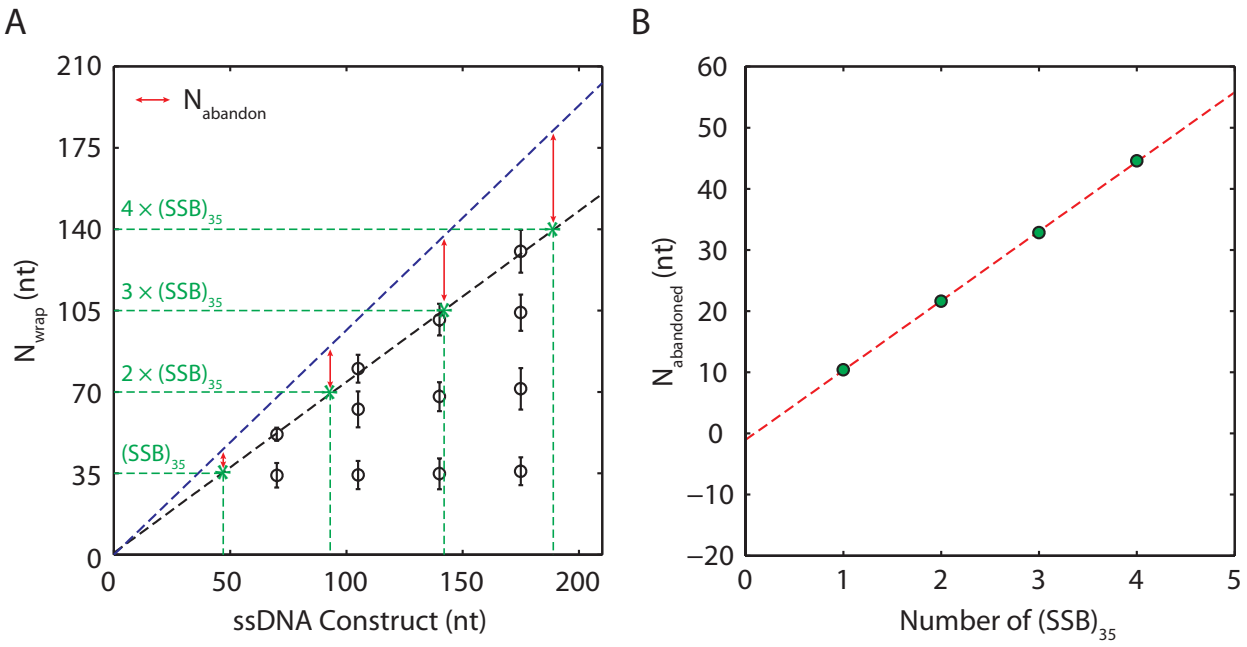

Figure 6.13: Abandoned nucleotides. (**A**) Data extrapolation demonstrating four DNA constructs of length 47, 94, 142, and 190 nt that wrap exactly 1, 2, 3, and 4 SSBs in $(SSB)_{35}$ binding mode (green lines). These SSBs only wraps 36, 72, 108, and 144 nt, abandoning ~11, 22, 34, and 46 nt, respectively (red arrowed lines). (**B**) Number of abandoned nucleotides vs. number of SSBs wrapping in $(SSB)_{35}$ binding mode. A red line is a linear fit to the data.

Next, we modeled our SSB oligomer as shown (Fig. 6.14). ssDNA is split into three segments. The first segment consists of nucleotides being wrapped by SSB, N_{wrap} (blue). The second segment contains nucleotides needed to bridge each pair of adjacent SSBs together, N_{link} (red). The last segment is composed of free nucleotides, N_{free} (green), which are randomly distributed along ssDNA, and not on SSBs.

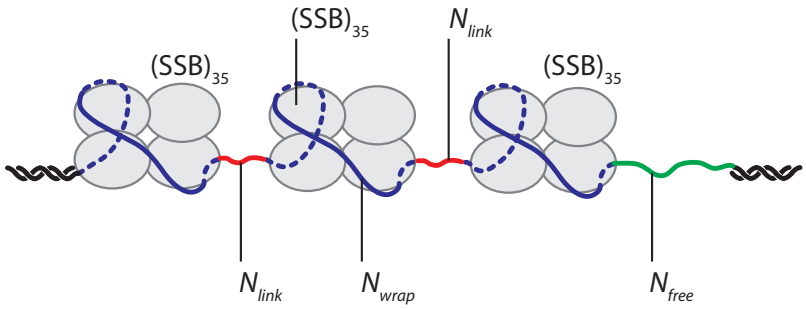

Figure 6.14: Model of SSB filament. Schematic representation of multiple SSBs forming a stable and long filament on ssDNA. A total number of nucleotides available is separated into three parts based on the location of nucleotides in the complex; (i) number of nucleotides wrapped by SSBs, N_{wrap} (blue), (ii) number of nucleotides bridged each pair of adjecant SSBs N_{link} (red), and (iii) number of free nucleotides N_{free} (green).

We assumed that the DNA construct contained M SSB and thus $M-1$ spacing between them. Putting all these together, the number of abandoned nucleotides, $N_{abandoned}$, was given by a simple equation:

$$\begin{aligned} N_{abandoned} &= N_{free} + (M-1)N_{link} \\ &= N_{link}M + (N_{free} - N_{link}) \end{aligned} \tag{6.3}$$

The equation (6.3) represents a linear function between the number of abandoned nucleotides, $N_{abandoned}$, and the number of SSBs, M, with a slope of N_{link} and a y-intercept of $N_{free}-N_{link}$. Fitting this equation to a plot in Figure 6.13(B), N_{link} and N_{free} are determined to be ~11 nt and ~10 nt, respectively. A summarized illustration of our model is shown (Fig. 6.15). For a DNA construct containing a single SSB, SSB wraps ~36 nt, and has extra ~10 nt of free nucleotides to diffuse around (Fig. 6.15(A)). For DNA constructs containing multiple SSBs, each SSB wraps ~36 nt. Approximately 11 nt are required to link a pair of adjacent SSBs together. Additional ~10 nt from the free nucleotides can be anywhere including the spaces between SSBs and the spaces between SSB and dsDNA, but not on any SSB (Fig. 6.15(B)).

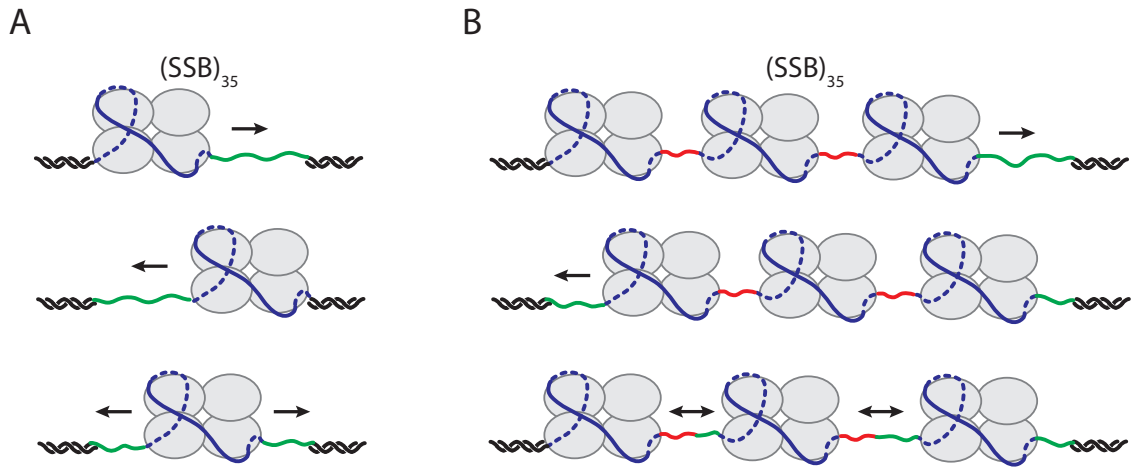

Figure 6.15: Model of SSB(s) wrapping. (**A**) Model of a single SSB wrapping and diffusing around ssDNA. (**B**) Model of multiple SSB wrapping ~36 nt ssDNA each (blue). Approximately 11 nt are required to link a pair of adjacent SSBs together (red). Free nucleotides can be anywhere, but not on any SSB (green).

Coupling these observations to a sliding diffusion mechanism of SSB in the $(SSB)_{35}$ binding mode (Chapter 5) provides insights into how SSB could be redistributed along ssDNA by other ssDNA binding proteins seeking access to unbound ssDNA. Previous work has proposed that different wrapping modes may be used selectively in different DNA metabolic processes (replication vs. recombination) [2]. How and which of these modes are used for particular processes remains unclear. We anticipate that the control of SSB wrapping modes into different SSB oligomerizations by applied force maybe a useful experimental tool to test this hypothesis.

Chapter 7

Interaction of SSB with RecA

Previous chapters described how a single SSB wraps ssDNA in different binding modes: $(SSB)_{65}$, $(SSB)_{56}$, $(SSB)_{35}$ and $(SSB)_{17}$, which wraps 65, 56, 35 and 17 nt of ssDNA, respectively. The same experiments also demonstrated that applying a mechanical force to the DNA tether, in particular at 5 pN, brings the SSB into the $(SSB)_{56}$ and $(SSB)_{35}$ wrapping mode selectively. Working at the solution conditions that favor these particular wrapping modes, we directly observed distinct SSB filament characteristics as well as their distinguishable filament formation processes. Under low salt and high SSB-to-ssDNA ratio, SSBs form a stable filament of $(SSB)_{35}$ on ssDNA. In contrast, high salt and low SSB-to-ssDNA ratio allow SSBs to form a bistable cluster wrapping in the $(SSB)_{35}$ and $(SSB)_{56}$ mode transiently.

In this chapter, we consider a possibility that these different SSB formations coupled with their capabilities to diffuse on ssDNA act as a controlling platform, and regulate other proteins accessibility to ssDNA. To validate our predition, we use a combined optical tweezers and confocal microscope (Fleezers) to first investigate a competitive behavior between a single SSB and many *E. coli* RecA on the ssDNA. Then, we examine the effect of multiple SSBs in different filament configurations on nucleation and filament formation of RecA.

We discovered that when RecA is added to ssDNA coated with a single SSB, filament formation is inhibited at low tensions. At higher tensions, where the SSB can partially unwrap from ssDNA, RecA forms a long filament after an extended lag time. During this process, the bound SSB is displaced and eventually replaced by RecA in a step-wise manner. Oligomerization of multiple SSBs, additionally, affects the nucleation rate of RecA. When SSBs are formed in isolate clusters of $(SSB)_{35}$/$(SSB)_{56}$, nucleation rate of RecA is slowed down by a factor of ~3.5 compare to the RecA nucleation rate on a bare DNA. When SSBs are stably bound as a long filament, nucleation rate further reduced by another ~1.5 fold. Our result reveals an importance of SSB binding modes and their oligomerizations to DNA recombination, and suggests that the $(SSB)_{35}$ binding mode is unlikely responsible for this

process.

7.1 Introduction

DNA inside a cell is continuously damaged through several channels, including environmental exposure to irradiation, chemical agents, or UV light. Products of the cell's own metabolism such as reactive oxygen species can also damage the DNA. These damages are usually categorized into two main types: a single-stranded DNA (ssDNA) damage and a double-stranded DNA (dsDNA) break. Single-stranded DNA damages, a nick or a lesion for examples, can be repaired by removing a damaged nucleotide and replacing it with an intact DNA using the other strand as a template. Double-stranded DNA breaks, in contrast, are harder to fix and more lethal than ssDNA damage due to a possibility of genome rearrangement.

Some DNA metabolic processes such as DNA replication can turn a ssDNA damage into a dsDNA break. During DNA replication, nucleoprotein complexes at the replication fork may encounter the sites of DNA damage or other obstacles. This results in a collapse of replication forks, creating a dsDNA break in the process (Fig. 7.1). An elaborate collaboration of many DNA metabolism enzymes is required to repair this collapse, and restart the replication on-site (independent of the origin).

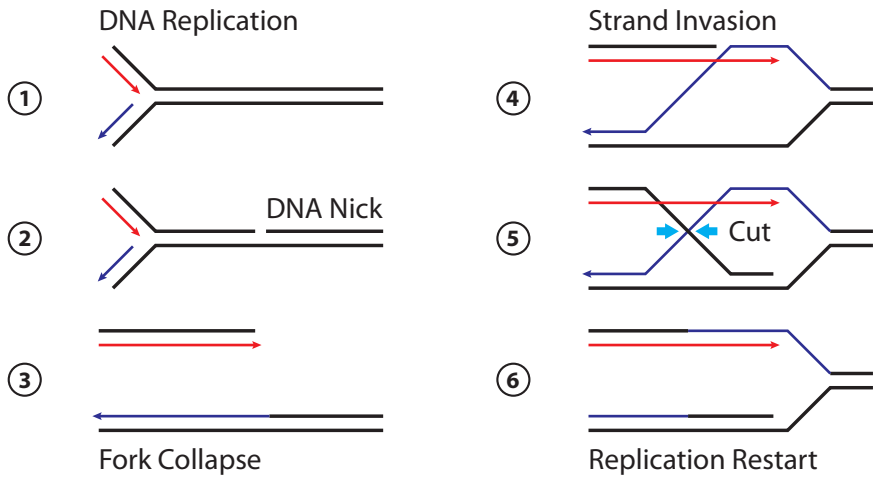

Figure 7.1: Repair of the double-stranded DNA break. A single-stranded DNA damage can lead into a double-stranded DNA break during a DNA replication (1-3). Cell selects homologous recombination to repair this break and restart the process (4-6). Colors are used to distinguish the DNA products from the DNA template. Illustrations were adapted from [102].

One of the repairing pathway in *E. coli*, for example, utilizes a set of proteins including

RecBCD helicase, RecA recombinase, and SSB protein to process the broken dsDNA end into a 3' ssDNA overhang, and reconnects it with the other strand through homologous recombination. RecBCD is involved primarily in unwinding and cleaving the broken dsDNA end, and is not discussed further. Previous chapters have extensively described and investigated SSB and its interaction with the DNA. This chapter, we introduce an *E. coli* recombinase named RecA and its functionality. Interaction between RecA and SSB is also reviewed.

7.1.1 *E. coli* RecA and its Functionality

E. coli RecA is a DNA-dependent ATPase and an ATP-dependent DNA binding protein. It consists of 352 amino acid residues and weighs ~38 kDa. Under normal conditions, there are ~8,000 to 10,000 monomers of RecA per cell. This number can increase to 70,000 upon DNA damage [103].

X-ray crystal structure revealed three important domains of *E. coli* RecA ([104], Fig. 7.2): a central core, an N-terminal, and a C-terminal domain. The N-terminal domain is considered to be involved specifically in monomer-monomer interactions [104, 105]. The core domain (34-269 AA) is highly conserved among bacteria species and even among eukaryotic homologs. It contains an ATP binding site (47-74 AA) and possible DNA binding sites [102]. Studies have speculated that two disordered loops, L1 (151-176 AA) and L2 (190-227 AA), are responsible for the DNA binding [106–108]. In contrast to the core domain, the C-terminal domain (270-352 AA) exhibits almost no sequence conservation. Studies suggested that it may be responsible for an active or inactive state of the RecA filament [109]. The last 25 residues of RecA (328-352) was found to be highly negative charged. It has been proposed that these negatively charged residues regulate the direct binding of RecA to dsDNA by electrostatically repelling the phosphate backbone of the DNA [110, 111].

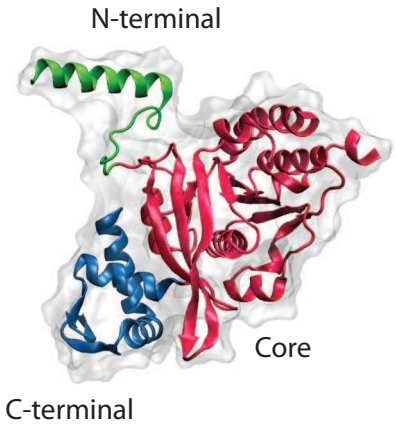

Figure 7.2: *E. coli* RecA. Crystal structure of *E. coli* RecA monomer showing three domains. The core domain (red) contains an ATP and DNA binding sites. The N-terminal domain facilitates an interaction between two RecA monomers, while the C-terminal domain regulates a double-stranded DNA binding.

E. coli RecA binds to DNA in multiple steps that results in an establishment of a nucleoprotein filament. Slow nucleation of RecA onto the DNA occurs first, followed by a rapid elongation of the filament. Nucleation is much faster on ssDNA than on dsDNA, and generally sequence-independent. Recent studies have shown that ~2 [5] or ~5 [112] RecA monomers are required to nucleate filaments. Types of nucleotide cofactor and concentration of magnesium ion plays an important role in the nucleation speed [5].

After nucleation, RecA monomers polymerize DNA to form a long filament. In the presence of ATP or its analog (ATP-γ-S), the filament is considered *active*, forming a right-handed helical filament. Each turn of the filament consists of six RecA monomers, and each monomer occupies three nucleotides of DNA [104]. Upon filament formation, DNA is extended by ~50-60% relative to the B-form DNA [113, 114]. On the other hand, RecA filament is not stable or *inactive* in the absence of ATP. It exhibits a smaller helical pitch and a smaller axial rise [115] than the active one. Filament growth is bidirectional on both ssDNA and dsDNA although faster in the 5' to 3' direction [5].

7.1.2 Influence of SSB on RecA Filament Formation

In the initial state of homologous recombination, RecBCD binds to dsDNA break and proceeds to unwind while simultaneously cleaves one of the DNA strands, resulting in a 3' single-stranded DNA overhang. At this point, ssDNA is exposed to the surrounding envin-

ronment and prone to nucleolytic and chemical attacks. Due to a slow nucleation of RecA onto ssDNA, SSB generally outcompetes RecA, and occupies most of the nucleotides (Fig. 7.3, top panel). Previous studies have demonstrated that SSB kinetically blocks RecA assembly by continuously binding and sequestering ssDNA [5]. The presence of already bound SSB also inhibits RecA filament formation on ssDNA, slowing down its nucleation rate [116, 117]. Since this inhibitory behavior of SSB is very strong, several studies suggested that accessory proteins are necessary to help loading RecA onto ssDNA [118, 119].

7.1.3 Previous Studies & Open Questions

Interaction between SSB and RecA on ssDNA has been extensively investigated. Bulk studies by Kowalczykowski et al. demonstrated that a number of variables such as order of addition, temperature, types of ssDNA, and magnesium concentration has an effect on SSB-RecA binding to ssDNA [34]. In general, when SSB is added to the ssDNA solution prior to the addition of RecA, a significant inhibition of RecA activity is observed. On the contrary, if SSB is added after RecA nucleoprotein filament is already formed, RecA activity varies based on the effect of other variables. The other study considered a possibility that SSB binding configurations might have a direct impact on RecA formation. Using electron microscopy, Griffith et al. showed that RecA is capable of assembling on ssDNA coated with beads-on-a-string $(SSB)_{65}$ clusters where the protein-free linker regions between SSB clusters provided access to the DNA [3].

Recent development in single-molecule techniques have shed some light on deeper understanding of SSB-RecA interaction. Joo et al. used single-molecule FRET to show that RecA can displace SSB with little resistance, and therefore the binding of SSB must be very weak compared to the force exerted by RecA filament [112]. In addition to Joo's studies, Roy et al. developed a three-color FRET to measure the displacement and removal rate of SSB while the RecA filament formation occurred. The study demonstrated that extension rate of RecA filament is comparable to the SSB displacement rate, and both are much higher than the removal rate of the SSB [4]. Direct imaging from TIRF microscopy exhibited that RecA is capable of nucleating and growing the filament on an SSB-coated ssDNA substrate [5]. The study also showed that both nucleation and growth rate depend on various conditions, including magnesium concentration, pH, and types of nucleotide cofactor. Magnetic tweezers experiment by Fu et al. used force to probe a physical picture of the competition between

RecA and SSB. The study showed that applying force to the ssDNA displaces SSB, and allows RecA to assemble filament [6].

Despite tremendous effort, the fundamental mechanism behind SSB displacement and dislodgement by RecA remains unclear. To date, many studies have only shown that RecA is capable of replacing SSB by pushing the SSB of the 3' end (Fig. 7.3). However, not all SSBs experience the same removal mechanism. Bell et al. demonstrated that growth of RecA filament is bidirectional and several filaments can be formed randomly along the ssDNA [5]. Following this observation, we predict that when these filaments grow in the opposite direction, some SSBs sandwiched by two RecA filaments are squeezed, and eventually dismissed from ssDNA. Moreover, SSB residing at the dsDNA-ssDNA junction encounters similar situation where it is pushed and possibly forced out by RecA.

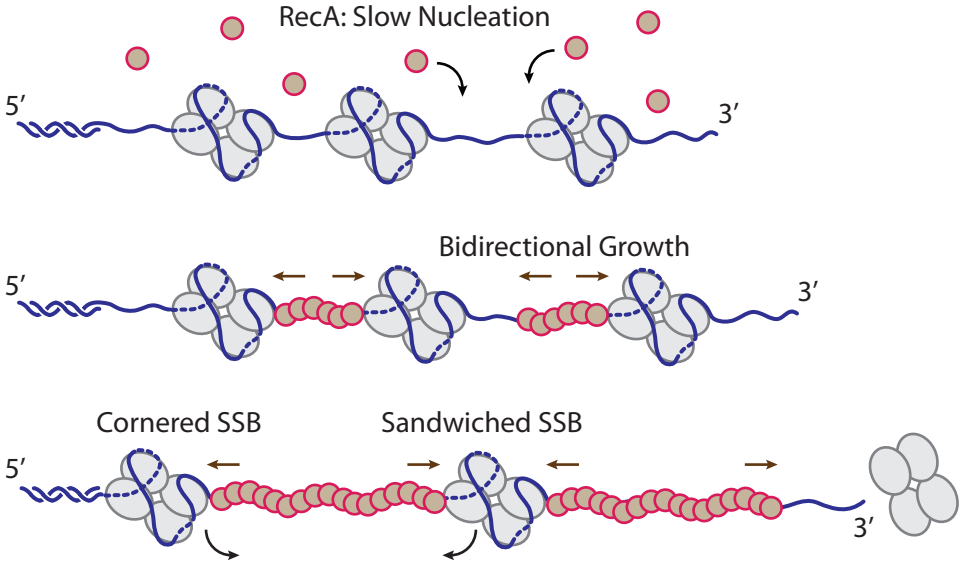

Figure 7.3: Model of initial state of homologous recombination. Cartoon schematics showing competitive behaviors between SSB and RecA. SSB quickly occupies exposed ssDNA due to its high affinity and a slow nucleation rate of RecA (top). After a period of time, RecA successfully nucleates on ssDNA (middle), and starts displacing SSB from ssDNA either by pushing the SSB off or forcing the SSB out (bottom).

The relationship between SSB binding configurations and RecA filament formation is also still ambiguous. Studies have shown that SSB binding in $(SSB)_{65}/(SSB)_{56}$ mode serves as an assembly factor for RecA binding to ssDNA by leaving gaps between bead-liked clusters [3]. On the other hand, unlimited cooperativity binding of SSB in $(SSB)_{35}$ mode is expected to inhibit RecA filament formation by fully occluding the ssDNA.

Using a high-resolution optical tweezers combined with a confocal microscope, we observe how SSBs in different binding configurations affect RecA filament formation on ssDNA. The same experiments also reveal competitive behaviors as well as the dissociation of SSB by RecA filament formation.

7.2 Experimental Procedure

Previously designed in Chapter 6, two DNA constructs containing 70-nt and 140-nt ssDNA binding site were initially used in the RecA experiment (dT70, dT140: Appendix A). Soon after, these constructs were modified to an improved version which contains PEG-liked linkers on both ends of the ssDNA (dT70sp and dT140sp: Appendix A). We used these improved constructs throughout the rest of the chapter.

Wild type *E. coli* SSB (SSB) and fluorescently labeled *E.coli* SSB (SSB_f) were generously provided by the Lohman's lab (Appendix A). In a typical RecA experiment, three trapping buffers containing 125 nM RecA plus 125 μM ATP-γ-S, 0.5 nM SSB, and protein-free were prepared (Appendix A). These buffers contained the ionic concentration that was known to favor the $(SSB)_{65}$ binding mode. An oxygen triple-state quencher was added to prevent fluorophore blinking [91] if SSB_f was used in the experiment.

In section 7.5, two additional buffers containing different ionic conditions were used (Appendix A). Concentration of RecA and ATP-γ-S was adjusted to suit the experiment which will be described in the section.

Depending on the experiment, only two buffers were chosen at a time. These selected buffers, beads, and DNA were loaded to the chamber in the same way previously described in Chapter 2. We trapped and calibrated the beads, formed tether in a non-RecA stream, and executed the tether qualification.

7.3 Filament Formation of RecA on ssDNA

In order to achieve our main goal to understand the interaction between RecA and SSB on a ssDNA, we first needed to understand fundamental properties of RecA-ssDNA complex. A constant force of various magnitudes was used to hold a DNA construct containing 70-nt ssDNA in the protein-free stream. The tethered construct was moved into the buffer containing RecA plus ATP-γ-S, maintaining a constant tension throughout. After some

time, RecA nucleated on ssDNA, and filaments were formed (Fig. 7.4(A)). Positive change in extension illustrated DNA stretching done by RecA [113, 114]. A controlled experiment was performed on a DNA construct containing dsDNA handles alone (no ssDNA). Under our experimental condition, we did not observe any RecA filament formation, Δx ~0, in all force ranges (Fig. 7.4(B)).

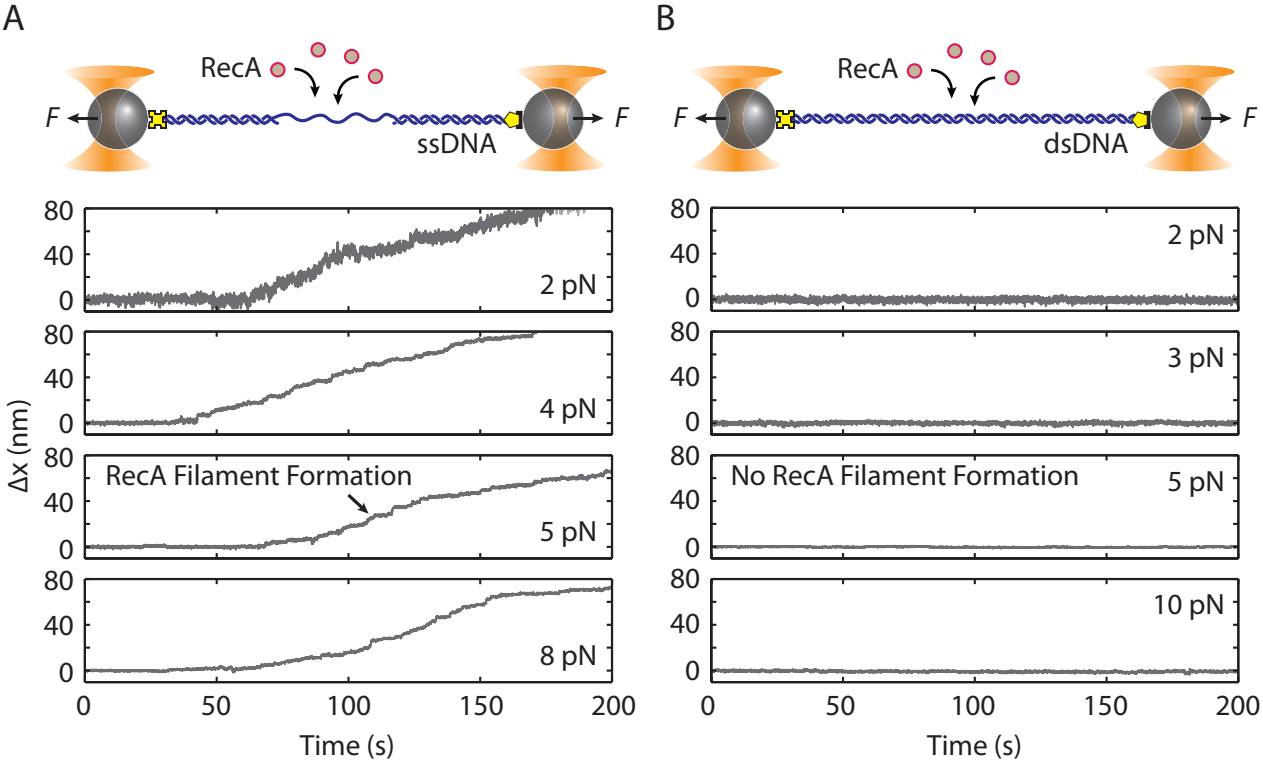

Figure 7.4: RecA filament formation on ssDNA. (**A**) A DNA construct containing 70 nt poly-dT ssDNA is held under a constant tension between 2-10 pN in the presence of RecA and ATP-γ-S. After a period of incubation, positive changes in extension are observed, indicating that RecA forms filament and extends the DNA. (**B**) No RecA filament formation is observed on dsDNA regardless of tension.

Previous studies have reported that RecA filament extended the ssDNA by 50-60% compared to B-form dsDNA [113, 114]. Since our ssDNA construct only contained 70-nt of ssDNA, we expected our change in extension to be in the range of ~10-20 nm based on the polymer elasticity model [93]. Interestingly, our results demonstrated otherwise. Under all tensions, changes in extension increased beyond what we expected. We considered a possibility that RecA nucleated on ssDNA, polymerized onto the dsDNA, and therefore extended all available DNA for a long period of time (Fig. 7.5).

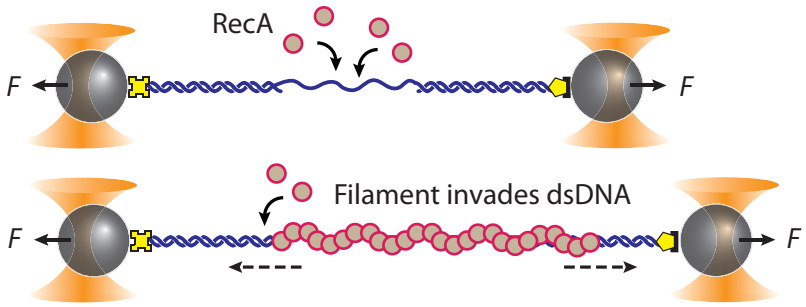

Figure 7.5: Polymerization of RecA on double-stranded DNA. Cartoon schematics demonstrating nucleation of RecA filament on ssDNA. Additional RecAs elongate filament onto both size of the dsDNA handles. Experimental data in (Fig. 7.4(A)) confirms our interpretation.

In fact, RecA's ability to elongate into the dsDNA hindered our observation. We were unable to distinguish RecA polymerization along the ssDNA from that along the dsDNA handles. Changes in extension measured from the optical traps would be the combination of the two.

To overcome this issue, we incorporated two spacers consisting of a PEG-liked molecule to both ends of the ssDNA segment (Fig. 7.6(A), PEG18). The spacer provided an extra length to separate ssDNA from dsDNA handles, preventing RecA to assemble through. We repeated the RecA assembly experiment on this new construct under a constant force of 5 pN , and found out that RecA filament formation stopped upon reaching the spacers (Fig. 7.6(B)). Change in extension of RecA-bound DNA gradually increased from 0 nm (bare DNA) to ~9 nm, and stayed constant for a very long time. A combined extension change distribution from many filament formation events at 5 pN confirmed this pausing. We predicted that RecA polymerized along ssDNA, reached the spacers, and stopped the filament formation.

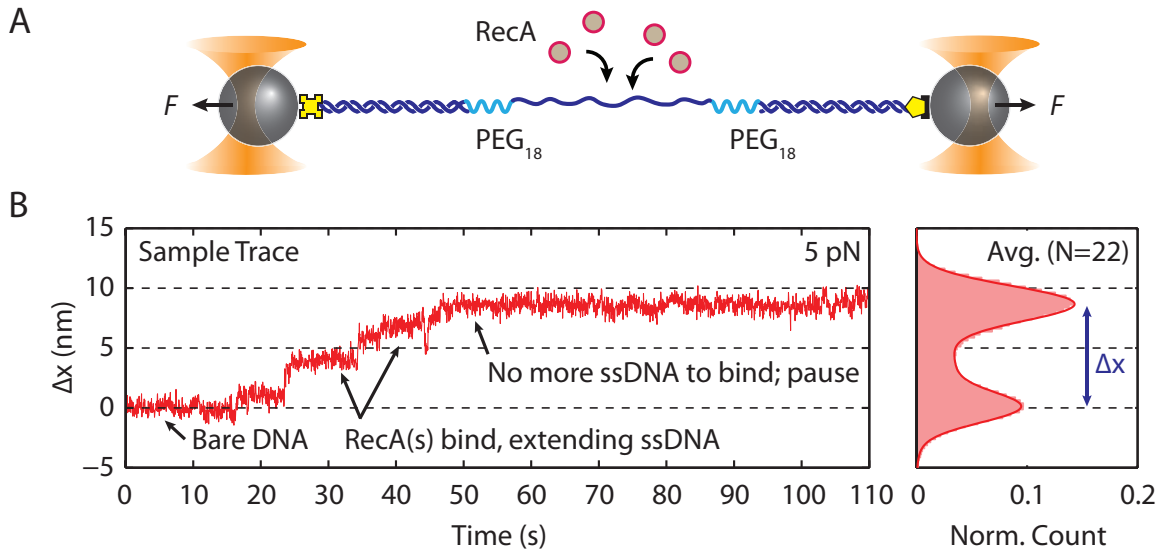

Figure 7.6: RecA filament formation on modified ssDNA. (**A**) A standard DNA construct consisting of a 70-nt ssDNA is engineered to contain two PEG-liked spacers locating at both ss-dsDNA junctions (PEG18, cyan). (**B**) Representative change in extension vs. time trace showing RecA filament formation stops upon reaching the spacers. A combined population distribution demonstrates the RecA pausing

The difference between two peaks of the distribution, Δx_{trap}, was compared against the polymer model of elasticity [93, 94] to validate our prediction.

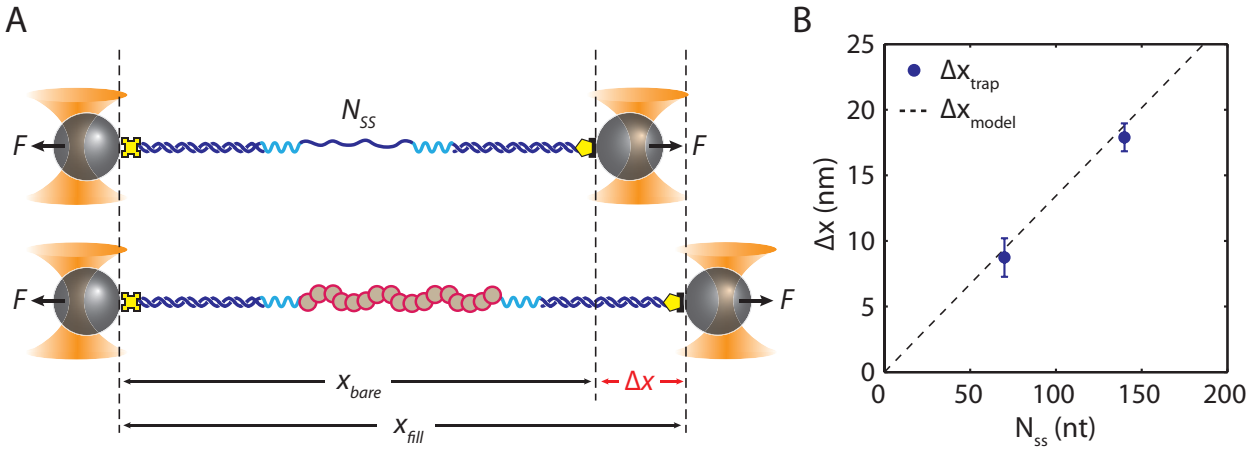

Figure 7.7: DNA extension upon formation of RecA. (**A**) A modified DNA construct containing N_{ss}-nt ssDNA illustrating its extension before (x_{bare}) and after (x_{fill}) RecA filament formation. *Deltax* denotes an extension difference between a bare DNA and a RecA-filled DNA. (**B**) The extension difference obtained from experiment (blue dots) are in an excellent agreement with the polymer model of elasticity (black dashed line).

As shown in Figure 7.7(A), the extension of the bare DNA, x_{bare} is given by Eq. (2.1):

$$x_{bare} = \xi_{ss}(F) \cdot N_{ss} + \xi_{ds}(F) \cdot N_{ds}$$

Filling the ssDNA with RecA extends the DNA by 50% compared to B-form dsDNA. The extension of the filled DNA molecule, x_{fill} is thus:

$$x_{fill} = 1.5 \times (\xi_{ds}(F) \cdot N_{ss}) + \xi_{ds}(F) \cdot N_{ds}$$

The extension change upon assembling, Δx_{model}, is simply the difference between x_{fill} and x_{bare}:

$$\Delta x_{model} = N_{ss} \left(1.5 \times \xi_{ds}(F) - \xi_{ss}(F)\right)$$

The predicted extension change, Δx_{model} was illustrated against the number of ssDNA nucleotides bound by RecA (Fig. 7.7(B), black). Our experimental data agreed well with the prediction (blue circle), indicating that RecA fully polymerizes on ssDNA and stops the elongation process at the ss-dsDNA junctions.

7.4 Interaction of RecA Filament with Single SSB

To examine behaviors of the DNA molecule in the presence of a single SSB and RecA, we modified our solution streams in the experimental chamber slightly. One stream contained trapping buffer plus 125 nM RecA and 125 μM ATP-γ-S, while the other contained buffer plus 0.5 nM SSB (Fig. 7.8). We formed a DNA tether in the SSB stream, maintaining it under a constant tension (Position 1). After one SSB bound, the tether was moved into a stream containing RecA (Position 2).

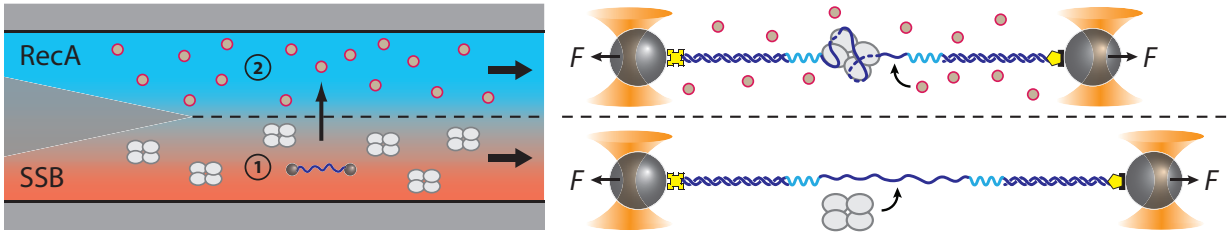

Figure 7.8: RecA filament formation on a single SSB assay. Two separate streams containing experimental buffer plus SSB (red, Position 1) and buffer plus RecA and ATP-γ-S (blue, Position 2) form a laminar interface. After a single SSB binds to ssDNA, the tether is moved into the RecA stream where the observation is made.

At low tension (~2 pN), we observed individual SSBs to bind and compact ssDNA in a single step (Fig. 7.9, blue interval). Based on our analysis from Chapter 4, this negative change in extension corresponded to a single SSB binding in the $(SSB)_{56}$ binding mode. The SSB remained bound in this binding mode upon entering the RecA stream (red interval). Despite being surrounded by a very high concentration of RecA, the SSB stayed bound to ssDNA for a very long period of time ($>$ 600 s). A combined extension change distribution from many events at ~2 pN confirmed our observation. RecA could not nucleate on ssDNA, and the filament formation was prohibited. We considered a possibility that RecA did not have enough ssDNA nucleotide to nucleate on. Previous work from Joo et al. showed that ~5 monomers of RecA occupying ~17 nt are required to initiate the nucleation [112]. In our case, 56 nt of ssDNA was wrapped by the SSB, leaving merely 14 nt available. In additions, experimental result from Chapter 5 demonstrated a capability of SSB to diffuse along ssDNA while wrapping in different modes. This diffusion results in even less number of effective nucleotides for RecA to nucleate on at any given time.

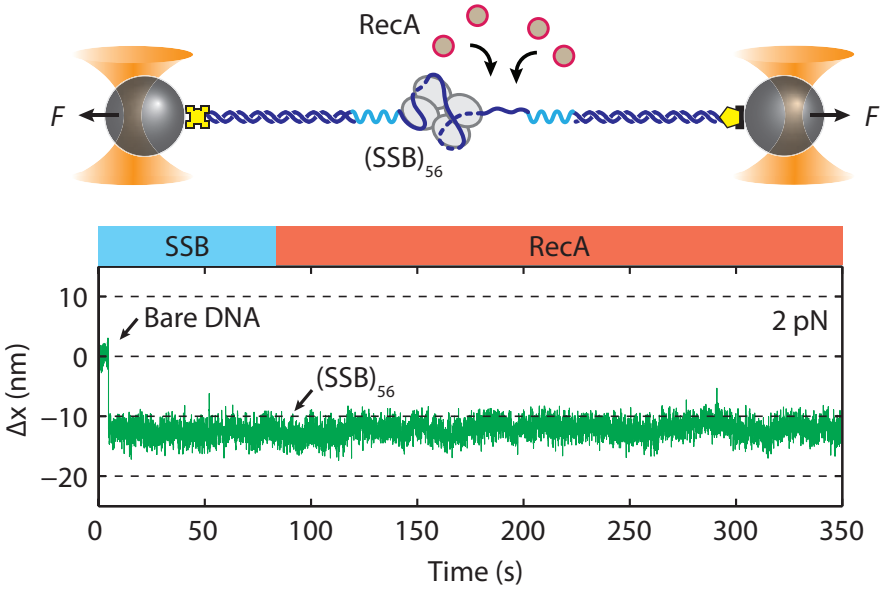

Figure 7.9: Inhibition of RecA filament formation. A single SSB wrapping ssDNA in $(SSB)_{56}$ binding mode under a constant tension of 2 pN (top). Under this wrapping mode, RecA filament formation is inhibited as indicated by no change in extension of the DNA after a very long time (bottom).

In contrast, we observed a drastically distinct outcome under high tension (~5 pN). In the absence of RecA, a single SSB bound and condensed ssDNA in two steps which corresponds to the $(SSB)_{35}$ and $(SSB)_{56}$ binding configuration, respectively (Fig. 7.10, blue interval). Under this condition, SSB may diffuse or transiently switch between binding modes without dissociating from ssDNA. The dynamic transitions between two modes persisted upon a movement of the nucleoprotein complex into the stream containing RecA (red interval). Interestingly, RecA formed filament when SSB wrapped ssDNA in the $(SSB)_{35}$, but not in the $(SSB)_{56}$ binding mode (orange arrow).

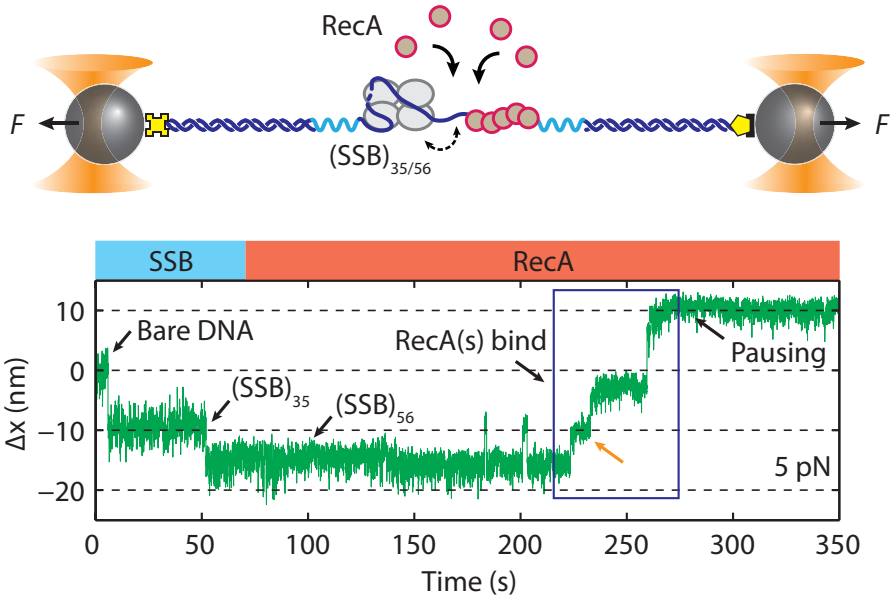

Figure 7.10: Facilitation of RecA filament formation. Transient wrapping-unwrapping between $(SSB)_{56}$ and $(SSB)_{35}$ binding modes of a single SSB under a constant tension of 5 pN facilitates RecA filament formation. Formation of RecA extends DNA (blue box), displaces the SSB, and stops after reaching PEG-liked spacers at the ss-dsDNA junctions.

Similar to RecA filament formation on a bare DNA (Fig. 7.6(B)), a long pause of the RecA filament formation on an SSB-bound DNA was also observed. Interestingly, these pause occurred at the same extension change of ~9 nm. Since we initially defined $\Delta x = 0$ nm as a bare DNA, $\Delta x = 9$ nm indicated a complete polymerization of RecA on the ssDNA. Our result not only showed that RecA can nucleate and form filament, but it also demonstrated that filament formation is capable of removing SSB from the ssDNA.

To investigate the removal of SSB by RecA further, we selected and examined a range of data from the moment filament formation started to the moment formation ended (Fig. 7.10, blue box). A combined extension change distribution from many SSB removal events were shown (Fig. 7.11). Surprisingly, RecA does not gradually replace SSB. Instead, the removal appears to happen in several bursts. We correlated this result with the SSB wrapping configurations, and hypothesized that RecA utilized the transient switching between SSB modes to displace the SSB.

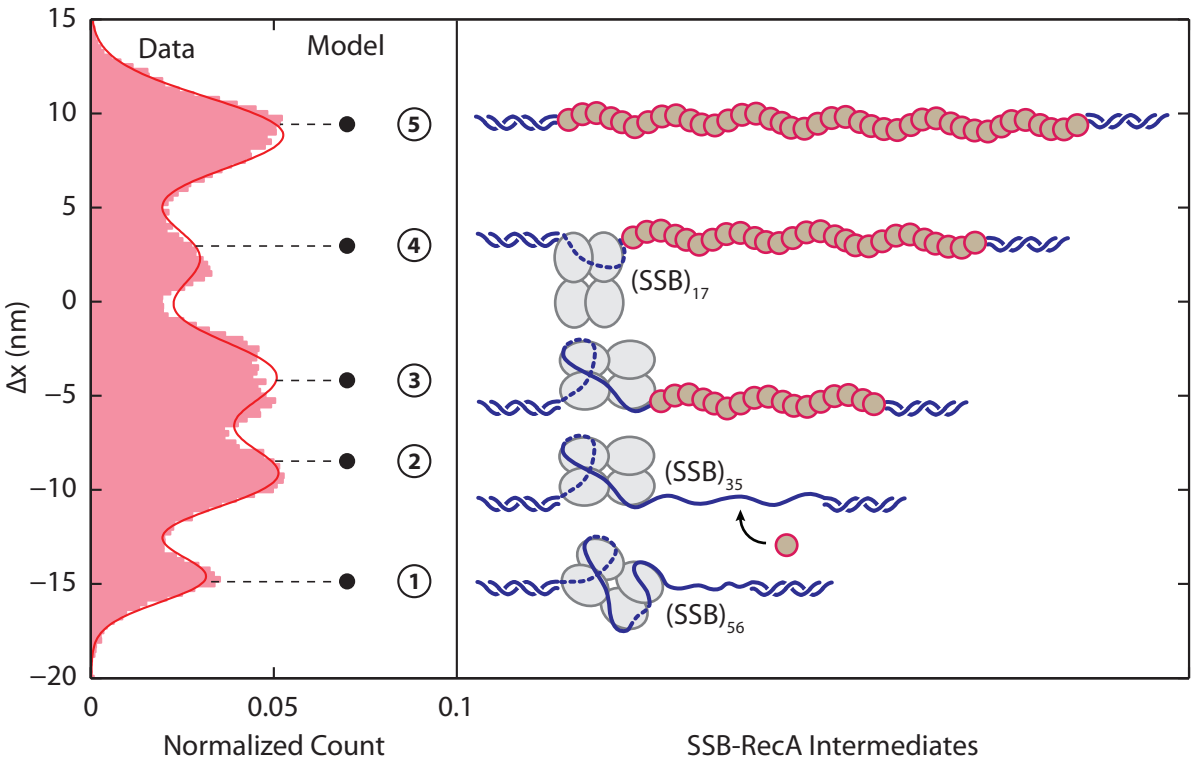

Figure 7.11: Dissociation of SSB upon RecA filment formation. Extension change distribution of RecA formation events (N=40) at a constant tension of 5 pN (pink). A solid red line is a multi-Gaussian fit to the distribution. Five states representing SSB-RecA dissociation intermediates are illustrated and assigned to peaks of the distribution. Polymer model of elasticity predictd the DNA extension according to the illustration, and demonstrated an excellent agreement with the data (black dots).

In order to validate our prediction, we developed a simple model using basic geometry and polymer elasticity theories [93, 94]. First, we assigned five states representing SSB-RecA removal intermediates to the peaks of distribution (Fig. 7.11). The first two states were previously established in Chapter 4. State *'1'* represented SSB wrapping in $(SSB)_{56}$ mode, while state *'2'* corresponded to SSB wrapping in $(SSB)_{35}$ mode. State *'5'* was recently demonstrated to be a state where RecA fully assembled on ssDNA. We made an assumption that RecA polymerized and filled all unwrapped nucleotides in state *'3'*. In state *'4'*, we predicted that RecA polymerized ssDNA further and forced SSB to be in $(SSB)_{17}$ wrapping mode. Schematics of five nucleoprotein states were displayed next to the histogram accordingly (Fig. 7.11).

Next, we defined the extension of the DNA molecule at each state as:

$$
\begin{aligned}
x_1 &= x_{hd}(F) + x_{SSB}^{eff}(N_w{\sim}56, F) + \xi_{ss}(F) \cdot (N_{ss}{\sim}14) \\
x_2 &= x_{hd}(F) + x_{SSB}^{eff}(N_w{\sim}35, F) + \xi_{ss}(F) \cdot (N_{ss}{\sim}35) \\
x_3 &= x_{hd}(F) + x_{SSB}^{eff}(N_w{\sim}35, F) + 1.5 \times (\xi_{ds}(F) \cdot (N_{ss}{\sim}35)) \\
x_4 &= x_{hd}(F) + x_{SSB}^{eff}(N_w{\sim}17, F) + 1.5 \times (\xi_{ds}(F) \cdot (N_{ss}{\sim}53)) \\
x_5 &= x_{hd}(F) + 1.5 \times (\xi_{ds}(F) \cdot (N_{ss}{\sim}70))
\end{aligned}
$$

where $x_{hd}(F)$ is the extension of the dsDNA handles at force, F, and $x_{SSB}^{eff}(N_w, F)$ is an effective size of the SSB wrapping N_w nucleotides. By setting x_5 ~9 nm, the relationship between our predicted DNA extension and nucleoprotein state was shown (Fig. 7.11, black dots). Overlapping experimental data obtained from the distribution on top of the plot revealed consistency between our results and a model (black dashed lines).

7.5 Interaction of RecA Filament with SSB Oligomers

Results from the previous section coupled with an observation of SSBs forming SSB filament from Chapter 6 provided us a capability to investigate the interaction between multiple SSBs and RecA. Briefly, the experiments in Chapter 6 demonstrated that applying force of 5 pN in suitable solution conditions populated multiple SSBs into two different configurations: (i) a long and stable SSB filament, (ii) isolated SSB clusters separated by ssDNA gaps. By Adding RecA into these DNA-SSBs configurations, we expected to observe distinguishable roles of these SSB configurations on RecA accessibility to ssDNA.

To examine this matter, we initially held a 140-nt poly-dT ssDNA construct accommodating two PEG-spaces in three different solution conditions containing no RecA nor ATP-γ-S (Fig. 7.12, Position 1). The first solution contains RecA trapping buffer only (left). The second solution consists of a solution that is favorable to $(SSB)_{65}$ binding mode and 0.5 nM SSB (middle). In this condition, SSBs form isolated clusters of $(SSB)_{56}$ on the DNA. The last solution contains a solution that favors $(SSB)_{35}$ binding mode and 5 nM SSB (right). A long SSB filament is formed in this condition as shown schematically. The tethered DNA was then moved into the top channel containing RecA trapping buffer (Appendix A) plus 375 nM RecA and 375 μM ATP-γ-S for observation (Position 2).

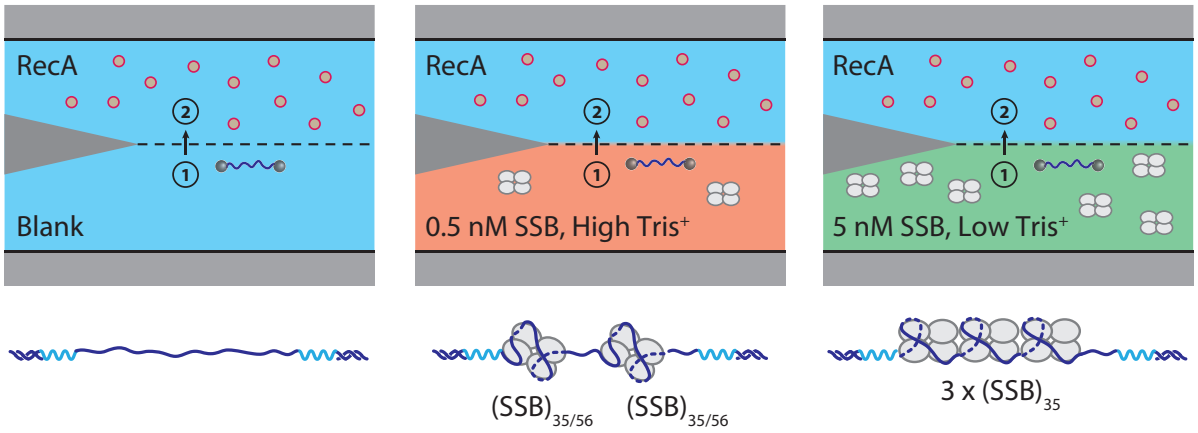

Figure 7.12: RecA filament formation on SSB oligomerization assay. Cartoon schematics of three experimental chambers containing different solution conditions in the bottom streams; (i) RecA trapping buffer containing no protein (blue), (ii) $(SSB)_{65}$ trapping buffer plus 0.5 nM SSB (red), and (iii) $(SSB)_{35}$ trapping buffer plus 5 nM SSB (green). The top stream of all three consists of RecA trapping buffer plus 375 nM RecA and 375 μM ATP-γ-S. A 140-nt poly-dT ssDNA construct is initially held at a constant force of 5 pN in the bottom stream (Position 1). The DNA is moved into the top stream for an observation of RecA filament assembly.

Figure 7.13 demonstrated three distinct representative time traces from experimental setups described above. Time $t = 0$ was recorded when the tether crossed the laminar interface into solutions containing RecA. Extension changes were offset to the positions where $\Delta x = 0$ nm corresponds to a bare DNA and $\Delta x \sim -30$ nm indicates two and three SSBs bind in $(SSB)_{56}$ and $(SSB)_{35}$ binding modes, respectively.

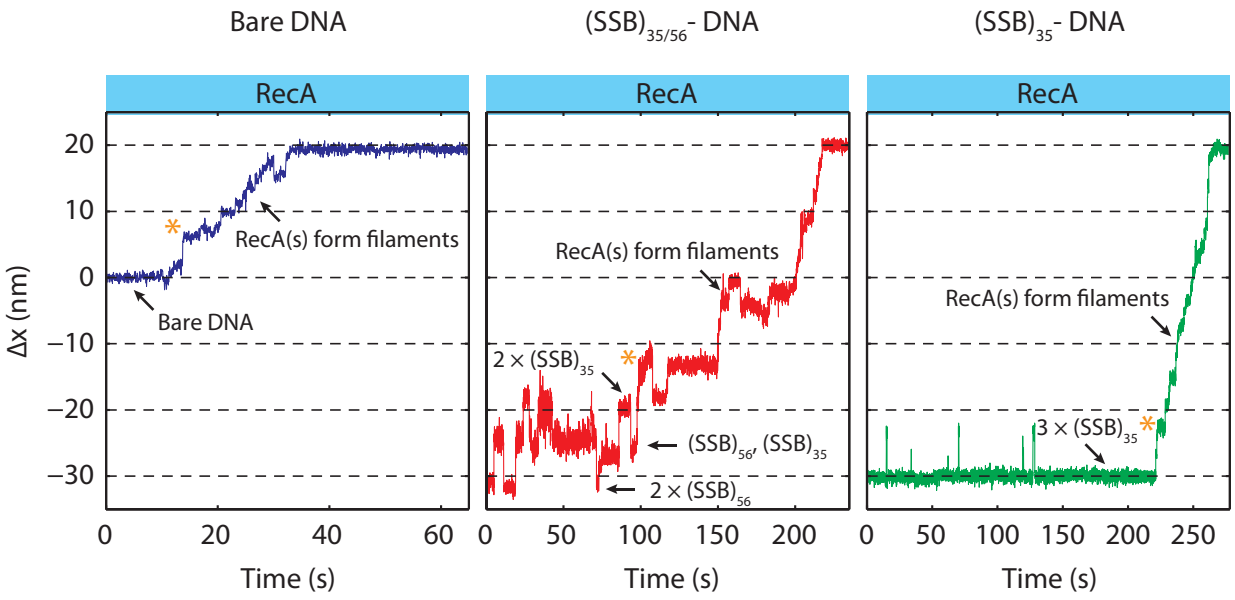

Figure 7.13: Effect of SSB binding modes on RecA filament formation. Representative time traces of showing RecA filament formation on a 140-nt construct containing no protein, two SSB transiently wrapping in $(SSB)_{56}$, and three SSB stably binding in $(SSB)_{35}$ binding mode. Extension change of Δx ~19 nm depicts a state where a RecA filament fully fills the ssDNA, displacing all SSBs in the process.

Without any quantitative data analysis, we already noticed many interesting features from these example traces. First, we observed long pauses of the RecA filament formation process in all three cases. For a bare DNA (left), RecA formed filament and stopped at Δx ~19 nm, in an agreement with the previous report (Fig. 7.7(B)). When the DNA was bound by SSBs (middle and right), RecA assembled filaments, and paused at the same extension change Δx ~20 nm, indicating that all SSBs were completely removed by the RecA filament. In additions, we observed the time waited for the RecA to polymerize varied significantly among different cases. RecA nucleated and formed filament quickly in the absence of SSB (left), while the same process occurred much slower if SSBs were present (middle and right). We considered a possibility that multiple SSBs oligomerization affected the RecA accessibility to ssDNA. Representative time traces demonstrated that RecA filament formation occurred faster when RecA was added to ssDNA wrapped by isolate clusters of $(SSB)_{56}$ (middle) than ssDNA wrapped by long filaments of $(SSB)_{35}$ (right).

To investigate this further, we determined a timestamp measured when RecA began the polymerization in all three scenarios (Fig. 7.13, asterisks). In some events, RecA did not form filaments after a very long time (t > 300 s). Timestamps in these cases were recorded

when the data acquisition stopped. Combining all events together, we counted how many times the polymerization have succeeded at time t $N_{success}(t)$, and compared to the number of polymerization failures, $N_{failure}(t)$. The probability of RecA filament formation after time t has passed, $p_{success}(t)$, could be expressed as

$$p_{success}(t) = \frac{N_{success}(t)}{N_{success}(t) + N_{failure}(t)} \tag{7.1}$$

Figure 7.14 demonstrated $p_{success}(t)$ distributions of three different ssDNA constructs over time (solid lines). In general, at any given time, RecA has a higher chance to successfully polymerize on a bare DNA (blue) than on a bound DNA (red and green). We fitted these distribution to a cumulative distribution function, $1 - e^{-t/\tau}$, to determine an average time spent waiting for the polymerization to occur, τ.

In the absence of SSB, RecA nucleated on ssDNA rapidly (blue). On average, it took τ_{bare} ~48 s for RecA to nucleate on a bare ssDNA. When isolated clusters of SSBs were present on ssDNA, in contrast, the nucleation time increased to $\tau_{cluster}$ ~144 s (red). We also noticed a time delay of ~20 s where RecA never formed before this timestamp. Adding this time delay to the nucleation time, we determined a lag time before filament formation to be ~164 s. The result demonstrated a consistency with the previous studies where the presence of already bound SSB inhibits RecA filament formation on ssDNA by slowing down its nucleation rate [116, 117]. Interestingly, when multiple SSBs were allowed to preform a stable and long filament of the $(SSB)_{35}$ binding mode on ssDNA, RecA took an even longer time to nucleate. The lag time including a very long time delay was determined to be ~237 s.

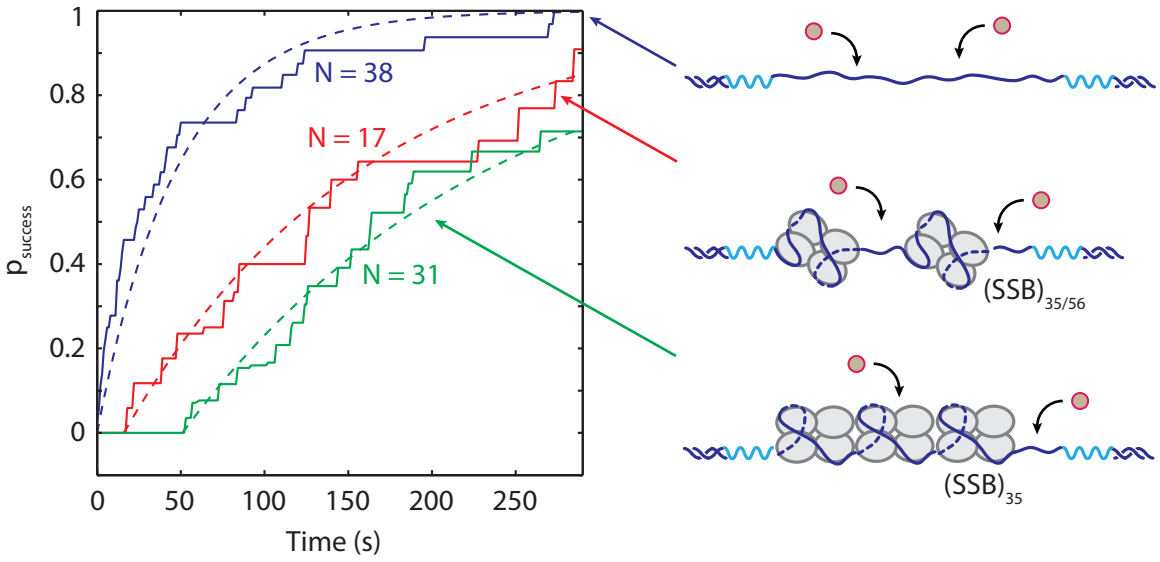

Figure 7.14: Success rate of RecA filament formation. Cumulative probability distributions showing a success chance of RecA filament formation on three different DNA constructs containing no protein (blue), two SSB transiently wrapping in $(SSB)_{56}$ (red), and three SSB stably binding in $(SSB)_{35}$ binding mode (green). Dashed lines are cumulative distribution function, $1 - e^{-t/\tau}$, fits to the distributions.

Our results demonstrated the effect of SSB binding modes on RecA filament formation. In the presence of SSBs regardless of their binding modes, nucleation rate of RecA on ssDNA was slowed down. The transient wrapping-unwrapping behaviors of SSB in $(SSB)_{56}$ isolated clusters lowered the nucleation rate of RecA by a factor of ~3.5 compare to that on a bare DNA. Forcing the SSBs to bind stably in a $(SSB)_{35}$ filament reduced the nucleation rate further. Since the nucleation of RecA initiates the homologous recombination, we suggested that the nucleation rate of RecA acts as a good indicator to determine whether the DNA repair can function properly.

This finding revealed an importance of SSB binding modes and their oligomerizations to DNA recombination, and further confirmed that $(SSB)_{65}/(SSB)_{56}$ binding modes are more likely to facilitate recombinase RecA during the DNA repair. The $(SSB)_{35}$ binding mode, on the contrary, inhibited RecA filament formation, and is believed to not play an important role in this recombination process. Even though the proposal has been made that $(SSB)_{35}$ binding mode would be best suited for DNA replication, the real function of $(SSB)_{35}$ is yet to be determined.

Appendix A

Sample and Protocols

A.1 Proteins, Beads, and Trapping Solutions

A.1.1 Proteins

The genotypes of all *E. coli* SSB used in this study are shown in Table A.1. SSB is a wild type SSB used mainly in most experiments. SSB_m is a mutated modification of the wild type SSB, where a tryptophan residue at the 54^{th} location is substituted by a serine residue. This mutant was previously shown to favor $(SSB)_{35}$ wrapping mode [95]. SSB_f is AlexaFluor555 labeled SSB used in the Fleezers experiment. The labeling position (122C) is chosen to locate outside the ssDNA binding motif (1-112) to ensure that fluorescence dyes do not interfere with the SSB binding.

Name	Modification	Comment
SSB	None (Wild Type)	Most experiments
SSB_m	Replacing W54 with S54	Favor $(SSB)_{35}$ binding mode
SSB_f	AlexaFluor555 labeled at C122	

Table A.1: SSB genotypes.

RecA is purchased from New England Biolabs (M0249S). No further purification is needed before the experiment. RecA requires ATP-γ-S (A1388, Sigma-Aldrich) to form a stable filament on ssDNA.

A.1.2 Beads

Two types of polystyrene bead are used to tether the DNA construct. Streptavidin-coated polystyrene bead of ~790-810 nm diameter is purchased from Spherotech (SVP-08-10).

Anti-digoxigenin bead is custom-made by cross-linking Protein-G-coated polystyrene bead (PGP-08-5, Spherotech) of ~880 nm diameter with anti-digoxigenin antibody (11333089001, Roche). Prior to the experiment, both beads are sonicated (5 s) and vortexed (10 s) to remove bead aggregation occurred during storage. Streptavidin beadd are then incubated with DNA constructs for 1 h at room temperature.

A.1.3 Trapping Solutions

Three trapping solution conditions are used for different experiments. In all experiments containing fluorescently labeled SSB, an oxygen triplet-state quencher (Trolox; Sigma-Aldrich) is added to the trapping buffers (0.1% w/v) to prevent fluorophore blinking.

$(SSB)_{65}$ trapping buffer

$(SSB)_{65}$ trapping buffer contains solution with high $Tris^+$, which is suitable for SSB to wrap ssDNA in the $(SSB)_{65}$ binding mode. It consists of 100 mM Tris-Cl (pH 7.6), 10 mM NaCl, 0.1 mM EDTA, and an oxygen scavenging system to reduce oxidative damage created by an infrared trapping laser at the bead-DNA junctions [120]. Low concentration of SSB (0.5 nM) and the oxygen scavenging system are added to this buffer immediately before the experiment.

$(SSB)_{35}$ trapping buffer

$(SSB)_{35}$ trapping buffer contains solution with low $Tris^+$ and low Na^+, which is suitable for SSB to wrap ssDNA in the $(SSB)_{35}$ binding mode. It consists of 10 mM Tris-Cl (pH 7.6), 10 mM NaCl, 0.1 mM EDTA, and an oxygen scavenging system. High concentration of SSB (5 nM) and the oxygen scavenging system are added to this buffer immediately before the experiment.

RecA trapping buffer

RecA trapping buffer consists of 20 mM Tris-AcO (pH 7.5), 10 mM NaCl, 4 mM Mg-$(AcO)_2$, and an oxygen scavenging system. To this buffer, 125 nM of RecA protein is added along with 125 μM of ATP-γ-S. ATP-γ-S is required by RecA to form a stable filament on ssDNA.

Experiments in section 7.5 are performed under a condition containing higher concentration of both RecA and ATP-γ-S. 375 nM of RecA protein and 375 μM of ATP-γ-S are added to the RecA trapping buffer.

A.2 Experimental Protocols

A.2.1 DNA Construct

The single-stranded DNA construct consists of three separate fragments ligated together (Fig. A.1): a right handle (RH), a left handle (LH), and a SSB binding site (BS). The handles serve as functionalized linkers that connect to trapped beads through biotin-streptavidin and digoxigenin-anti-digoxigenin linkages and spatially separate the beads from the protein binding site. The DNA sequences of both LH and RH are conserved throughout the entire study. Sequences of the BS, however, vary based on the experiment.

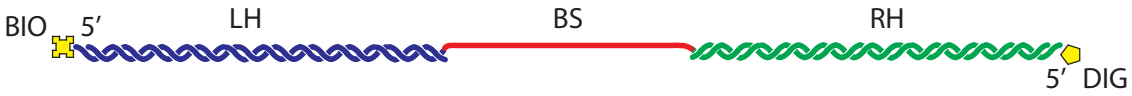

Figure A.1: Traditional DNA construct. A DNA construct consisting of three separate fragments: a right handle (RH), a left handle (LH), and an SSB binding site (BS).

Each fragment was prepared separately in multiple steps. First, we PCR-amplified LH and RH, followed by site-specific digestions to create nucleotide overhangs. The BS was custom-ordered and no further amplification was needed. It was ligated directly to the overhangs of the handles. The detailed protocols for each step were listed below.

Preparing Double-stranded DNA Handles

The LH was synthesized from PCR amplification of the pBR322 plasmid using a 5'-biotin-labeled forward primer (LF). The RH was PCR-amplified from the phage lambda DNA using a 5'-digoxigenin-labeled forward primer (RF). In both cases, the reverse primers (LR, RR) were chosen to make the handles approximately 1,700 base pairs long (Fig. A.2).

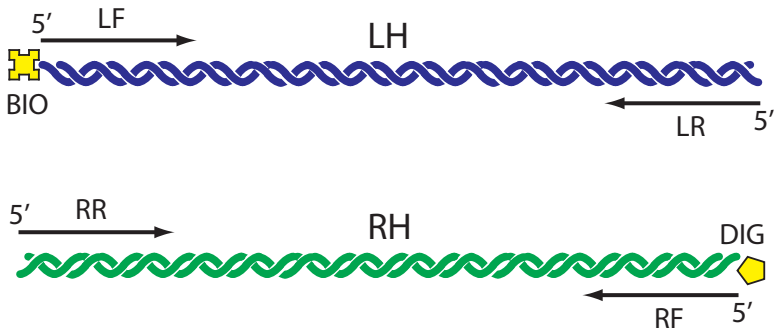

Figure A.2: Double-stranded DNA handles. Left Handle (LH) containing a 5'-biotin-labeled forward primer (LF), while Right Handle (RH) consisting of a 5'-digoxigenin-labeled forward primer (RF). Reverse primers (LR, RR) were chosen to create handles at desired lengths.

Material

- 2X Phusion Master Mix (M0531S, New England BioLabs)
- Left FWD Primer (5'-/5Biosg/TGA AGT GGT GGC CTA ACT AC/-3'): 10 µM
- Left REV Primer (5'-/CAA GCC TAT GCC TAC AGC AT/-3'): 10 µM
- Right FWD Primer (5'-/5DigN/GGG CAA ACC AAG ACA GCT AA/-3'): 10 µM
- Right REV Primer (5'-/CGT TTT CCC GAA AAG CCA GAA/-3'): 10 µM
- pBR322 DNA Plasmid (N3033S, New England BioLabs): 10 ng/µl
- Lambda DNA Plasmid (N3011S, New England BioLabs): 10 ng/µl
- 100% DMSO
- Nuclease-free H_2O
- PCR Purification Kit (28104, QIAGEN)

Procedure

1. For each DNA handle, mix materials according to the Table A.2.
2. Follow the profiles from Table A.3 to perform a PCR amplification.
3. After the PCR is completed, purify the DNA product with a QIA purification kit (Page 19).
4. The final volume for each handle should be around 30 ul.

	Amount (µl)	
	Left Handle	Right Handle
Phusion Master Mix	50	50
FWD Primer	5	5
REV Primer	5	5
DNA Plasmid	2 (pBR322)	2 (Lambda)
DMSO	3	3
H_2O	35	35

Table A.2: Materials for PCR-amplification of double-stranded DNA handles.

	Temperature (°C)	Time (s)	Cycle
Initial Denaturation	98	30	1
Denaturation	98	10	30
Primer Annealing	54	30	
Extension	72	30	
Final Extension	72	600	1

Table A.3: PCR-amplification profile for double-stranded DNA handles.

Digesting Double-stranded DNA Handles

The LH was digested to a 1,550-bp length with the PspGI restriction enzyme. This enzyme cleaved dsDNA at CCTGG or CCAGG sequence, creating an overhang of 5-nucleotide on the 5' end. The RH was cut with the TspRI restriction enzyme, resulting in a 1,710-bp dsDNA with a 9-nucleotide 3' overhang (Fig. A.3).

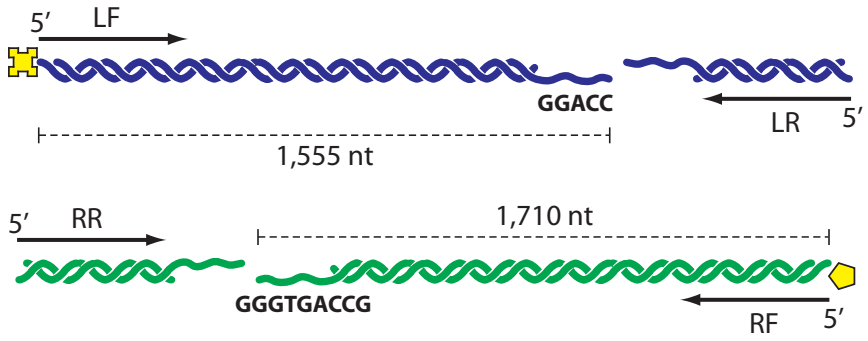

Figure A.3: Digested DNA handles. Site-specific restriction enzymes were used digest both dsDNA handles. Single-stranded DNA overhangs of 5-nt and 9-nt were created on the LH and RH, respectively.

Material

- Purified Left Handle
- Purified Right Handle
- PspGI Restriction Enzyme (R0611S, New England BioLabs)
- TspRI Restriction Enzyme (R0582S, New England BioLabs)
- 10X NEB4 (New England Biolabs Buffer No.4)
- PCR Purification Kit (28104, QIAGEN)

Procedure

1. For each DNA handle, mix materials according to the Table A.4.
2. Incubate mixtures at a given temperature for 2 h.
3. After the digestion finishes, purify the DNA product with a PCR purification kit (Page 19).
4. The final volume for each digested handle should be around 30 ul.

	Amount (μl)	
	Left Handle	Right Handle
DNA Handle	30	30
NEB Buffer No.4	3.5	3.5
Endonucleases	2 (PspGI)	2 (TspRI)
Incubation Temperature	75 °C	65 °C
Incubation Time	2 h	2 h

Table A.4: Materials and conditions for double-stranded DNA handles digestion.

Ligating Single-stranded DNA Binding Site to Handles

Throughout this study, different modifications and lengths of the BS are used in different biological systems interested (Table. A.5). Various lengths of Thymine and DNA modifications are designed to locate in the middle of the fragment. On each end, there is a 5-nt and 9-nt sequence that is complementary to the overhang of the LH and RH, respectively. By ligating all three fragments (LH, BS and RH) together with a DNA ligase, we obtained a final construct which has one digoxigenin and one biotin functional group on opposing ends. These functional groups serve as linkages to the trapping beads (Fig. A.4). Due to an inefficiency of the ligation, the final DNA product would require an extraction using an agarose gel electrophoresis detailed below.

Name	Length (nt)	IDT Sequence
dT70	70	/5Phos/CCTGG/$(T)_{70}$/CCCACTGGC
dT94	94	/5Phos/CCTGG/$(T)_{94}$/CCCACTGGC
dT105	105	/5Phos/CCTGG/$(T)_{105}$/CCCACTGGC
dT140	140	/5Phos/CCTGG/$(T)_{140}$/CCCACTGGC
dT175	175	/5Phos/CCTGG/$(T)_{175}$/CCCACTGGC
dT70sp	70	/5Phos/CCTGG/iSp18/$(T)_{70}$/iSp18/CCCACTGGC
dT140sp	140	/5Phos/CCTGG/iSp18/$(T)_{140}$/iSp18/CCCACTGGC
dT70cy5	70	/5Phos/CCTGG/iSp18/$(T)_{70}$/iSp18/CCCACTGGC

Table A.5: Sequences of the SSB binding site (BS).

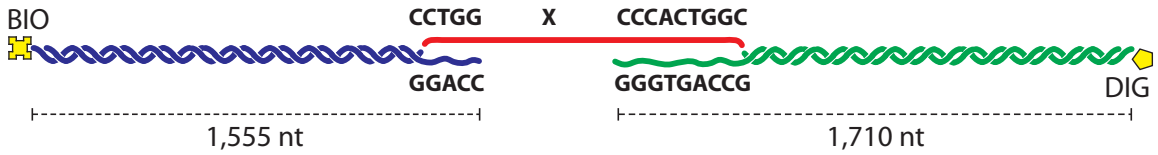

Figure A.4: Ligated DNA construct. Three DNA segments; LH, RH, and BS, are ligated together using a DNA ligase. Parts of the BS sequence are designed to match those complementary overhangs of the dsDNA handles. 'X' denotes a variation of BS sequence.

Material

- Digested Left Handle
- Digested Right Handle
- Single-stranded DNA Binding Site: 1 μM
- 10X T4 DNA Ligase (M0202S, New England BioLabs)
- 25X T4 DNA Ligase Buffer (came with T4 ligase)
- 1X TBE Buffer
- Agarose Gel (BP160-100, Fisher Scientific)
- Loading Dye (Novel Juice; LD001-1000, GeneDirex)
- DNA Ladder (N3232S, New England BioLabs)
- Gel Extraction Kit (28704, QIAGEN)

Procedure: DNA Ligation

1. Measure and make sure that the concentration of both handles is ~100 ng/μl.
2. Mix materials according to the Table A.6
3. Follow the profiles from the Table A.7 to perform the DNA ligation.

	Amount (μl)
Digested Left Handle	30
Digested Right Handle	30
Single-straned DNA Binding Site	4
T4 DNA Ligase	8
T4 DNA Ligase Buffer	8

Table A.6: Materials for DNA ligation

	Temperature (°C)	Time (min)	Cycle
Ligation	20	60	1
Enzyme Deactivation	65	15	1

Table A.7: DNA ligation profile.

Procedure: DNA Gel Extraction

1. Prepare a 1% gel using 1X TBE buffer (0.6 g of agarose gel into 60 ml of 1X TBE). Let it solidify at room temperature for ~1 h.
2. For both ligated DNA product and DNA ladder, mix materials according to the Table. A.8.
3. Load both mixtures into the gel filled with 1X TBE.
4. Perform an electrophoresis using the profile shown in Table. A.8
5. After the electrophoresis finishes, check the ligated DNA product against the DNA ladder.
6. Cut the gel containing ligated DNA product under the blue lamp.
7. Extract the DNA product using a gel extraction kit (Page 25).
8. The final volume should be around 30 ul. Dilute and store at 4 °C as desired.

	Amount (µl)	
	Ligated DNA Product	DNA Ladder
DNA	80	5
Labeling Dye	24	3
1X TBE	16	2
Electrophoresis Voltage	90 V	90 V
Electrophoresis Time	~1 h	~1 h

Table A.8: Materials and conditions for gel electrophoresis of ligated DNA construct.

A.2.2 Microfluidic Chamber

Trap experiments were performed in a custom-designed laminar flow chamber (Fig. A.5, [92]), consisting of two glass slides sandwiching melted Nescofilm patterned with channels. Holes with a diameter of 2-mm were drilled onto one of the slides by a laser engraver system

to create inlets and outlets. The chamber was mounted on an anodized aluminum frame into which inlet and outlet tubing was connected.

Constructing Glass Chamber

Material

- Glass Slide (Size) (12-545-M, ThermoFisher)
- Nescofilm (Karlan)
- Glass Capillary (OD = 100 ± 10 μm, ID = 25.0 ± 6.4 μm; Garner Glass Co., Claremont, CA)
- Laser Engraver System (VLS2.30, Universal Laser Systems)
- Glass Cleaning Jar (Coplin Jar)
- Acetone
- Ethanol
- Milli-Q Water

Procedure

1. Drill 8 holes onto a slide using a laser engraver system with a profile shown in Table A.9.
2. Clean both drilled and intact slides by sonicating them in a cleaning jar containing acetone and ethanol for 5 minutes each.
3. Rinse slides with Milli-Q water. Let them dry.
4. Create a pattern of the flow channels by cutting a piece of Nescofilm with a laser engraver with a profile shown in Table A.9.
5. Carefully attach the cut pattern to the drilled slide. Make sure that all holes are aligned nicely with the channels.
6. Cut two, 5-mm long pieces of glass capillary. Place them as shown (Fig. A.5).
7. Sandwich the pattern with an intact slide. Gently press the chamber such that all components mildly attach to each other.
8. Heat both sides of the chamber equally on a hotplate (heat setting = 4) for 3-4 minutes.

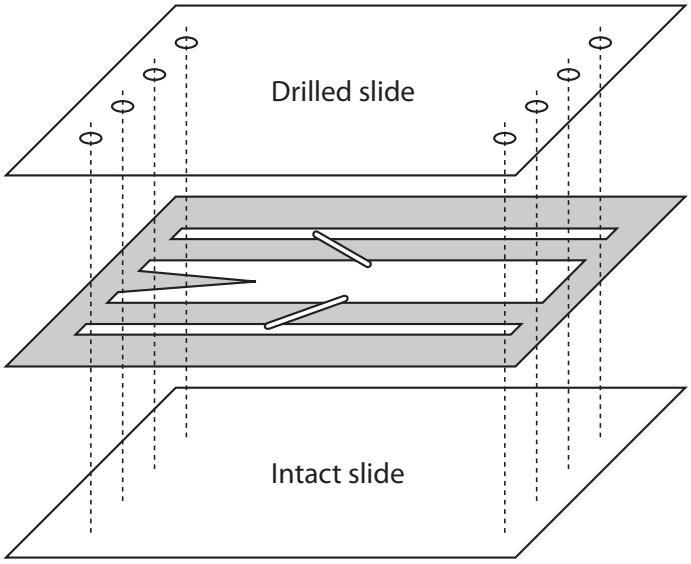

Figure A.5: Glass chamber. A custom-designed laminar flow chamber consisting of two glass slides sandwiching melted Nescofilm patterned with channels (shaded). Holes are drilled on one of the slide to create inlets and outlets (circle). Two pieces of glass capillary are used to connect channels together.

Setting	Glass	Nescofilm
Power	15%	8%
Speed	10%	10%
PPI	250	250
Repeat	15	1

Table A.9: Laser engraver profile.

Assembling Chamber onto Bracket

Material

- Finished Glass Chamber
- Custom-built Anodized Aluminum Frame with Two Holders and Screws.
- Tygon Tubing (ABW00001, Saint-Gobain)
- PE Tubing (PE20, Becton Dickinson and Company)
- Inlet Needles

Procedure

1. Cut 8 pieces of Tygon tubing, each with a length of 4-cm.

2. Cut 8 pieces of PE tubing, each with a length of ~30-cm.
3. Assemble Tygon tubing, PE tubing, and a screw together as shown (Fig. A.6). Repeat for all tubing.
4. Mount a finished glass chamber onto the bracket. Gently screw the holders to hold the chamber in place. Do not break the chamber!
5. Insert all tubing from the back of the bracket. Make sure all tubes are aligned with the inlets and outlets.
6. Test the chamber by flushing Milli-Q water into every channel one-by-one. Check for any leakage.

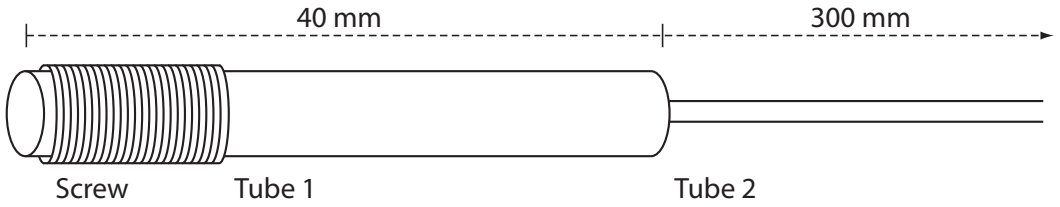

Figure A.6: Chamber tubing. Two types of plastic tube connected to each other are inserted into a metal screw to create an inlet or outlet.

Appendix B

Data Analysis

B.1 Data Analysis

B.1.1 DNA Polymer Elasticity Modeling

Extension of the DNA tether was modeled using two polymer elasticity theories [93, 94]. The total extension, x_{DNA}, was decomposed into two components: dsDNA (x_{ds}) and ssDNA (x_{ss}). We computed the extension of each of these segments separately,

$$\begin{aligned} x_{DNA} &= x_{ds} + x_{ss} \\ x_{DNA} &= \xi_{ds}(F) \cdot N_{ds} + \xi_{ss}(F) \cdot N_{ss} \end{aligned} \tag{B.1}$$

where $\xi_{ds}(F)$ and $\xi_{ss}(F)$ are the extension of one dsDNA base pair and one ssDNA nucleotide at a tension F, respectively, and N_{ds} is the total length of the dsDNA handles while N_{ss} is length of the ssDNA loading site. The dsDNA segment was modeled with an extensible worm-like chain (XWLC) model [93]. Parameters for dsDNA were taken directly from the previous study [121]. The persistence length of dsDNA was 50 nm, the stretch modulus for dsDNA was 1,200 pN, and the contour length per single dsDNA base pair was 0.34 nm·bp^{-1}. The ssDNA segment was fitted to a snake-like chain (SLC) model [94]. Since the ionic condition in the solution affects the properties of the ssDNA, parameters used in this model vary significantly among experiments. We compared our buffer containing different ionic conditions with a lookup table provided in the literature [94], and obtained all necessary parameters as following:

Trapping Buffer	f_c (pN)	γ	L_0 (nm)	L_c/L_0
$(SSB)_{35}$	0.28	0.58	$N_{ss}/2$	0.28
$(SSB)_{65}$	0.7	0.61	$N_{ss}/2$	0.32
RecA	1.4	0.64	$N_{ss}/2$	0.38

Table B.1: Parameters for snake-like chain polymer modeling.

Our traditional DNA construct consists of 3,260 bp dsDNA handles and a short ssDNA binding site. To validate our choice of these parameters, we performed a stretching experiment on DNA constructs containing various lengths of the ssDNA binding site in different buffer conditions, and compared the results with predictions from the elasticity models.

Polymer Modeling in $(SSB)_{65}$ Trapping Buffer

DNA constructs containing 70-nt (dT70) and 140-nt (dT140) ssDNA molecules were stretched and relaxed in the $(SSB)_{65}$ trapping buffer (Appendix A). Force-extension curves (FEC) of many DNA molecules (Fig. B.1; dT70 (red) and dT140(orange)) are in excellent agreement with the models (black).

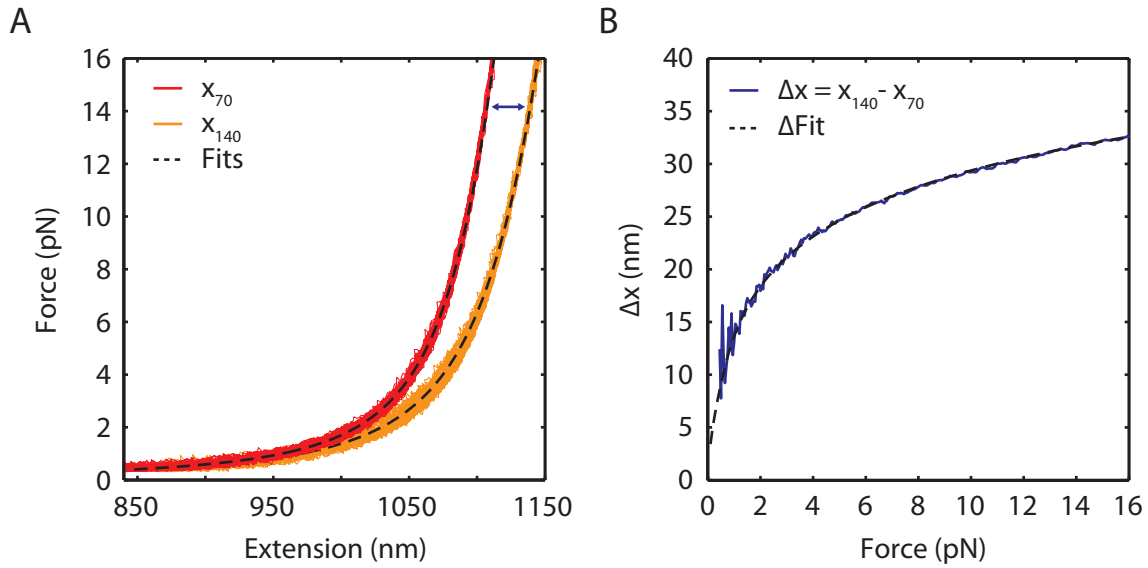

Figure B.1: Single-stranded DNA polymer modeling in $(SSB)_{65}$ trapping buffer. (**A**) Representative force-extension curves (FEC) of stretching and relaxing a DNA construct containing 3,260-bp dsDNA handles and 70-nt (red) or 140-nt (orange) ssDNA. Black dashed lines are fits to the constructs. (**B**) Extension difference (blue) between 70-nt and 140-nt ssDNA constructs in (A) vs. force. The fit illustrates the validity of the ssDNA elasticity model over short lengths (70-nt).

Polymer Modeling in $(SSB)_{35}$ Trapping Buffer

Four DNA constructs consisting of 70-dT, 105-dT (dT105), 140-dT and 175-dT (dT175) ssDNA segments were stretched and relaxed in the $(SSB)_{35}$ trapping buffer (Appendix A). Figure B.2 demonstrates the validity of the model showing representative FECs (red, green, orange, and cyan) along with their fits (black).

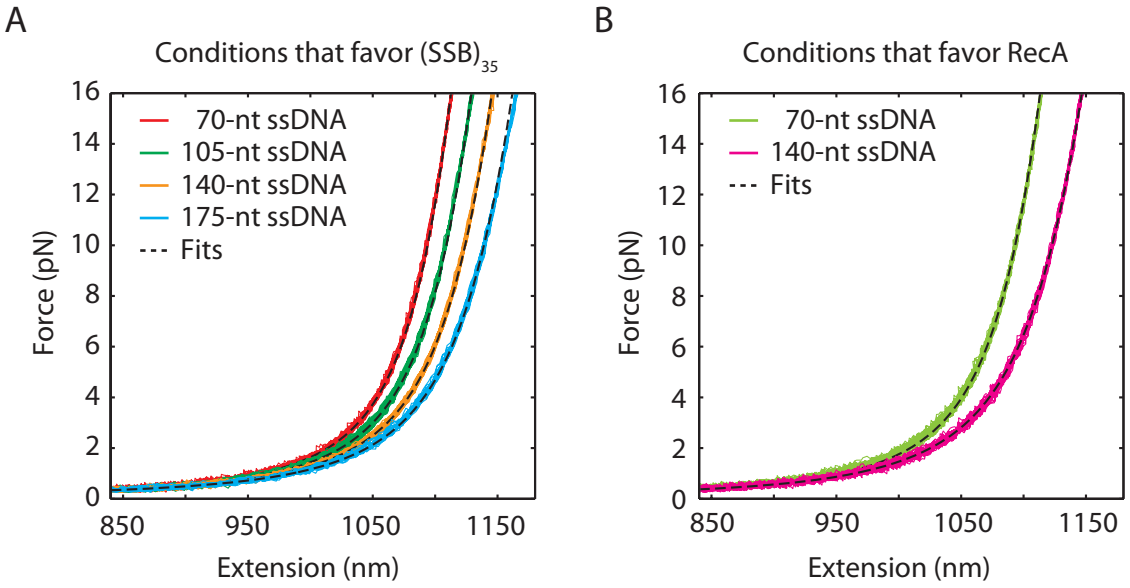

Figure B.2: Single-stranded DNA polymer modeling in $(SSB)_{35}$ and RecA trapping buffers. (**A**) Representative force-extension curves (FEC) of stretching and relaxing a DNA construct containing 70-nt (red), 105-nt (green), 140-nt (orange), and 175-nt (cyan) ssDNA in conditions that favor $(SSB)_{35}$ binding mode. Black dashed lines are fits to the constructs. (**B**) Representative FECs of stretching and relaxing a DNA construct containing 70-nt (green) and 140-nt (pink) ssDNA in conditions that are suitable for RecA filament formation.

Polymer Modeling in RecA Trapping Buffer

Many dT70 and dT140 ssDNA constructs were stretched and relaxed under a range of tension (0-25 pN). Representative force extension curves (FEC) of many dT70 (green) and dT140 (pink) ssDNA molecules are shown in comparison with the fits (Fig. B.2).

Bibliography

[1] W. Bujalowski and T. M. Lohman. "Escherichia coli single-strand binding protein forms multiple, distinct complexes with single-stranded DNA". *Biochemistry* 25.24 (1986), pp. 7799–802.

[2] T. M. Lohman and M. E. Ferrari. "Escherichia coli single-stranded DNA-binding protein: multiple DNA-binding modes and cooperativities". *Annu Rev Biochem* 63 (1994), pp. 527–70.

[3] J. D. Griffith, L. D. Harris, and 3rd Register J. "Visualization of SSB-ssDNA complexes active in the assembly of stable RecA-DNA filaments". *Cold Spring Harb Symp Quant Biol* 49 (1984), pp. 553–9.

[4] R. Roy, A. G. Kozlov, T. M. Lohman, and T. Ha. "SSB protein diffusion on single-stranded DNA stimulates RecA filament formation". *Nature* 461.7267 (2009), pp. 1092–7.

[5] J. C. Bell, J. L. Plank, C. C. Dombrowski, and S. C. Kowalczykowski. "Direct imaging of RecA nucleation and growth on single molecules of SSB-coated ssDNA". *Nature* 491.7423 (2012), pp. 274–8.

[6] H. Fu, S. Le, H. Chen, K. Muniyappa, and J. Yan. "Force and ATP hydrolysis dependent regulation of RecA nucleoprotein filament by single-stranded DNA binding protein". *Nucleic Acids Res* 41.2 (2013), pp. 924–32.

[7] R. R. Meyer and P. S. Laine. "The single-stranded DNA-binding protein of Escherichia coli". *Microbiol Rev* 54.4 (1990), pp. 342–80.

[8] B. M. Alberts and L. Frey. "T4 bacteriophage gene 32: a structural protein in the replication and recombination of DNA". *Nature* 227.5265 (1970), pp. 1313–8.

[9] N. Sigal, H. Delius, T. Kornberg, M. L. Gefter, and B. Alberts. "A DNA-unwinding protein isolated from Escherichia coli: its interaction with DNA and with DNA polymerases". *Proc Natl Acad Sci U S A* 69.12 (1972), pp. 3537–41.

[10] J. de Vries and W. Wackernagel. "Cloning and sequencing of the Serratia marcescens gene encoding a single-stranded DNA-binding protein (SSB) and its promoter region". *Gene* 127.1 (1993), pp. 39–45.

[11] E. I. Golub and K. B. Low. "Conjugative plasmids of enteric bacteria from many different incompatibility groups have similar genes for single-stranded DNA-binding proteins". *J Bacteriol* 162.1 (1985), pp. 235–41.

[12] G. Martin and M. Salas. "Characterization and cloning of gene 5 of Bacillus subtilis phage phi 29". *Gene* 67.2 (1988), pp. 193–201.

[13] E. Scherzinger, F. Litfin, and E. Jost. "Stimulation of T7 DNA polymerase by a new phage-coded protein". *Mol Gen Genet* 123.3 (1973), pp. 247–62.

[14] M. P. Fairman and B. Stillman. "Cellular factors required for multiple stages of SV40 DNA replication in vitro". *EMBO J* 7.4 (1988), pp. 1211–8.

[15] C. R. Wobbe, L. Weissbach, J. A. Borowiec, F. B. Dean, Y. Murakami, P. Bullock, and J. Hurwitz. "Replication of simian virus 40 origin-containing DNA in vitro with purified proteins". *Proc Natl Acad Sci U S A* 84.7 (1987), pp. 1834–8.

[16] S. J. Brill and B. Stillman. "Yeast replication factor-A functions in the unwinding of the SV40 origin of DNA replication". *Nature* 342.6245 (1989), pp. 92–5.

[17] P. G. Mitsis, S. C. Kowalczykowski, and I. R. Lehman. "A single-stranded DNA binding protein from Drosophila melanogaster: characterization of the heterotrimeric protein and its interaction with single-stranded DNA". *Biochemistry* 32.19 (1993), pp. 5257–66.

[18] P. A. Pavco and G. C. Van Tuyle. "Purification and general properties of the DNA-binding protein (P16) from rat liver mitochondria". *J Cell Biol* 100.1 (1985), pp. 258–64.

[19] V. Tiranti, M. Rocchi, S. DiDonato, and M. Zeviani. "Cloning of human and rat cDNAs encoding the mitochondrial single-stranded DNA-binding protein (SSB)". *Gene* 126.2 (1993), pp. 219–25.

[20] M. D. Challberg. "A method for identifying the viral genes required for herpesvirus DNA replication". *Proc Natl Acad Sci U S A* 83.23 (1986), pp. 9094–8.

[21] A. Atrazhev, S. Zhang, and F. Grosse. "Single-stranded DNA binding protein from calf thymus. Purification, properties, and stimulation of the homologous DNA-polymerase-alpha-primase complex". *Eur J Biochem* 210.3 (1992), pp. 855–65.

[22] J. W. Chase and K. R. Williams. "Single-stranded DNA binding proteins required for DNA replication". *Annu Rev Biochem* 55 (1986), pp. 103–36.

[23] S. Raghunathan, A. G. Kozlov, T. M. Lohman, and G. Waksman. "Structure of the DNA binding domain of E. coli SSB bound to ssDNA". *Nat Struct Biol* 7.8 (2000), pp. 648–52.

[24] L. B. Overman, W. Bujalowski, and T. M. Lohman. "Equilibrium binding of Escherichia coli single-strand binding protein to single-stranded nucleic acids in the (SSB)65 binding mode. Cation and anion effects and polynucleotide specificity". *Biochemistry* 27.1 (1988), pp. 456–71.

[25] U. Curth, J. Greipel, C. Urbanke, and G. Maass. "Multiple binding modes of the single-stranded DNA binding protein from Escherichia coli as detected by tryptophan fluorescence and site-directed mutagenesis". *Biochemistry* 32.10 (1993), pp. 2585–91.

[26] M. I. Khamis, J. R. Casas-Finet, A. H. Maki, J. B. Murphy, and J. W. Chase. "Investigation of the role of individual tryptophan residues in the binding of Escherichia coli single-stranded DNA binding protein to single-stranded polynucleotides. A study by optical detection of magnetic resonance and site-selected mutagenesis". *J Biol Chem* 262.23 (1987), pp. 10938–45.

[27] A. G. Kozlov, M. M. Cox, and T. M. Lohman. "Regulation of single-stranded DNA binding by the C termini of Escherichia coli single-stranded DNA-binding (SSB) protein". *J Biol Chem* 285.22 (2010), pp. 17246–52.

[28] S. R. Wessel, A. H. Marceau, S. C. Massoni, R. Zhou, T. Ha, S. J. Sandler, and J. L. Keck. "PriC-mediated DNA replication restart requires PriC complex formation with the single-stranded DNA-binding protein". *J Biol Chem* 288.24 (2013), pp. 17569–78.

[29] B. Bhattacharyya, N. P. George, T. M. Thurmes, R. Zhou, N. Jani, S. R. Wessel, S. J. Sandler, T. Ha, and J. L. Keck. "Structural mechanisms of PriA-mediated DNA replication restart". *Proc Natl Acad Sci U S A* 111.4 (2014), pp. 1373–8.

[30] S. N. Savvides, S. Raghunathan, K. Futterer, A. G. Kozlov, T. M. Lohman, and G. Waksman. "The C-terminal domain of full-length E. coli SSB is disordered even when bound to DNA". *Protein Sci* 13.7 (2004), pp. 1942–7.

[31] M. E. Kuil, K. Holmlund, C. A. Vlaanderen, and R. van Grondelle. "Study of the binding of single-stranded DNA-binding protein to DNA and poly(rA) using electric field induced birefringence and circular dichroism spectroscopy". *Biochemistry* 29.35 (1990), pp. 8184–9.

[32] E. V. Bobst, F. W. Perrino, R. R. Meyer, and A. M. Bobst. "An EPR study to determine the relative nucleic acid binding affinity of single-stranded DNA-binding protein from Escherichia coli". *Biochim Biophys Acta* 1078.2 (1991), pp. 199–207.

[33] T. Matsumoto, Y. Morimoto, N. Shibata, T. Kinebuchi, N. Shimamoto, T. Tsukihara, and N. Yasuoka. "Roles of functional loops and the C-terminal segment of a single-stranded DNA binding protein elucidated by X-Ray structure analysis". *J Biochem* 127.2 (2000), pp. 329–35.

[34] S. C. Kowalczykowski, J. Clow, R. Somani, and A. Varghese. "Effects of the Escherichia coli SSB protein on the binding of Escherichia coli RecA protein to single-stranded DNA. Demonstration of competitive binding and the lack of a specific protein-protein interaction". *J Mol Biol* 193.1 (1987), pp. 81–95.

[35] K. Muniyappa, K. Williams, J. W. Chase, and C. M. Radding. "Active nucleoprotein filaments of single-stranded binding protein and recA protein on single-stranded DNA have a regular repeating structure". *Nucleic Acids Res* 18.13 (1990), pp. 3967–73.

[36] S. W. Morrical, J. Lee, and M. M. Cox. "Continuous association of Escherichia coli single-stranded DNA binding protein with stable complexes of recA protein and single-stranded DNA". *Biochemistry* 25.7 (1986), pp. 1482–94.

[37] R. D. Shereda, A. G. Kozlov, T. M. Lohman, M. M. Cox, and J. L. Keck. "SSB as an organizer/mobilizer of genome maintenance complexes". *Crit Rev Biochem Mol Biol* 43.5 (2008), pp. 289–318.

[38] A. G. Kozlov and T. M. Lohman. "Stopped-flow studies of the kinetics of single-stranded DNA binding and wrapping around the Escherichia coli SSB tetramer". *Biochemistry* 41.19 (2002), pp. 6032–44.

[39] W. Bujalowski and T. M. Lohman. "Negative co-operativity in Escherichia coli single strand binding protein-oligonucleotide interactions. II. Salt, temperature and oligonucleotide length effects". *J Mol Biol* 207.1 (1989), pp. 269–88.

[40] R. Roy, A. G. Kozlov, T. M. Lohman, and T. Ha. "Dynamic structural rearrangements between DNA binding modes of E. coli SSB protein". *J Mol Biol* 369.5 (2007), pp. 1244–57.

[41] R. Zhou, A. G. Kozlov, R. Roy, J. Zhang, S. Korolev, T. M. Lohman, and T. Ha. "SSB functions as a sliding platform that migrates on DNA via reptation". *Cell* 146.2 (2011), pp. 222–32.

[42] K. S. Lee, A. B. Marciel, A. G. Kozlov, C. M. Schroeder, T. M. Lohman, and T. Ha. "Ultrafast redistribution of E. coli SSB along long single-stranded DNA via intersegment transfer". *J Mol Biol* 426.13 (2014), pp. 2413–21.

[43] M. J. Comstock, T. Ha, and Y. R. Chemla. "Ultrahigh-resolution optical trap with single-fluorophore sensitivity". *Nat Methods* 8.4 (2011), pp. 335–40.

[44] A. Ashkin. "Acceleration and Trapping of Particles by Radiation Pressure". *Physical Review Letters* 24.4 (1970), p. 156.

[45] A. Ashkin and J. M. Dziedzic. "Optical Levitation by Radiation Pressure". *Applied Physics Letters* 19.8 (1971), p. 283.

[46] A. Ashkin and J. M. Dziedzic. "Optical Trapping and Manipulation of Viruses and Bacteria". *Science* 235.4795 (1987), pp. 1517–1520.

[47] A. Ashkin, J. M. Dziedzic, and T. Yamane. "Optical Trapping and Manipulation of Single Cells Using Infrared-Laser Beams". *Nature* 330.6150 (1987), pp. 769–771.

[48] T. T. Perkins, D. E. Smith, and S. Chu. "Direct Observation of Tube-Like Motion of a Single Polymer-Chain". *Science* 264.5160 (1994), pp. 819–822.

[49] T. T. Perkins, D. E. Smith, R. G. Larson, and S. Chu. "Stretching of a Single Tethered Polymer in a Uniform-Flow". *Science* 268.5207 (1995), pp. 83–87.

[50] J. C. Crocker and D. G. Grier. "Microscopic Measurement of the Pair Interaction Potential of Charge-Stabilized Colloid". *Physical Review Letters* 73.2 (1994), pp. 352–355.

[51] P. T. Korda, M. B. Taylor, and D. G. Grier. "Kinetically locked-in colloidal transport in an array of optical tweezers". *Physical Review Letters* 89.12 (2002).

[52] T. L. Min, P. J. Mears, I. Golding, and Y. R. Chemla. "Chemotactic adaptation kinetics of individual Escherichia coli cells". *Proc Natl Acad Sci U S A* 109.25 (2012), pp. 9869–74.

[53] J. Liphardt, B. Onoa, S. B. Smith, Jr. Tinoco I., and C. Bustamante. "Reversible unfolding of single RNA molecules by mechanical force". *Science* 292.5517 (2001), pp. 733–7.

[54] B. Onoa, S. Dumont, J. Liphardt, S. B. Smith, Jr. Tinoco I., and C. Bustamante. "Identifying kinetic barriers to mechanical unfolding of the T. thermophila ribozyme". *Science* 299.5614 (2003), pp. 1892–5.

[55] C. Bustamante, Z. Bryant, and S. B. Smith. "Ten years of tension: single-molecule DNA mechanics". *Nature* 421.6921 (2003), pp. 423–7.

[56] V. Garces-Chavez, D. McGloin, H. Melville, W. Sibbett, and K. Dholakia. "Simultaneous micromanipulation in multiple planes using a self-reconstructing light beam". *Nature* 419.6903 (2002), pp. 145–7.

[57] M. P. MacDonald, L. Paterson, K. Volke-Sepulveda, J. Arlt, W. Sibbett, and K. Dholakia. "Creation and manipulation of three-dimensional optically trapped structures". *Science* 296.5570 (2002), pp. 1101–3.

[58] J. R. Moffitt, Y. R. Chemla, D. Izhaky, and C. Bustamante. "Differential detection of dual traps improves the spatial resolution of optical tweezers". *Proc Natl Acad Sci U S A* 103.24 (2006), pp. 9006–11.

[59] L. Paterson, M. P. MacDonald, J. Arlt, W. Sibbett, P. E. Bryant, and K. Dholakia. "Controlled rotation of optically trapped microscopic particles". *Science* 292.5518 (2001), pp. 912–4.

[60] C. Gosse and V. Croquette. "Magnetic tweezers: micromanipulation and force measurement at the molecular level". *Biophys J* 82.6 (2002), pp. 3314–29.

[61] K. Visscher, S. P. Gross, and S. M. Block. "Construction of multiple-beam optical traps with nanometer-resolution position sensing". *Ieee Journal of Selected Topics in Quantum Electronics* 2.4 (1996), pp. 1066–1076.

[62] K. Visscher and S. M. Block. "Versatile optical traps with feedback control". *Molecular Motors and the Cytoskeleton, Pt B* 298 (1998), pp. 460–489.

[63] J. E. Molloy, J. E. Burns, J. C. Sparrow, R. T. Tregear, J. Kendrick-Jones, and D. C. White. "Single-molecule mechanics of heavy meromyosin and S1 interacting with rabbit or Drosophila actins using optical tweezers". *Biophys J* 68.4 Suppl (1995), 298S–303S, 303S–305S.

[64] F. Gittes and C. F. Schmidt. "Interference model for back-focal-plane displacement detection in optical tweezers". *Opt Lett* 23.1 (1998), pp. 7–9.

[65] M. W. Allersma, F. Gittes, M. J. deCastro, R. J. Stewart, and C. F. Schmidt. "Two-dimensional tracking of ncd motility by back focal plane interferometry". *Biophys J* 74.2 Pt 1 (1998), pp. 1074–85.

[66] K. Svoboda, C. F. Schmidt, B. J. Schnapp, and S. M. Block. "Direct observation of kinesin stepping by optical trapping interferometry". *Nature* 365.6448 (1993), pp. 721–7.

[67] K. Visscher, M. J. Schnitzer, and S. M. Block. "Single kinesin molecules studied with a molecular force clamp". *Nature* 400.6740 (1999), pp. 184–9.

[68] P. J. Pease, O. Levy, G. J. Cost, J. Gore, J. L. Ptacin, D. Sherratt, C. Bustamante, and N. R. Cozzarelli. "Sequence-directed DNA translocation by purified FtsK". *Science* 307.5709 (2005), pp. 586–90.

[69] M. D. Wang, M. J. Schnitzer, H. Yin, R. Landick, J. Gelles, and S. M. Block. "Force and velocity measured for single molecules of RNA polymerase". *Science* 282.5390 (1998), pp. 902–7.

[70] G. J. Wuite, S. B. Smith, M. Young, D. Keller, and C. Bustamante. "Single-molecule studies of the effect of template tension on T7 DNA polymerase activity". *Nature* 404.6773 (2000), pp. 103–6.

[71] Y. R. Chemla, K. Aathavan, J. Michaelis, S. Grimes, P. J. Jardine, D. L. Anderson, and C. Bustamante. "Mechanism of force generation of a viral DNA packaging motor". *Cell* 122.5 (2005), pp. 683–92.

[72] J. R. Moffitt, Y. R. Chemla, K. Aathavan, S. Grimes, P. J. Jardine, D. L. Anderson, and C. Bustamante. "Intersubunit coordination in a homomeric ring ATPase". *Nature* 457.7228 (2009), pp. 446–50.

[73] M. T. Woodside, P. C. Anthony, W. M. Behnke-Parks, K. Larizadeh, D. Herschlag, and S. M. Block. "Direct measurement of the full, sequence-dependent folding landscape of a nucleic acid". *Science* 314.5801 (2006), pp. 1001–4.

[74] S. B. Smith, Y. Cui, and C. Bustamante. "Overstretching B-DNA: the elastic response of individual double-stranded and single-stranded DNA molecules". *Science* 271.5250 (1996), pp. 795–9.

[75] J. Enger, M. Goksor, K. Ramser, P. Hagberg, and D. Hanstorp. "Optical tweezers applied to a microfluidic system". *Lab Chip* 4.3 (2004), pp. 196–200.

[76] P. Jordan, J. Leach, M. Padgett, P. Blackburn, N. Isaacs, M. Goksor, D. Hanstorp, A. Wright, J. Girkin, and J. Cooper. "Creating permanent 3D arrangements of isolated cells using holographic optical tweezers". *Lab Chip* 5.11 (2005), pp. 1224–8.

[77] X. Wang, S. Chen, M. Kong, Z. Wang, K. D. Costa, R. A. Li, and D. Sun. "Enhanced cell sorting and manipulation with combined optical tweezer and microfluidic chip technologies". *Lab Chip* 11.21 (2011), pp. 3656–62.

[78] Z. Li, B. Anvari, M. Takashima, P. Brecht, J. H. Torres, and W. E. Brownell. "Membrane tether formation from outer hair cells with optical tweezers". *Biophys J* 82.3 (2002), pp. 1386–95.

[79] J. Dai and M. P. Sheetz. "Mechanical properties of neuronal growth cone membranes studied by tether formation with laser optical tweezers". *Biophys J* 68.3 (1995), pp. 988–96.

[80] M. C. Zhong, X. B. Wei, J. H. Zhou, Z. Q. Wang, and Y. M. Li. "Trapping red blood cells in living animals using optical tweezers". *Nat Commun* 4 (2013), p. 1768.

[81] G. Knoner, B. E. Rolfe, J. H. Campbell, S. J. Parkin, N. R. Heckenberg, and H. Rubinsztein-Dunlop. "Mechanics of cellular adhesion to artificial artery templates". *Biophys J* 91.8 (2006), pp. 3085–96.

[82] P. J. Mears, S. Koirala, C. V. Rao, I. Golding, and Y. R. Chemla. "Escherichia coli swimming is robust against variations in flagellar number". *Elife* 3 (2014), e01916.

[83] E. A. Abbondanzieri, W. J. Greenleaf, J. W. Shaevitz, R. Landick, and S. M. Block. "Direct observation of base-pair stepping by RNA polymerase". *Nature* 438.7067 (2005), pp. 460–5.

[84] Z. Qi, R. A. Pugh, M. Spies, and Y. R. Chemla. "Sequence-dependent base pair stepping dynamics in XPD helicase unwinding". *Elife* 2 (2013), e00334.

[85] W. Cheng, S. G. Arunajadai, J. R. Moffitt, Jr. Tinoco I., and C. Bustamante. "Single-base pair unwinding and asynchronous RNA release by the hepatitis C virus NS3 helicase". *Science* 333.6050 (2011), pp. 1746–9.

[86] M. Sen, R. A. Maillard, K. Nyquist, P. Rodriguez-Aliaga, S. Presse, A. Martin, and C. Bustamante. "The ClpXP protease unfolds substrates using a constant rate of pulling but different gears". *Cell* 155.3 (2013), pp. 636–46.

[87] M. A. Dijk, L. C. Kapitein, Jv Mameren, C. F. Schmidt, and E. J. Peterman. "Combining optical trapping and single-molecule fluorescence spectroscopy: enhanced photobleaching of fluorophores". *J Phys Chem B* 108.20 (2004), pp. 6479–84.

[88] R. R. Brau, P. B. Tarsa, J. M. Ferrer, P. Lee, and M. J. Lang. "Interlaced optical force-fluorescence measurements for single molecule biophysics". *Biophys J* 91.3 (2006), pp. 1069–77.

[89] W. Bujalowski and T. M. Lohman. "Monomer-tetramer equilibrium of the Escherichia coli ssb-1 mutant single strand binding protein". *J Biol Chem* 266.3 (1991), pp. 1616–26.

[90] T. M. Lohman, J. M. Green, and R. S. Beyer. "Large-scale overproduction and rapid purification of the Escherichia coli ssb gene product. Expression of the ssb gene under lambda PL control". *Biochemistry* 25.1 (1986), pp. 21–5.

[91] I. Rasnik, S. A. McKinney, and T. Ha. "Nonblinking and long-lasting single-molecule fluorescence imaging". *Nat Methods* 3.11 (2006), pp. 891–3.

[92] L. R. Brewer and P. R. Bianco. "Laminar flow cells for single-molecule studies of DNA-protein interactions". *Nat Methods* 5.6 (2008), pp. 517–25.

[93] C. Bustamante, J. F. Marko, E. D. Siggia, and S. Smith. "Entropic elasticity of lambda-phage DNA". *Science* 265.5178 (1994), pp. 1599–600.

[94] O. A. Saleh, D. B. McIntosh, P. Pincus, and N. Ribeck. "Nonlinear low-force elasticity of single-stranded DNA molecules". *Phys Rev Lett* 102.6 (2009), p. 068301.

[95] M. E. Ferrari, J. Fang, and T. M. Lohman. "A mutation in E. coli SSB protein (W54S) alters intra-tetramer negative cooperativity and inter-tetramer positive cooperativity for single-stranded DNA binding". *Biophys Chem* 64.1-3 (1997), pp. 235–51.

[96] J. R. Casas-Finet, M. I. Khamis, A. H. Maki, and J. W. Chase. "Tryptophan 54 and phenylalanine 60 are involved synergistically in the binding of E. coli SSB protein to single-stranded polynucleotides". *FEBS Lett* 220.2 (1987), pp. 347–52.

[97] M. I. Khamis, J. R. Casas-Finet, A. H. Maki, J. B. Murphy, and J. W. Chase. "Role of tryptophan 54 in the binding of E. coli single-stranded DNA-binding protein to single-stranded polynucleotides". *FEBS Lett* 211.2 (1987), pp. 155–9.

[98] K. R. Williams, J. B. Murphy, and J. W. Chase. "Characterization of the structural and functional defect in the Escherichia coli single-stranded DNA binding protein encoded by the ssb-1 mutant gene. Expression of the ssb-1 gene under lambda pL regulation". *J Biol Chem* 259.19 (1984), pp. 11804–11.

[99] W. Bujalowski and T. M. Lohman. "Monomers of the Escherichia coli SSB-1 mutant protein bind single-stranded DNA". *J Mol Biol* 217.1 (1991), pp. 63–74.

[100] C. Bustamante, S. B. Smith, J. Liphardt, and D. Smith. "Single-molecule studies of DNA mechanics". *Curr Opin Struct Biol* 10.3 (2000), pp. 279–85.

[101] B. Maier, D. Bensimon, and V. Croquette. "Replication by a single DNA polymerase of a stretched single-stranded DNA". *Proc Natl Acad Sci U S A* 97.22 (2000), pp. 12002–7.

[102] S. L. Lusetti and M. M. Cox. "The bacterial RecA protein and the recombinational DNA repair of stalled replication forks". *Annu Rev Biochem* 71 (2002), pp. 71–100.

[103] S. Sommer, F. Boudsocq, R. Devoret, and A. Bailone. "Specific RecA amino acid changes affect RecA-UmuD'C interaction". *Mol Microbiol* 28.2 (1998), pp. 281–91.

[104] R. M. Story, I. T. Weber, and T. A. Steitz. "The structure of the E. coli recA protein monomer and polymer". *Nature* 355.6358 (1992), pp. 318–25.

[105] A. I. Roca and M. M. Cox. "RecA protein: structure, function, and role in recombinational DNA repair". *Prog Nucleic Acid Res Mol Biol* 56 (1997), pp. 129–223.

[106] H. G. Nastri and K. L. Knight. "Identification of residues in the L1 region of the RecA protein which are important to recombination or coprotease activities". *J Biol Chem* 269.42 (1994), pp. 26311–22.

[107] V. A. Malkov and R. D. Camerini-Otero. "Photocross-links between single-stranded DNA and Escherichia coli RecA protein map to loops L1 (amino acid residues 157-164) and L2 (amino acid residues 195-209)". *J Biol Chem* 270.50 (1995), pp. 30230–3.

[108] Y. Wang and K. Adzuma. "Differential proximity probing of two DNA binding sites in the Escherichia coli recA protein using photo-cross-linking methods". *Biochemistry* 35.11 (1996).

[109] X. Yu, S. A. Jacobs, S. C. West, T. Ogawa, and E. H. Egelman. "Domain structure and dynamics in the helical filaments formed by RecA and Rad51 on DNA". *Proc Natl Acad Sci U S A* 98.15 (2001), pp. 8419–24.

[110] S. Tateishi, T. Horii, T. Ogawa, and H. Ogawa. "C-terminal truncated Escherichia coli RecA protein RecA5327 has enhanced binding affinities to single- and double-stranded DNAs". *J Mol Biol* 223.1 (1992), pp. 115–29.

[111] R. C. Benedict and S. C. Kowalczykowski. "Increase of the DNA strand assimilation activity of recA protein by removal of the C terminus and structure-function studies of the resulting protein fragment". *J Biol Chem* 263.30 (1988), pp. 15513–20.

[112] C. Joo, S. A. McKinney, M. Nakamura, I. Rasnik, S. Myong, and T. Ha. "Real-time observation of RecA filament dynamics with single monomer resolution". *Cell* 126.3 (2006), pp. 515–27.

[113] T. Nishinaka, Y. Ito, S. Yokoyama, and T. Shibata. "An extended DNA structure through deoxyribose-base stacking induced by RecA protein". *Proc Natl Acad Sci U S A* 94.13 (1997), pp. 6623–8.

[114] R. Galletto, I. Amitani, R. J. Baskin, and S. C. Kowalczykowski. "Direct observation of individual RecA filaments assembling on single DNA molecules". *Nature* 443.7113 (2006), pp. 875–8.

[115] R. W. Ruigrok, B. Bohrmann, E. Hewat, A. Engel, E. Kellenberger, and E. DiCapua. "The inactive form of recA protein: the 'compact' structure". *EMBO J* 12.1 (1993), pp. 9–16.

[116] M. V. Madiraju, P. E. Lavery, S. C. Kowalczykowski, and A. J. Clark. "Enzymatic properties of the RecA803 protein, a partial suppressor of recF mutations". *Biochemistry* 31.43 (1992), pp. 10529–35.

[117] Q. Shan, J. M. Bork, B. L. Webb, R. B. Inman, and M. M. Cox. "RecA protein filaments: end-dependent dissociation from ssDNA and stabilization by RecO and RecR proteins". *J Mol Biol* 265.5 (1997), pp. 519–40.

[118] D. G. Anderson and S. C. Kowalczykowski. "The translocating RecBCD enzyme stimulates recombination by directing RecA protein onto ssDNA in a chi-regulated manner". *Cell* 90.1 (1997), pp. 77–86.

[119] J. J. Churchill, D. G. Anderson, and S. C. Kowalczykowski. "The RecBC enzyme loads RecA protein onto ssDNA asymmetrically and independently of chi, resulting in constitutive recombination activation". *Genes Dev* 13.7 (1999), pp. 901–11.

[120] M. P. Landry, P. M. McCall, Z. Qi, and Y. R. Chemla. "Characterization of photoactivated singlet oxygen damage in single-molecule optical trap experiments". *Biophys J* 97.8 (2009), pp. 2128–36.

[121] C. G. Baumann, S. B. Smith, V. A. Bloomfield, and C. Bustamante. "Ionic effects on the elasticity of single DNA molecules". *Proc Natl Acad Sci U S A* 94.12 (1997), pp. 6185–90.